

Magnetic resonance imaging of the right ventricle in human pulmonary hypertension

A thesis by

Kevin G Blyth MBChB, MRCP

Submitted for the degree of Doctor of Medicine

to

The University of Glasgow

2007

Principal Supervisor: Professor Andrew Peacock

Adviser: Ms. Tania Sprott

Division: Cardiovascular & Medical Sciences

Funding Sources: Chest Heart & Stroke Scotland

British Heart Foundation

National Services Division of the Scottish Executive

Dedication

To Karen

Declaration

The work reported in this thesis was undertaken during my tenure as a Clinical Research Fellow at the Scottish Pulmonary Vascular Unit, Western Infirmary, Glasgow. All of the studies reported herein have either been published or submitted to journals for consideration of publication. A list of these papers and other published abstracts relating to the work reported is included. All of the work reported in this thesis was undertaken by me, with the assistance of a number of colleagues who are formally acknowledged overleaf. All of the statistical analyses herein were performed by me and the manuscript was written solely by me.

Signed

Kevin Blyth, September 2007

Acknowledgements

The work reported in this thesis was performed under the supervision of Professor Andrew Peacock. I am indebted to him for the opportunity to work as a Clinical Research Fellow at the Scottish Pulmonary Vascular Unit (SPVU). His enthusiasm for physiology in general and for pulmonary vascular disease, in particular, was an inspiration throughout my time in the unit. The work in this thesis would have been possible without the staff of the Glasgow Cardiac Magnetic Resonance Unit (GCMRU). Tracey Steedman showed much good humour and patience while guiding me through the subtleties of image acquisition and analysis while the tuition given by Dr. John Foster regarding magnetic resonance theory was invaluable. I am grateful to them both. I must also thank Professor Henry Dargie for the opportunity to join the GCMRU team and for his interest in my research. Dr. David Welsh, who is in charge of basic science research at the SPVU, should have had little interest in my, strictly clinical, research project. Therefore, his constant encouragement, friendship and assistance on matters ranging from publication methods to bike maintenance were appreciated all the more. The work in this thesis was funded by a project grant from Chest, Heart & Stroke Scotland. The MRI scanner at the Western Infirmary was partly funded by the British Heart Foundation. I am indebted to the charity workers of both organisations whose efforts afforded me the luxury of two years of dedicated clinical research. Finally, and most importantly, I must thank the patients with pulmonary hypertension who took part in the studies in this thesis. Their positive attitude and willingness to help, in spite of a devastating illness, was hugely appreciated.

CONTENTS

	<i>Page</i>
Dedication	1
Declaration	2
Acknowledgements	3
Contents	4
List of Figures	12
List of Tables	15
Abbreviations	17
Publications relating to this thesis	20
Presentations and Abstracts	21
Abstract	23
<u>Chapter 1:</u>	<u>Introduction</u>
1.	General introduction 25
1.1	Structure and function of the normal pulmonary circulation 27
1.1.1	Normal pulmonary vascular anatomy 27
1.1.1.1	The pulmonary macrocirculation 28
1.1.1.2	The pulmonary microcirculation 30
1.1.1.2.1	Extra-alveolar vessels 30
1.1.1.2.2	Alveolar vessels 31
1.1.2	Normal pulmonary vascular function 33
1.1.3	Normal regulation of pulmonary haemodynamics 34

1.1.3.1	Passive regulation of pulmonary haemodynamics	34
1.1.3.2	Active regulation of pulmonary haemodynamics	36
1.1.3.2.1	Hypoxic pulmonary vasoconstriction	36
1.1.3.2.2	Neural influences upon pulmonary haemodynamics	37
1.1.3.2.3	Humeral influences upon pulmonary haemodynamics	38
1.1.4	Normal right ventricular structure and function	39
1.1.4.1	Anatomical considerations	39
1.1.4.1.1	The location and shape of the right ventricle	39
1.1.4.1.2	Topography of the right ventricular cavity	42
1.1.4.1.3	The layering and myoarchitecture of the right ventricular wall	43
1.1.4.1.4	The layering and myoarchitecture of the left ventricular wall	45
1.1.4.1.5	Right ventricular blood supply	46
1.1.4.2	Normal right ventricular function	46
1.2	The pulmonary circulation and right ventricle in pulmonary hypertension	47
1.2.1	The aetiology of pulmonary hypertension	47
1.2.2	The pathophysiology of pulmonary arterial hypertension	50
1.2.3	Pulmonary vascular remodelling	51
1.2.3	Right ventricular failure in pulmonary hypertension	52
1.3	Current methods of assessment of the pulmonary circulation and right ventricle	53
1.3.1	Echocardiography	54
1.3.1.1	Detection of pulmonary hypertension	54
1.3.1.2	Quantitative assessment of right ventricular function	55

1.3.2	Right heart catheterisation	56
1.3.3	The six-minute walk test	59
1.3.4	Natriuretic peptides	60
1.3.4.1	Natriuretic peptides and left heart disease	61
1.3.4.2	Natriuretic peptides and Pulmonary Hypertension	62
1.3.5	Summary	63
1.4	Cardiovascular Magnetic Resonance (CMR) imaging	64
1.4.1	Magnetic resonance theory	64
1.4.1.1	Nuclear magnetic resonance fundamentals	64
1.4.1.2	Magnetic fields and magnets	68
1.4.1.3	Radiofrequency pulses and transverse magnetisation	71
1.4.1.4	Relaxation	73
1.4.1.4.1	T1 relaxation	74
1.4.1.4.2	T2 relaxation	79
1.4.1.5	Tissue contrast	82
1.4.1.5.1	T1 contrast	83
1.4.1.5.2	T2 contrast	84
1.4.1.6	Magnetic field gradients and spatial localisation of tissue	88
1.4.1.6.1	Slice-selection gradients	89
1.4.1.6.2	Frequency and phase encoding gradients	91
1.4.1.7	K-space	92
1.4.1.8	Pulse sequences	96
1.4.1.8.1	Gradient echo	96
1.4.1.8.1	Spin Echo	98
1.4.2	Components of a modern CMR scanner	98

1.4.3	Previous use of CMR in patients with PH	102
1.4.3.1	Right ventricular volumes, function and mass	102
1.4.3.2	Contrast enhanced-CMR imaging	103
1.4.3.2.1	Myocardial infarction	105
1.4.3.2.2	Hypertrophic cardiomyopathy	108
1.4.3.2.3	Myocarditis	108
1.4.3.3	Right ventricular stroke volume and Pulmonary Artery Flow Mapping	111
1.4.3.4	Dobutamine stress-CMR imaging	112
1.5	Hypotheses and aims of this thesis	112
<u>Chapter 2:</u>	<u>Materials and Methods</u>	
2.1	Patient recruitment	116
2.2	Routine diagnostic assessment	122
2.2.1	Non-invasive assessment	122
2.2.2	Right heart catheterisation	122
2.3	Cardiovascular Magnetic Resonance imaging	123
2.3.1	Patient preparation and positioning	125
2.3.2	CMR image acquisition	127
2.3.2.1	Standard imaging	127
2.3.2.2	Contrast enhanced-CMR imaging	132
2.3.2.3	Dobutamine stress-CMR imaging	133
2.3.2.3.1	Dobutamine infusion	134
2.3.2.3.2	Stress imaging	135
2.3.2.4	Common problems encountered during CMR imaging	135

2.3.3	Data storage	136
2.3.4	Analysis of Cardiovascular Magnetic Resonance images	136
2.3.4.1	Standard imaging	137
2.3.4.2	Contrast enhanced-CMR imaging	141
2.3.4.3	Dobutamine stress-CMR imaging	144
2.3.4.3.1	Right and left ventricular volumes	144
2.3.4.3.2	Right and left ventricular stroke volume and ejection fraction	144
2.3.4.4	Common problems encountered during CMR image analysis	148

Chapter 3: Definition of an NT-proBNP threshold for the non-invasive detection of RV systolic dysfunction in pulmonary hypertension

3.1	Introduction	150
3.2	Methods	152
3.2.1	Patients	152
3.2.2	Venous blood sampling and measurement of NT-proBNP	154
3.2.3	CMR image acquisition and analysis	154
3.2.4	Clinical assessment and right heart catheterisation	154
3.2.5	Statistical analysis	155
3.3	Results	156
3.3.1	Clinical assessment and right heart catheterisation	156
3.3.2	CMR imaging	157
3.3.3	Correlation analyses	159

3.3.4	Differences in log ₁₀ [NT-proBNP] in subgroups of patients	159
3.3.5	RV systolic dysfunction	159
3.3.6	Diagnostic performance of NT-proBNP	162
3.3.7	Predictors of [NT-proBNP]	162
3.4	Discussion	163
3.4.1	Physiological determinants of NT-proBNP	164
3.4.2	Clinical implications	165
3.4.3	RV ejection fraction	166
3.4.4	NT-proBNP and LV stroke volume	166
3.4.5	Study limitations	167
3.4.6	Conclusion	168

Chapter 4: Contrast enhanced-Cardiovascular Magnetic Resonance imaging in patients with pulmonary hypertension

4.1	Introduction	170
4.2	Methods	171
4.2.1	Patients	171
4.2.2	CMR image acquisition	173
4.2.3	Pre-contrast CMR image analysis	173
4.2.4	Contrast enhanced-CMR image analysis	173
4.2.5	Clinical assessment and right heart catheterisation	173
4.2.6	Statistical Analysis	173
4.3	Results	174
4.3.1	Right heart catheterisation	174
4.3.2	Pre-contrast CMR imaging	175

4.3.3	Contrast enhanced CMR imaging	176
4.4	Discussion	184
4.4.1	Potential mechanisms of contrast enhancement	185
4.4.1.1	Myocardial ischaemia	185
4.4.1.2	Myocardial fibrosis	185
4.4.1.3	Elevated RV afterload	186
4.4.1.4	Mechanical wall stress	187
4.4.1.5	Summary of potential mechanisms of DCE	187
4.4.2	Study Limitations	188
4.4.3	Clinical implications	188
<u>Chapter 5:</u>	<u>Dobutamine stress -Cardiovascular Magnetic Resonance</u>	
	<u>imaging in patients with pulmonary hypertension</u>	
5.1	Introduction	190
5.2	Methods	191
5.2.1	Study participants and clinical assessment	191
5.2.2	Dobutamine stress-CMR imaging	192
5.2.3	Dobutamine stress-CMR image analysis	192
5.2.4	Statistics	192
5.3	Results	193
5.3.1	Clinical characteristics and demographics	193
5.3.2	Symptoms	195
5.3.3	CMR results	195
5.3.3.1	Resting analyses	197
5.3.3.2	Stress analyses	197

5.3.4	Correlates of the right and left ventricular stroke volume response to dobutamine	199
5.4	Discussion	202
5.4.1	Right ventricle	202
5.4.2	Left ventricle	204
5.4.3	Conclusions	207
<u>Chapter 6:</u>	<u>General Discussion and Summary</u>	
6.1	Clinical background	209
6.2	The limitations of the current diagnostic method	210
6.3	The advantages of CMR imaging	210
6.4	Conclusions and future work	212
References		217

List of Figures

<u>Chapter 1</u>	<i>Page</i>	
Figure 1.1	Surface anatomy of the human right ventricle	40
Figure 1.2	Cut-away diagram of the normal right ventricular cavity	41
Figure 1.3	Random natural orientation of hydrogen proton spins	66
Figure 1.4	Precession of protons within a strong magnetic field	67
Figure 1.5	The net magnetisation vector of protons in a strong magnetic field	69
Figure 1.6	Magnetic field orientation (B_0) in a superconducting electromagnet	70
Figure 1.7	Schematic representation of a 90° excitation pulse	72
Figure 1.8	Schematic representation of T1 relaxation	75
Figure 1.9	T1-weighted sagittal image of the lumbar spine	78
Figure 1.10	Schematic representation of T2 relaxation	80
Figure 1.11	Comparative T1- and T2 -weighted images of the brain	86
Figure 1.12	Diagrammatic representation of a slice-selection gradient	90
Figure 1.13	Diagrammatic representation of K-space	94
Figure 1.14	Components of a modern MRI scanner	101
Figure 1.15	An example of sub-endocardial delayed contrast enhancement typical of an acute myocardial infarction	107
Figure 1.16	An example of patchy, mid-wall delayed contrast enhancement typical of hypertrophic cardiomyopathy	109
Figure 1.17	An example of diffuse, mid-wall delayed contrast enhancement typical of acute myocarditis	110

Chapter 2

Figure 2.1	Information sheet and consent form used in recruiting patients	118
Figure 2.2	Description of patient recruitment for the three experiments described in this thesis	121
Figure 2.3	The Siemens Sonata 1.5 Tesla system	124
Figure 2.4	Safety questionnaire	126
Figure 2.5	Typical scout images used to localise the heart within the thoracic cavity during cardiovascular magnetic resonance imaging	128
Figure 2.6	Image 1 of a vertical long axis cine	129
Figure 2.7	Image 1 of a horizontal long axis cine	130
Figure 2.8	Image 1 of a basal short axis cine	131
Figure 2.9	Planimetry analyses of RV volumes and mass	139
Figure 2.10	Analysis of contrast enhanced-cardiovascular magnetic resonance images	142
Figure 2.11	Explanation of the method used to define the spatial boundaries of the RV insertion points in Chapter 4	143
Figure 2.12	Analysis of velocity encoded flow mapping	146

Chapter 3

Figure 3.1	Correlation and diagnostic performance of NT-proBNP measurements compared with CMR measurements of RV systolic function in patients with pulmonary hypertension	161
------------	---	-----

Chapter 4

Figure 4.1	Example of delayed contrast enhancement in a patient with pulmonary hypertension	178
------------	--	-----

Figure 4.2	Correlation between delayed contrast enhancement mass and various right ventricular measurements and invasive pulmonary haemodynamics	181
Figure 4.3	Example of interventricular septal bowing in a patient with pulmonary hypertension	183
<u>Chapter 5</u>		
Figure 5.1	RV stroke volume index measured at rest and during dobutamine stress-CMR imaging	198
Figure 5.2	Correlation between RV stroke volume index and LV end-diastolic volume index at rest and during dobutamine stress-CMR imaging	201

List of Tables

Chapter 1

Table 1.1	Clinical classification of pulmonary hypertension	49
Table 1.2	T1 relaxation times of commonly imaged tissues	76
Table 1.3	T2 relaxation times of commonly imaged tissues	81

Chapter 3

Table 3.1	Results of right heart catheterisation	156
Table 3.2	Ventricular dimensions and function by cardiovascular magnetic resonance imaging in patients and controls	158
Table 3.3	Correlation co-efficients between \log_{10} [NT-proBNP] (ng/l) and measurements acquired during cardiovascular magnetic resonance imaging and right heart catheterisation	160

Chapter 4

Table 4.1	Final diagnoses reached in 25 patients with pulmonary hypertension	171
Table 4.2	Group demographics for patients and control subjects	172
Table 4.3	Results of right heart catheterisation in 25 patients with pulmonary hypertension	175
Table 4.4	Ventricular dimensions and function by cardiovascular magnetic resonance imaging in patients with pulmonary hypertension and control subjects	177

Chapter 5

Table 5.1	Invasive haemodynamic measurements in 16 patients with pulmonary hypertension	194
Table 5.2	Cardiac function at rest and during dobutamine-stress CMR	196

imaging in 16 patients and 6 controls

Table 5.3	Correlates of the effect of dobutamine on right and left ventricular stroke volumes in 16 patients with pulmonary hypertension	200
-----------	--	-----

List of Abbreviations

BSA	Body Surface Area
BNP	B-type Natriuretic Peptide
CI	Cardiac Index
Ce-CMR	Contrast Enhanced- Cardiovascular Magnetic Resonance
CHD	Congenital Heart Disease
CMR	Cardiovascular Magnetic Resonance
CO	Cardiac Output
CPET	Cardiopulmonary Exercise Testing
CT	Computed Tomography
CTD	Connective Tissue Disease
CTEPH	Chronic Thromboembolic Pulmonary Hypertension
CXR	Chest Radiograph
DCE	Delayed Contrast Enhancement
Ds-CMR	Dobutamine Stress- Cardiovascular Magnetic Resonance
ECG	Electrocardiogram
ED	End-Diastole
EDV	End-Diastolic Volume
EDVI	End-Diastolic Volume Index
EF	Ejection Fraction
ES	End-Systole
ESV	End-Systolic Volume
ESVI	End-Systolic Volume Index
FISP	Fast Imaging With Steady State Precession
FoV	Field of View

FLASH	Fast Low Angle Shot
Gd-DTPA	Gadolinium-Diethylene Triaminepentaacetic Acid
HLA	Horizontal Long Axis
HPV	Hypoxic Pulmonary Vasoconstriction
IPAH	Idiopathic Pulmonary Arterial Hypertension
IVS	Interventricular Septum
LV	Left Ventricle/Ventricular
LVEDV	Left Ventricular End-Diastolic Volume
LVEDVI	Left Ventricular End-Diastolic Volume Index
LVEF	Left Ventricular Ejection Fraction
LVESV	Left Ventricular End-Systolic Volume
LVESVI	Left Ventricular End-Systolic Volume Index
LVH	Left Ventricular Hypertrophy
LVM	Left Ventricular Mass
MR	Magnetic Resonance
MRI	Magnetic Resonance Imaging
MVO ₂	Mixed Venous Oxygen Saturation
NT-proBNP	N terminal pro B-type Natriuretic Peptide
NYHA	New York Heart Association
PAH	Pulmonary Arterial Hypertension
PAOP	Pulmonary Artery Occlusion Pressure
PAP	Pulmonary Artery Pressure
PH	Pulmonary Hypertension
PVR	Pulmonary Vascular Resistance
RAP	Right Atrial Pressure

RF	Radiofrequency
ROI	Region of Interest
RV	Right Ventricle/Ventricular
RVEDV	Right Ventricular End-Diastolic Volume
RVEDVI	Right Ventricular End-Diastolic Volume Index
RVEF	Right Ventricular Ejection Fraction
RVESV	Right Ventricular End-Systolic Volume
RVESVI	Right Ventricular End-Systolic Volume Index
RVH	Right Ventricular Hypertrophy
RVIP	Right Ventricular Insertion Point
RVM	Right Ventricular Mass
RVMI	Right Ventricular Mass Index
RVSD	Right Ventricular Systolic Dysfunction
RVSV	Right Ventricular Stroke Volume
RVSVI	Right Ventricular Stroke Volume Index
SA	Short Axis
SSFP	Steady State Free Precession
SV	Stroke Volume
SVI	Stroke Volume Index
T	Tesla
TE	Echo Time
TI	Inversion Time
TR	Repetition Time
VLA	Vertical Long Axis
6MWT	Six Minute Walk Test

Publications Relating To This Thesis

Contrast enhanced-cardiovascular magnetic resonance imaging in patients with pulmonary hypertension

KG Blyth, BA Groenning, TN Martin, JE Foster, PB Mark, HJ Dargie & AJ Peacock
European Heart Journal 2005; (26), 1993-1999

NT-proBNP can be used to detect RV systolic dysfunction in pulmonary hypertension.

KG Blyth, BA Groenning, PB Mark, TN Martin, JE Foster, T Steedman, JJ Morton, HJ Dargie & AJ Peacock
European Respiratory Journal 2007 Apr; 29(4):737-44. Epub Nov 29 2006

Stroke volume responses in pulmonary hypertension assessed by dobutamine-stress cardiovascular MRI

KG Blyth, JE Foster, T Steedman, HJ Dargie & AJ Peacock
Submitted to European Respiratory Journal

Presentations and Abstracts

Brain Natriuretic Peptide levels predict the extent of right ventricular dysfunction, determined by cardiovascular magnetic resonance imaging, in patients presenting with pulmonary hypertension

KG Blyth, BA Groenning, JJ Morton, PB Mark, JE Foster, HJ Dargie & AJ Peacock

Presented to British Thoracic Society, December 2005

Runner-up in BTS/BLF Young Investigators Award

Contrast enhanced-cardiovascular magnetic resonance imaging allows the detection of occult myocardial abnormalities within the interventricular septum of patients with severe pulmonary hypertension

KG Blyth, TN Martin, PB Mark, JE Foster, BA Groenning, HJ Dargie & AJ Peacock

Presented to American Thoracic Society, May 2005

Distensibility of the main pulmonary artery by cardiovascular magnetic resonance imaging predicts pulmonary haemodynamics in patients with severe pulmonary hypertension

KG Blyth, PB Mark, JE Foster, HJ Dargie & AJ Peacock

Presented to American Thoracic Society, May 2005

Contrast enhanced-cardiac magnetic resonance imaging in patients with pre-capillary pulmonary hypertension

KG Blyth, TN Martin, PB Mark, JE Foster, BA Groenning, HJ Dargie & AJ Peacock

Presented to Royal Medico-Chirurgical Society of Glasgow, March 2005

Contrast enhanced-cardiac magnetic resonance imaging provides a novel marker of myocardial injury in patients with severe pulmonary hypertension

KG Blyth, TN Martin, PB Mark, JE Foster, BA Groenning, HJ Dargie & AJ Peacock

Presented to British Thoracic Society, 1 December 2004

Late gadolinium enhancement - a novel marker of myocardial injury in patients with severe pulmonary hypertension

KG Blyth, TN Martin, PB Mark, JE Foster, BA Groenning, HJ Dargie & AJ Peacock

Presented to Scottish Thoracic Society, 19 November 2004

Late gadolinium enhancement (LGE), a marker of myocardial damage, can be detected by contrast enhanced-cardiac magnetic resonance imaging within the right ventricle of patients with severe pulmonary hypertension. The extent of LGE relates to RV performance.

KG Blyth, TN Martin, PB Mark, JE Foster, BA Groenning, HJ Dargie & AJ Peacock

Presented to European Respiratory Society, 6 September 2004

Abstract

Pulmonary Hypertension (PH) is a rare but devastating illness which results in progressive right ventricular (RV) failure and early death. RV function determines survival in all patients with PH but it is difficult to measure accurately using existing clinical techniques. The choice and design of the experiments in this thesis was driven by a desire to improve our understanding of the reasons for right, and left, ventricular dysfunction in this context. Cardiovascular magnetic resonance (CMR) imaging was utilized throughout as it allows the non-invasive, direct and accurate study of both ventricles; at rest and during stress. In Chapter 3, CMR imaging was used to identify an NT-proBNP threshold (1685 ng/l, sensitivity 100%, specificity 94%) for the non-invasive detection of RV systolic dysfunction in patients with PH. In Chapter 4, contrast-enhanced-CMR was utilized for the first time in PH patients and revealed previously unidentified areas of myocardial fibrosis within the RV insertion points and interventricular septum. The extent of these areas correlated inversely with RV ejection fraction ($r = -0.762$, $p < 0.001$). Septal contrast enhancement was particularly associated with bowing of the interventricular septum. Finally, in Chapter 5, dobutamine stress-CMR was used to determine the individual reasons for right and left ventricular stroke volume impairment during exercise in PH patients. Δ RV stroke volume appeared limited by diminished contractile reserve as Δ RVEF was lower in PH patients (27%) compared to controls (38%) and Δ RVEF correlated with Δ RV stroke volume ($r = 0.94$, $p < 0.001$). Δ LV stroke volume appeared limited by impaired filling, probably due to reduced LV preload as RV stroke volume and LV end-diastolic volume remained closely related at rest ($r = 0.821$, $p < 0.001$) and stress ($r = 0.693$, $p = 0.003$).

Chapter 1

Introduction

1. General Introduction

Pulmonary Hypertension (PH) results from a variety of conditions which affect the pulmonary circulation. A progressive rise in pulmonary vascular resistance (PVR) results from obliteration or obstruction of the pulmonary vascular bed. This rise in PVR leads to a rise in pulmonary arterial pressure (PAP) and eventually results in right ventricular (RV) failure and early death in the majority of patients. Prognosis in PH is largely dictated by RV function. Data recorded in the 1980's by the US National Institutes of Health Registry indicate that, without treatment, median survival in Pulmonary Arterial Hypertension is only 2.8 years from diagnosis with equivalent 1-year, 3-year and 5-year survival rates of only 68%, 48% and 34%, respectively. (1)

Nevertheless, the twenty years that have elapsed since the collection of these data have been marked by steady and significant scientific advance. We have seen a complete re-classification of the numerous conditions that result in PH and there has been a sea change in our conception of the processes that mediate vascular remodelling and the development of pulmonary arterial hypertension (PAH). We have moved away from the vasoconstrictive hypothesis originally proposed regarding the origins of PAH and now acknowledge the primarily vasoproliferative origin of this condition. New intracellular therapeutic targets have thus been identified in PAH and other causes of PH. This progress has driven the development of new breed of targeted antiproliferative therapies for the treatment of PAH (e.g. Prostanoids, Endothelin antagonists, and Phosphodiesterase inhibitors) and increasingly, PH associated with other diseases. As a direct result of this progress survival rates in

PAH now approach 90% at 1 year and are over 60 % at 5 years in selected groups (2, 3).

The advent of these new therapies brings with it new challenges for physicians managing patients with this heterogeneous group of conditions. The pulmonary circulation is largely hidden from clinical examination and conventional imaging technologies. As a result the acquisition of accurate measurements within it has always been difficult and fraught with error. Even now, at the dawn of the twenty-first century, physicians remain reliant for an assessment right ventricular function, which is the principal determinant of survival in PH patients, upon techniques that are either prohibitively invasive, as is the case with right heart catheterisation or technically flawed, albeit non-invasive, in the case of transthoracic echocardiography. The need for an accurate diagnostic method with which to identify, and accurately document, prognostically significant RV dysfunction in PH patients has, therefore, never been greater. In addition, our understanding of the reasons for RV failure in PH remains incomplete. Novel approaches to filling this gap in our knowledge base are essential. Furthermore, considerable importance has been placed, by both expert clinician bodies and organisations asked to fund clinical research trials, upon the development of novel imaging technologies and new techniques which provide a more accurate and less invasive assessment of the pulmonary circulation in patients with PH.

Over the last decade Cardiovascular Magnetic Resonance (CMR) imaging has become accepted as the gold standard technique for the assessment of the proximal pulmonary circulation and the morphology and function of the right ventricle. CMR

technology offers tremendous further potential as a non-invasive, multiplanar method capable of providing a more complete assessment of the right ventricle in PH patients than that currently available.

The general aim of this thesis is to generate new and clinically relevant information regarding RV function in PH using CMR imaging. The premise on which this aim is based is RV function dominates prognosis in patients with PH and that a better means of detecting, measuring and understanding RV function in PH might result in an improved outcome for patients. Before contemplating the diseased pulmonary circulation in PH a review of the structure and function of the normal pulmonary circulation and right ventricle is appropriate.

1.1. Structure and function of the normal pulmonary circulation

1.1.1 Normal pulmonary vascular anatomy

Unlike the systemic vasculature, which is optimised to maintain oxygen delivery to the tissues, the pulmonary circulation is designed to facilitate gas exchange with the environment. It must be able to function under a variety of conditions and adjust rapidly to changes in ambient atmospheric and haemodynamic pressure. In terms of both anatomical structure and physiological function, the pulmonary circulation is supremely adapted to meet these demands. The vessels of the human pulmonary circulation, like those within the systemic circulation, are comprised of an intima, a media and an adventitia. In the normal pulmonary circulation a single sheet of endothelial cells constitutes the intimal layer, outside of which lies a medial layer of

smooth muscle cells which thins and eventually disappears from normal arteries beyond the level of the respiratory bronchioles. Internal and external elastic lamina envelop this medial smooth muscle layer, outside of which lies an adventitia comprised of a protein matrix secreted by resident fibroblasts. The adventitial layer of the pulmonary circulation, like the media, thins and disappears from pulmonary arteries as they subdivide and coalesce to form the dense pulmonary capillary network.

In comparison with equivalently sized systemic vessels, the medial layer of smooth muscle cells within vessels of the pulmonary circulation is significantly thinner for any given calibre of vessel examined, e.g. the wall of a healthy main pulmonary artery is up to 30% thinner than that of a healthy ascending aorta. This relative amuscularity reflects the lower pressures normally prevalent within the lung circulation.

1.1.1.1 The pulmonary macrocirculation

Following ejection from the right ventricle, the structure and function of which is discussed in detail in Section 1.1.4, mixed venous blood crosses the pulmonary (semi-lunar) valve and enters the main pulmonary artery (or pulmonary trunk). After around 5 cm of travel this vessel bifurcates to form right and left pulmonary arteries (RPA and LPA). The RPA travels horizontally behind the ascending aorta to the root of the right lung. It then further sub-divides into two branches; the smaller upper branch accompanies the right upper lobe bronchus and subdivides within this area of lung. The larger, lower branch of the RPA accompanies Bronchus Intermedius and delivers mixed venous blood for saturation within the middle and lower lobes of the right lung.

The left main pulmonary artery runs horizontally in front of the descending aorta and on reaching the left hilum undergoes similar bifurcation with the upper branch supplying the left upper lobe and the lower branching providing desaturated blood to the left lower lobe.

Unlike the systemic circulation in which the subsequent branching of the vasculature can be summarised by subdivision into large conducting arteries, arterioles, capillaries, venules and veins, the pulmonary arterial tree branches in a manner which appears more unfamiliar to the non-specialist. Arterioles and venules do not exist in the pulmonary vascular bed. Instead unique transitional vessels transmit blood between conducting pulmonary arteries and alveolar capillaries. These transitional pulmonary vessels are termed 'pre-capillary arteries' and 'post-capillary veins'.

Large conducting pulmonary arteries enter the wedge shaped units of the lung parenchyma (either lobules or acini) associated with a bronchus/bronchiole and surrounded by a loose connective tissue sheath. The fibrous insertion points of the alveolar septae, which constitute the crucial, gas exchanging portions of the lung parenchyma, insert radially into this connective tissue sheath. This arrangement is crucial to gas exchange function within the normal pulmonary circulation and will be discussed later.

Following transmission into the lung parenchyma, the conducting pulmonary arteries, which whilst they run alongside a bronchiole are termed 'axial' spawn subjugate 'supernumerary' arteries at apparently random intervals and angles. These 'supernumerary' arteries far outnumber their axial progenitors. Supernumerary

arteries, instead of remaining alongside their parent bronchioles penetrate directly into the adjacent alveolar parenchyma, subdividing further into smaller arteries and eventually entering the alveolar capillary network which surrounds the alveoli.

This supernumerary branching pattern means that a single lobule or acinus, although oxygenated by the bronchus or bronchiole at its apex, is not necessarily perfused solely by blood within the conducting pulmonary artery that enters its own apex. Instead each wedge shaped unit can be partly perfused by supernumerary branches of the conducting pulmonary arteries which originally perfused one or more of several adjacent sections of lung parenchyma. No pulmonary artery (whether axial or supernumerary) is ever exposed directly to atmospheric (or alveolar) air pressures, and all are surrounded by the thin connective tissue sheath alluded to earlier. These vessels (which include both the arteries and accompanying veins) are unique to the lung in their configurations and are termed the 'extra-alveolar vessels' (4).

1.1.1.2 The pulmonary microcirculation

1.1.1.2.1 Extra-alveolar vessels

The term 'extra-alveolar vessels' was first coined in 1961 by Howell and describes all of the arteries and veins within the pulmonary circulation that are surrounded by a connective tissue sheath (4). Larger, axial, vessels share their connective tissue sheath with a bronchus, whilst smaller, supernumerary, vessels have a sheath of their own.

As described previously, this connective tissue sheath not only transmits the pulmonary arteries, veins and lymphatics into the lung parenchyma, it also accepts the radially arranged fibrous insertion points of the alveolar septae. It is now accepted that this fibrous sheath constitutes a 'fibrous continuum' that extends from each lung hilum to the corresponding parietal pleural surface, surrounding all extra-alveolar vessels and bronchi in between (5). It has been demonstrated previously that the interstitial pressure within this connective tissue sheath is sub-atmospheric, or 'negative' (6). It has also been established that this pressure becomes 'more negative' with increasing chest wall expansion as the fibrous mesh transmits the expansive forces generated across the thoracic cage during inspiration. The radial arrangement of the insertion points of the alveolar septae into the connective tissue sheath ensures that these forces result in an increase in extra-alveolar vessel diameter and length during inspiration. This configuration facilitates maximal capillary blood flow during inspiration.

1.1.1.2.2 Alveolar vessels

At the termination of the conducting bronchioles, both air and blood (within the accompanying, terminal, axial arteries) enters the (alveolar) gas exchange parenchyma. Air is transmitted along the alveolar ducts which are lined by alveolar septae. These organs constitute the primary gas exchange apparatus of the lung. Blood capillaries constitute over 90% of the substance of these septae. The accompanying terminal axial arteries undergo further final subdivision and join the alveolar capillary network within the alveolar septae. There, blood from the axial arteries is mixed with blood from supernumerary vessels which have already been

assimilated into this dense capillary network. At this point, alveolar air and pulmonary capillary blood are separated by an extremely thin membrane, which at its minimum is comprised of a single vascular endothelial cell, an associated alveolar epithelial cell with a fused basement membrane in between. It is across this membrane that gas exchange can occur.

‘Corner vessels’ are unique amongst the alveolar capillaries. Due to their anatomical location, at the corners of each alveolus, they alone are able to withstand increases in alveolar air pressure, e.g. during inspiration. Other alveolar vessels, residing within the walls of the alveolar septae are forced to collapse under these conditions. The corner vessels thus provide the sole constant mechanism for gas-exchange within the lung, even in the face of high alveolar air pressures. Serial microsectioning of these corner vessels has demonstrated that they are perfused on one side by a pre-capillary artery and drained on the other by a post-capillary vein (7). They therefore also provide a rapid and efficient gas exchange ‘short-cut’ between the right and left sides of the pulmonary circulation when the rest of the pulmonary vascular bed is collapsed, e.g. within the lungs of a ventilated patient using high Positive End-Expiratory Pressure (PEEP) settings. This concept is discussed in more detail in section 1.1.3.1, entitled ‘Passive regulation of pulmonary haemodynamics’.

Unlike the systemic circulation, in which the terminal, perfusing capillary bed is formed by the final branching of an arteriole and then drained by reconstitution of the capillaries to form a venule, the pulmonary capillary bed forms a seemingly chaotic network of intertwining capillaries with no obvious beginning or end. This configuration has prompted much debate as to the exact nature and pattern of blood

flow within the pulmonary vascular bed. Weibel argues that this blood flow is governed by the tubular shape of the pulmonary arteries and capillaries and so PVR can be computed by Poiseuille's law (8). In contrast, Fung and Sobin have proposed an alternative model suggesting lamellar (sheet-like) flow between fibrous 'posts' within the hexagonal capillary network mesh (9-11). Others have suggested that both flow conditions may co-exist depending on the prevailing atmospheric and haemodynamic conditions (12).

1.1.2 Normal pulmonary vascular function

The anatomical configuration of the pulmonary circulation described above provides much of the apparatus necessary for normal pulmonary function and efficient gas exchange. In health, the pulmonary circulation is a compliant, high flow, low resistance system. Unlike the systemic circulation the pulmonary circulation is nearly maximally vasodilated at rest. Healthy pulmonary arteries exhibit very low basal smooth muscle tone and normal PVR is approximately one-fifteenth of normal systemic vascular resistance (13). This allows the pulmonary circulation to accommodate the entire cardiac output, which flows through the lungs at pressures far lower than those seen in the systemic circulation. These low pressures prevent fluid migrating into the interstitial space, optimizing the conditions for gas exchange and allowing the RV to operate at minimum energy cost (14).

1.1.3 *Normal regulation of pulmonary haemodynamics*

1.1.3.1 *Passive regulation of pulmonary haemodynamics*

Pulmonary blood flow is greater in the dependant regions of the lung; the upright human lung is approximately 30 cm in height and so the influence of gravity cannot be underestimated. Gravity-dependant relationships between the transmural pressures of air, arterial blood and venous blood exert tremendous influence over the shape, and therefore, the function of the alveolar septae and the microvasculature they contain.

These three determinants of the net transmural alveolar pressure are present in various combinations depending on the location of an individual alveolus within the upright lung. These combinations have been reproduced in the laboratory and, following fixation of the vasculature, used by West to describe the three 'zones' within the upright human lung (15).

Zone 1 Alveolar air pressure is higher than both arterial and venous pressures

Upper zones of the upright lung

Zone 2 Arterial pressure is highest, followed by alveolar air pressure. Venous pressure is lowest.

Mid- zones of the upright lung

Zone 3 Both arterial and venous pressures are higher than alveolar air pressure

Lower zones of the upright lung

In Zone 1 high alveolar air pressure produces perfectly smooth alveolar septal surfaces with collapse of all but the corner capillary vessels. This configuration

rarely, if ever, exists *in vivo* except in the very apices of the lung and perhaps in the setting of profound hypovolaemia. Although Zone 1 conditions are detrimental to gas exchange, it has been demonstrated previously that the corner vessels, which are the sole capillaries open within this environment remain capable of maintaining gas exchange.

Zone 2 conditions are commonly encountered throughout the lungs of patients ventilated mechanically using high PEEP settings. As in zone 1 the relatively high alveolar pressures cause collapse of many of the septal capillaries. Those that remain open appear as slit-like vessels although, as in Zone 1, the majority of capillary blood flow is through corner vessels (or corner pleats, which are formed by infoldings of the alveolar wall where at least three alveolar septae, containing open corner vessels, meet). Although these conditions would, again, appear to compromise gas exchange, the corner pleats perform extremely efficiently in this regard.

Under Zone 3 conditions the optimum conditions for gas exchange exist. The relatively low alveolar air pressure allows distension and engorgement of the majority of the alveolar septal capillaries. Assuming alveolar ventilation is adequate and well distributed avid gas exchange across this huge surface area will be possible.

This zonal model of gas exchange function is clearly not strictly geographical or anatomical. Instead, West's model provides a useful basis for discussions regarding pulmonary circulation function under various environmental and haemodynamic conditions. In addition to these powerful 'passive' regulatory mechanisms which are

endowed upon the pulmonary circulation through its unique configuration, additional 'active' regulatory mechanisms also exist.

1.1.3.2 Active regulation of pulmonary haemodynamics

In healthy individuals, the active regulation of the pulmonary circulation is far less important than the passive mechanisms discussed in the previous section. Neuro-humeral factors play a fairly minor role in control of the healthy pulmonary circulation; however, Hypoxic Pulmonary Vasoconstriction (HPV) remains a powerful and important influence upon pulmonary haemodynamics under the appropriate conditions.

1.1.3.2.1 Hypoxic pulmonary vasoconstriction

The systemic and pulmonary circulations differ diametrically in their response to hypoxia. Whilst the systemic vasculature vasodilates in an attempt to maintain local tissue oxygenation the pulmonary circulation vasoconstricts. HPV is initiated by an unidentified oxygen sensor, which is probably located in the airways and is effected by shortening of the smooth muscle cells within the small (200-600 μm diameter) pulmonary arteries in the precapillary circulation. HPV is triggered within two minutes of a fall in inspired alveolar oxygen concentration below a threshold of around 10%. This reflex diverts deoxygenated blood away from under- or un-ventilated alveoli in an attempt to maintain ventilation/perfusion (V/Q) matching and arterial oxygen saturation.

The HPV reflex was first described by Bradford and Dean in the 1890's and more completely defined by von Euler and Liljestrand in the cat in 1946 (16). This reflex is found in all mammalian species although its intensity varies between species and individuals. The components and intracellular pathways which mediate HPV have been the subject of much research over recent years. Although significant progress has been made in animal models, the exact nature of the human HPV response is not yet fully understood. It is known that hypoxia causes an increase in both the influx and intracellular generation of calcium within pulmonary artery smooth muscle cells probably signalling through altered intracellular potassium channels (e.g. $K_{V2.1}$ and $K_{V1.5}$ which have been identified in rat pulmonary arteries).

HPV is most effective in response to localised V/Q mismatch when it can preserve arterial oxygen saturation without any rise in PAP. However, in the context of widespread V/Q mismatch or persistent inspired alveolar hypoxia, HPV results in the PH associated with Chronic Hypoxic Lung Disease and continuous residence at high altitude, respectively.

1.1.3.2.2 Neural influences upon pulmonary haemodynamics

Although the pulmonary circulation is suffused with both adrenergic and cholinergic nerve endings, this innervation is predominantly proximal and is not thought to be of great significance in the control of normal pulmonary vascular function. Adrenergic pathways have been shown to produce both vasodilatation (β agonists) and vasoconstriction (α agonists) depending on the receptor subtypes stimulated. Stimulation of the sympathetic nervous system has been shown to produce both

vasodilatation and vasoconstriction, whilst the parasympathetic nervous system appears to have no significant effect on the healthy pulmonary circulation.

1.1.3.2.3. Humeral influences upon pulmonary haemodynamics

Various circulating and endothelium derived-humeral factors have been shown to influence both the healthy and the diseased pulmonary circulation. Nitric Oxide and Prostacyclin, both derived from endothelial cells, have both been shown to consistently cause pulmonary vasodilatation and to inhibit cell replication and growth within the pulmonary circulation. In contrast, Thromboxane A₂ and Endothelin-1 which again are derived from the endothelium are potent constricting agents and growth factors. Disregulation of the production of these endothelium derived humeral factors appears central to the pathogenesis of various pulmonary vascular disorders including Pulmonary Arterial Hypertension. A large number of other mediators, e.g. histamine, serotonin, angiotensin II, acetylcholine have been shown to affect pulmonary vascular tone although none of these have shown consistent haemodynamic effects.

1.1.4 *Normal right ventricular structure and function*

1.1.4.1 *Anatomical considerations*

1.1.4.1.1 *The location and shape of the right ventricle*

The term ‘right ventricle’ is really a misnomer. The ‘rightness’ of the RV reflects the natural orientation of the explanted heart as it lies on the dissection table. In this position the RV, which is more accurately termed the anterior, or pulmonary, ventricle, lies on the operator’s right with the interventricular septum (IVS) in the midline and the cardiac apex pointing away. In the normally connected *in vivo* human heart the RV is an anterior structure lying almost in the midline.

The shape of the human RV is complex and has been likened to a truncated ellipsoid pyramid, draped around the cylindrical left ventricle (LV). The left posterior and left lateral borders of the RV cavity are therefore concave and formed by the IVS, whilst the tricuspid (or atrioventricular) valve plane forms the right posterior border. The basal surface of the RV lies upon the right hemi-diaphragm over the left lobe of the liver whilst the convex antero-superior surface, often termed the RV ‘free wall’ extends from right atrium to the apex and forms a large part of the sterno-costal surface of the heart. The upper left corner of the RV, as it resides in the chest, forms a conical pouch termed the *Infundibulum* (or *Conus Arteriosus*) from which the main pulmonary artery arises (see figure 1.1, overleaf).

Figure 1.1

Surface anatomy of the human RV as it lies in the thoracic cavity. Reproduced from the 20th edition of Gray's Anatomy of the Human Body, originally published in 1918 (copyright expired).

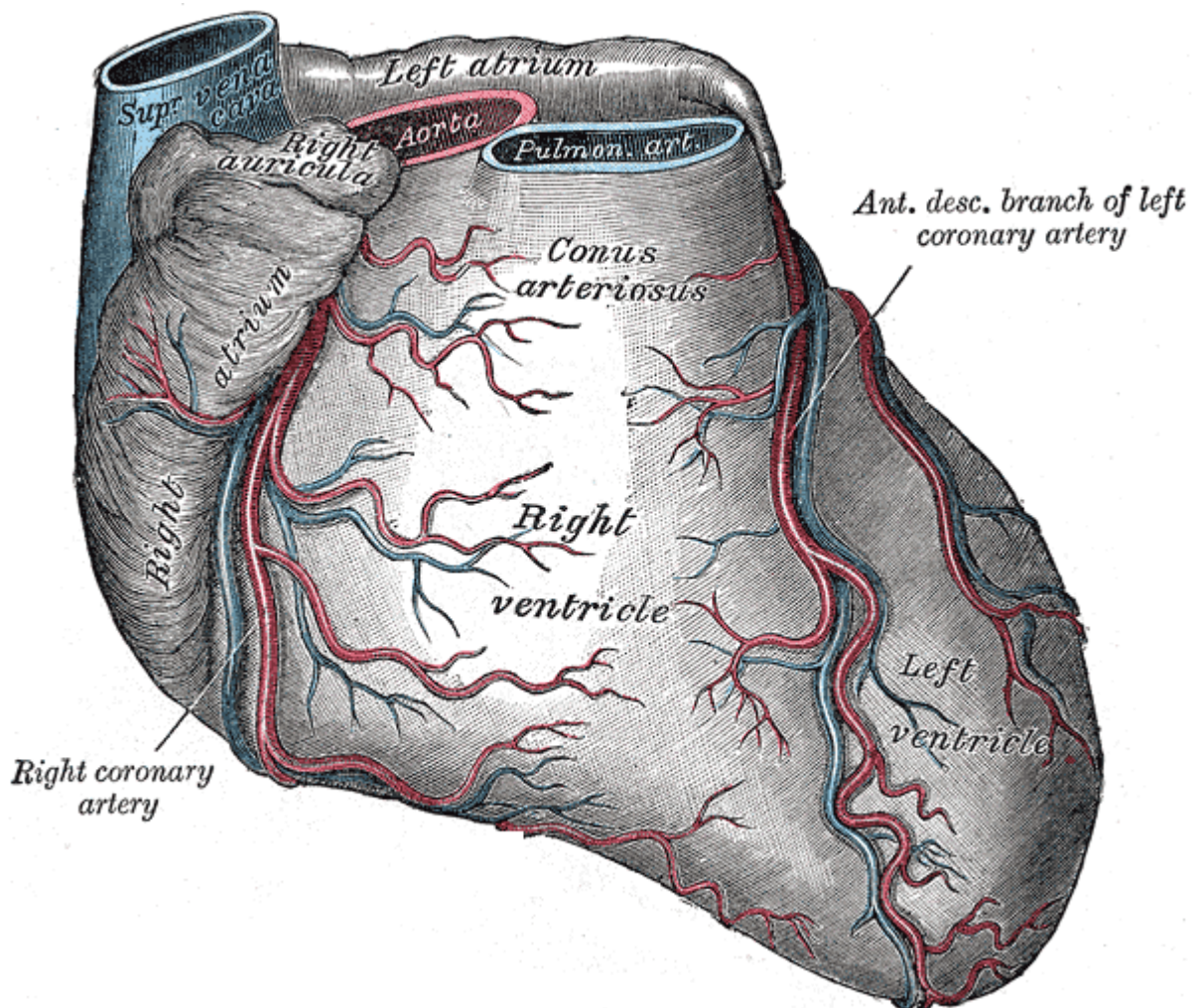
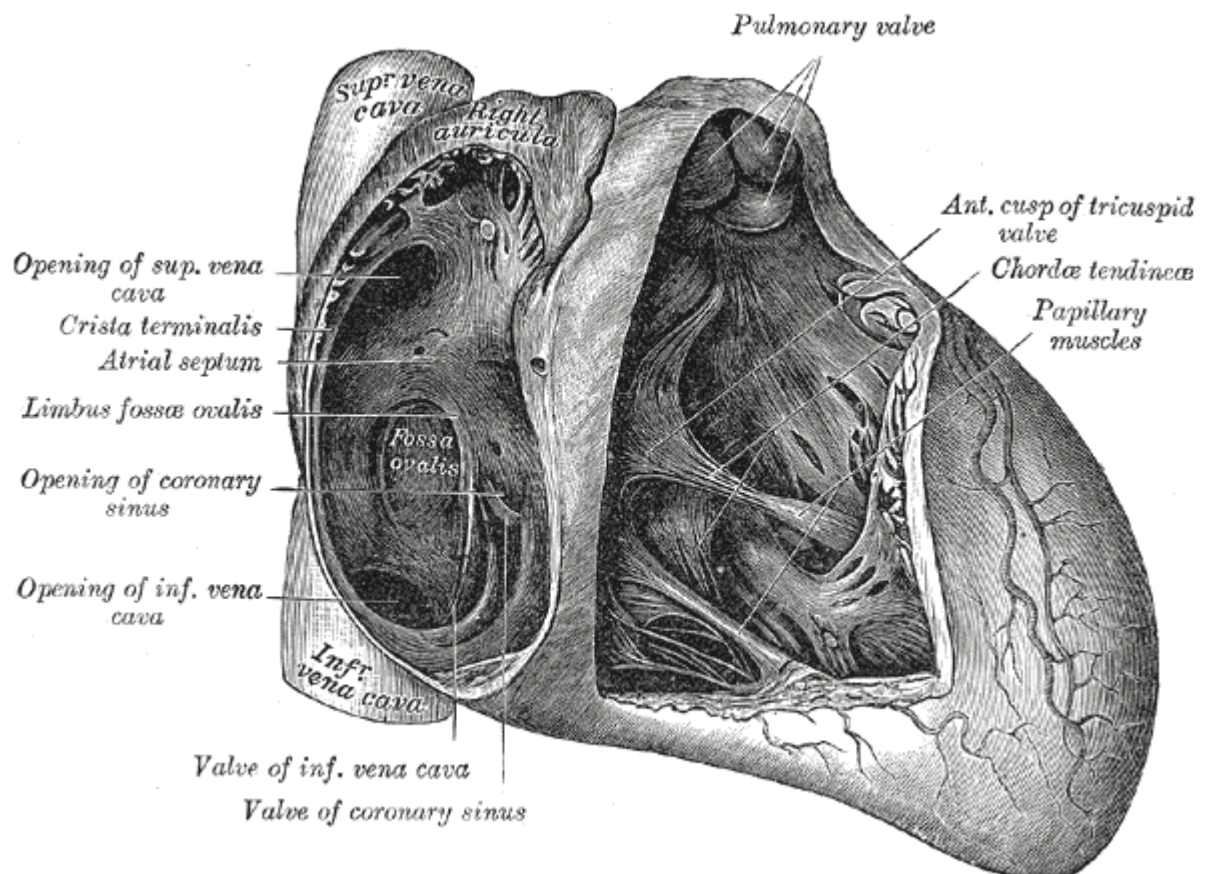


Figure 1.2

Cut-away diagram of the normal RV cavity. The RV outflow tract lies immediately inferior to the pulmonary valve. The moderator band is visible, but not labelled, at the bottom right of the RV cavity which it crosses to attach to the RV free wall (cut away). Reproduced from the 20th edition of Gray's Anatomy of the Human Body, originally published in 1918 (copyright expired).



1.1.4.1.2 *Topography of the right ventricular cavity*

The RV cavity is, by convention, divided into inlet and outlet (or sinus) portions separated by the supraventricular ridge (see figure 1.1 on page 40). The inlet portion of the RV is comprised of the tricuspid valve, the papillary muscles and their associated chordae tendinae, and the coarsely trabeculated myocardium that supports the tricuspid valve. The well defined muscle bands of the supraventricular ridge form an almost circular orifice separating this inlet portion of the RV from the contiguous outlet (or outflow) tract. Note: the RV outflow tract is sometimes referred to as the *Infundibulum* or the *Conus Arteriosus* (as it is in Figure 1.1). While the term *Infundibulum* more specifically refers to the muscular component of the RV that surrounds the outflow tract the terms, *Infundibulum* and RV outflow tract are often used inter-changeably. *Conus Arteriosus* is a term generally now confined to anatomy text books although it describes the same structure as *Infundibulum*.

The RV outflow tract is unique in that it is the only component of the RV cavity that has a smooth endocardial surface. It runs superiorly from the tricuspid valve plane to the pulmonary valve which lies at its summit. It is visible, but not labelled, immediately inferior to the pulmonary valve on figure 1.2 (page 41). The endocardial surface of the remainder of the RV cavity is coarsely trabeculated. These trabeculations appear straighter and fewer in number than those found within the LV cavity; some are simple ridges, others are more developed and although fixed at their ends, free in the middle. A further population of trabeculae are more heavily muscled and collectively form the papillary muscles, supporting the three leaflets of the tricuspid valve. The papillary muscles of the RV are more complex in there

arrangement than those supporting the mitral valve in the LV (17). A single large anterior papillary muscle arises from the RV free wall. In addition, multiple smaller papillary muscles attach partly to the postero-inferior RV free wall and partly to the septum and a further group of smaller papillary muscles arise from the interventricular septum. The uppermost of these septal papillary muscles is called the medial (conal) papillary muscle, also described as the Muscle of Lancisi or the Muscle of Luschka. Again these structures are visible in Figure 1.2 in which they are labelled simply as the papillary muscles. The septomarginal trabeculation is a particularly well developed trabeculation that extends apically along the interventricular septum from the Supraventricular Ridge. Just before this structure meets the RV free wall at the RV apex, a prominent ridge of muscle extends from it and crossed the RV cavity to meet the approaching RV free wall. This structure may assist in preventing over-distension of the RV, hence its name; the Moderator Band. The moderator band is visible, but not labelled at the bottom right corner of the RV cavity in figure 1.2.

1.1.4.1.3 The layering and myoarchitecture of the right ventricular wall

The human heart is supported by a flexible, fibrous skeleton fixed around the two atrioventricular (tricuspid and mitral) and the two arterial (pulmonary and aortic) valve orifices. Myocardial muscle fibres from all four cardiac chambers attach into this skeletal frame in a fashion that facilitates coordinated chamber and valve function.

Within the LV of the human heart a characteristic pattern of subepicardial (or superficial), middle and subendocardial (or deep) muscle layers can be identified.

This is in contrast to the RV in which only two identifiable muscle layers exist, a superficial layer and a deep layer (18, 19). Whether within the LV or the RV these muscles layers are not separated by myofascial planes but are instead defined by changes in the orientation of their constituent fibres. These orientations are, by convention, described relative to the plane of the atrioventricular grooves. Therefore, circumferential fibres run parallel to the atrioventricular grooves whilst longitudinal fibres run perpendicular to this plane. Oblique muscle fibres run in a direction interposed between these two axes (18).

The myocardial muscle fibres of the superficial (subepicardial) layer of the RV are anchored to the fibroskeleton of the heart around the tricuspid valve ring. These superficial fibres run obliquely from the base of the heart towards the apex. Some cross the anterior and posterior interventricular sulci on the sternocostal and diaphragmatic surfaces of the heart and merge with LV superficial fibres running longitudinally from around the mitral valve ring. On approaching the cardiac apex these superficial fibres, from both left and right ventricles, wind into tight vortices (one on the left and one on the right). These vortices eventually invaginate at the cardiac apex.

The wound fibres of this superficial layer, tucked in at the right and left cardiac vortices at the apex of the heart then give rise to the fibres of the deep (subendocardial) muscle layer of the RV and LV respectively. The deep fibres of the RV run longitudinally back towards the atrioventricular and pulmonary valve anulli and the papillary muscles, into which they insert and are anchored to. A significant component of the deep muscle layer of the RV also arises from the invagination of

some superficial fibres at the anterior and posterior interventricular sulci. These fibres form the right hand side of the interventricular septum before continuing basally. They ultimately become fixed to similar endocardial structures as those fibres that originated at the cardiac apex.

The fibres within the deepest of this deep RV layer are arranged in sheets that loop around both cardiac ventricles. This arrangement of the deep fibres and in particular the anchoring of these fibres to key structural elements within the heart is believed to facilitate normal synchronised ventricular function and coordinated atrio-ventricular valve closure in the normal human heart.

1.1.4.1.4 The layering and myoarchitecture of the left ventricular wall

As indicated earlier the LV, which includes the interventricular septum, contains an additional, middle, layer of muscle fibres. These fibres are arranged circumferentially and have no specific points of origin, termination or anchorage. The middle layer of the LV has been shown to be preferentially thickened in patients with systemic hypertension (20) and in those with congenital heart disease (19). Within the LV the superficial and deep muscle layers are arranged in a similar fashion to those within the RV, however, the superficial fibres of the LV must penetrate the middle, circumferential, layer to reach and become confluent with the deep muscle layer.

1.1.4.1.4. Right ventricular blood supply

In general, the Right Coronary Artery (RCA) supplies the RV myocardium. The sino-atrial node branch supplies the sino-atrial node in the RA, whilst other marginal branches of the RCA supply the RV free-wall. Inevitably there is some variability in this arrangement in humans, for example, in approximately 10% of individuals, branches of the circumflex artery, arising from the Left Coronary Artery (LCA), supply the posterior RV wall (21). In the majority of individuals the interventricular septum is supplied predominantly by four to six perpendicular branches of the Left Anterior Descending Artery, arising from the LCA. Detailed histopathological studies have however demonstrated a considerable contribution to septal blood supply, particularly within the postero-inferior portions of the septum from perpendicular branches of the Posterior Descending Artery (PDA) (21). In 85 % of individuals this vessel arises from the RCA (a right dominant coronary circulation) whilst in the remaining 15% the PDA arises from the Left Coronary Artery (LCA) (a left dominant coronary circulation). In this latter 15 % of individuals the interventricular septum will therefore receive almost all its blood supply from the left coronary circulation.

1.1.4.2 Normal right ventricular function

The RV under normal circumstances is a low pressure volume pump that moves desaturated blood out across the pulmonary valve into the pulmonary circulation. Desaturated blood returns from the systemic circulation via the vena cavae and the RA, finally crossing the tricuspid valve and entering the inlet portion of the RV

cavity. The normal RV ejects an equivalent volume of blood per contraction as the left ventricle (LV). Since resting pulmonary vascular resistance (PVR) is, however, only one-fifteenth of normal systemic vascular resistance the RV is able to operate at a far lower energy cost than the LV, per contraction. The low pressure environment within the pulmonary circulation is advantageous in that it prevents fluid migrating into the interstitial space and so provides optimal conditions for gas exchange. These low pressures do however make the pulmonary circulation in general, and the thin-walled RV in particular, poorly adapted to cope with rapid changes in pulmonary vascular resistance and rising pulmonary artery pressures (14).

1.2 The pulmonary circulation and right ventricle in Pulmonary Hypertension

1.2.1 The aetiology of pulmonary hypertension

The term ‘Pulmonary Hypertension’ describes a syndrome characterised haemodynamically by elevated PVR and PAP, and clinically by complaints of breathlessness, fatigue, chest pain and ankle swelling. The detection of Pulmonary Hypertension (PH) is therefore, in itself, not an adequate diagnosis as the syndrome can be caused by a variety of diseases which vary not only in origin but also in response to treatment and prognosis.

Following the 2nd WHO symposium on PH in Evian, France in 1998, a new classification of the diseases known to cause PH was proposed. This re-classification sought to classify diseases on the basis of the pathophysiological phenotype expressed

in each condition; as a result the preceding arbitrary division of the causes of PH into ‘primary’ and ‘secondary’ phenomena was discarded. It was hoped that this new classification would encourage the development of therapies targeted more specifically at the implicated and often common biological abnormalities. In addition the Evian classification aimed to allow the standardisation of diagnostic methods and facilitate more meaningful communication about individual patients between centres. The Evian classification was endorsed and updated at the 3rd world symposium held in Venice in 2003 and is presented in Table 1.1, overleaf.

Table 1.1 Clinical classification of Pulmonary Hypertension (Venice 2003)

1. Pulmonary arterial hypertension (PAH)

- 1.1. Idiopathic (IPAH)
- 1.2. Familial (FPAH)
- 1.3. Associated with (APAH):
 - 1.3.1. Connective tissue disease
 - 1.3.2. Congenital systemic to pulmonary shunts
 - 1.3.3. Portal hypertension
 - 1.3.4. HIV infection
 - 1.3.5. Drugs and toxins
 - 1.3.6. Others, e.g. thyroid disorders, glycogen storage disease, HHT, splenectomy
- 1.4. Associated with significant venous or capillary involvement
 - 1.4.1. Pulmonary veno-occlusive disease (PVOD)
 - 1.4.2. Pulmonary capillary haemangiomatosis (PCH)
- 1.5. Persistent pulmonary hypertension of the newborn (PPHN)

2. Pulmonary hypertension associated with left heart diseases

- 2.1. Left-sided atrial or ventricular heart disease
- 2.2. Left-sided valvular heart disease

3. Pulmonary hypertension associated with lung respiratory diseases and/or hypoxia

- 3.1. Chronic obstructive pulmonary disease
- 3.2. Interstitial lung disease
- 3.3. Sleep disordered breathing
- 3.4. Alveolar hypoventilation disorders
- 3.5. Chronic exposure to high altitude
- 3.6. Developmental abnormalities

4. Pulmonary hypertension due to chronic thrombotic and/or embolic disease

- 4.1. Thromboembolic obstruction of proximal pulmonary arteries
- 4.2. Thromboembolic obstruction of distal pulmonary arteries
- 4.3. Non-thrombotic pulmonary embolism, e.g. tumour, parasites, foreign material

5. Miscellaneous

Sarcoidosis, histiocytosis X, lymphangiomatosis, compression of pulmonary vessels

1.2.2 *The pathophysiology of Pulmonary Arterial Hypertension*

The unique functional configuration of the pulmonary circulation is maintained by a fine balance of locally synthesised and rapidly active modulators of cellular growth and pulmonary vascular smooth muscle tone. This balance maintains the microcellular structure of the vessels in the pulmonary circulation and is necessary to facilitate rapid responses to changes in atmospheric, haemodynamic or ventilatory conditions. However, this balance is disrupted in Pulmonary Arterial Hypertension (PAH), in which, aberrant intracellular signalling and functional abnormalities have been demonstrated within all three layers of the vascular wall. PAH is considered the prototype for the majority of primary disorders affecting the pulmonary vasculature including Idiopathic PAH (previously termed Primary Pulmonary Hypertension) and PAH associated with various conditions including connective tissue diseases, HIV infection and congenital systemic-to-pulmonary shunts. These intracellular abnormalities include:

1. Endothelial cell dysfunction (22-25) within the intima
2. Increased expression of 5-hydroxytryptamine transporter proteins (26, 27) and abnormal voltage-dependant potassium channels (28, 29) within pulmonary artery smooth muscle cells (PASMCs)
3. Abnormalities of adventitial metalloproteases and serine elastases (30-32)

1.2.3 *Pulmonary vascular remodelling*

Current evidence suggests that these aberrant intracellular processes, in combination, promote cellular proliferation and vasoconstriction and result in the typical histopathological abnormalities seen in PAH. These changes, often summarised by the term ‘vascular remodelling’, are characterised by the obliteration of pulmonary arterioles by intimal fibrosis, often with associated in-situ thrombosis and hypertrophy of the medial smooth muscle cells and adventitial fibroblasts. The classic ‘plexiform’ lesion is seen in up to two-thirds of patients with PAH (33, 34). This ominous mass of tangled vessels, endothelial cells and fibroblasts has been demonstrated in patients with idiopathic PAH (33, 34), PAH associated with scleroderma (35) and in PH secondary to congenital heart disease (34) and chronic thromboembolism (36). It has been demonstrated recently that endothelial cell proliferation within plexiform lesions is monoclonal in Idiopathic PAH but polyclonal in PH secondary to other causes (37). Plexiform arteriopathy is thought to represent an angiogenic response to local tissue ischaemia and/or hypoxia, occurring as a result of proximal vascular obstruction (38). Several authors have observed that the earliest stages of PH are characterised pathologically by medial hypertrophy alone (33, 34, 39), without plexiform arteriopathy, which would be in keeping with this hypothesis.

Our greater understanding of the intracellular mechanisms underlying vascular remodelling and recognition of the vasoproliferative origins of PAH has prompted development of the current, growing breed of anti-proliferative or ‘de-remodelling’ therapies. Despite the progress that has been made over the last decade, the triggers involved in the initiation and perpetuation of these complex remodelling processes are

not yet fully understood. Genetic (40, 41), haematological (42), inflammatory (43) and numerous other potential mechanisms have been implicated, and it appears likely that the underlying aetiology is multifactorial, perhaps involving a ‘second-hit’ upon a genetically susceptible individual.

1.2.4 Right ventricular failure in PH

As alluded to in the General Introduction, RV function is the principal haemodynamic determinant of survival in PH of all aetiologies. Of the numerous physiological variables that have prognostic significance in PH patients the vast majority are direct correlates of RV performance. These include cardiac output and index (1, 3, 44, 45), mixed venous oxygen saturation (45) and VO_2 max and peak oxygen pulse (46, 47), all of which outperform pulmonary arterial pressure as prognostic indicators in PH. Furthermore, RV failure before treatment initiation is associated with a poor outcome in patients with PAH (48) and is associated with increased morbidity and mortality related to Pulmonary Thromboendarterectomy for Chronic Thromboembolic PH (49, 50). This powerful prognostic influence reflects the fact that progressive RV failure is the usual, and unfortunately, inevitable cause of death in the vast majority of patients who develop PH.

The prognostic impact of poor RV function suggests an obvious clinical role as a means of detecting ‘at risk’ patients at presentation with PH. However, its clinical usefulness in this manner is greatly reduced by the limited means currently available to detect it. RV dysfunction, without overt RV failure (suggested by an elevated jugular venous pressure, peripheral oedema) is almost impossible to detect clinically.

Physicians are therefore overly reliant on diagnostic aids for the identification of RV failure in PH patients. The methods currently available for this purpose have significant limitations which will be discussed in detail in the sections that follow. One of the principal aims of this thesis was the establishment of a novel non-invasive means of detecting RV dysfunction in PH patients using NT-proBNP. This experiment is described in Chapter 3. Additionally, I hoped through the studies reported in Chapters 4 and 5 to uncover new information regarding the development of RV failure and the effect of RV failure on exercise capacity in PH patients. These goals are all based upon the supposition that RV failure is the catalyst for clinical decline and death in PH patients and that a better means of detecting and understanding it, are essential if the outcome for patients is to be improved.

1.3 Current methods of assessment of the pulmonary circulation and right ventricle

In contrast to the advances in therapy that have been seen over recent years, there has been little change in the tools used to assess the pulmonary circulation since the introduction of cardiac catheterisation in the 1970s and the deployment of portable, inexpensive transthoracic echocardiography machines in the 1980s. This lack of progress means that physicians remain reliant on these two techniques for the assessment of RV function in patients with PH. Unfortunately, neither method is ideally suited for this purpose.

1.3.1 *Echocardiography*

Medical echocardiography was developed in the years following World War II. During the war, pre-war experimentation with ultrasound technology had been intensified, resulting in the introduction of 'SONAR' which was successfully used during the conflict to track submarines underwater. In the 1950s, the Swedish physician and physicist, Inge Edler, subsequently dubbed the 'Father of Echocardiography' (51), modified these techniques to produce moving images of the human heart for the first time (52). By the 1970s and 80s echocardiography had become established as a useful clinical tool. Thirty years on from this, it is the most commonly performed cardiovascular investigation after electrocardiography and chest radiography (51). Echocardiography (a term which refers to trans-thoracic echocardiography throughout this thesis) has two principal uses in the assessment of patients with PH, 1) the detection of suspected PH in a symptomatic individual and 2) the measurement of RV dimensions and the quantitative assessment of RV function in patients already known to have PH.

1.3.1.1 *Detection of Pulmonary Hypertension*

Using echocardiography, Doppler-derived measurements of the peak velocity of blood traversing orifices, such as valves, within the cardiovascular system allows an estimation of the pressure gradient driving blood flow across such areas. This method employs a simplified version of Bernoulli's equation where the driving pressure gradient = $4 \times (\text{peak velocity of blood flow})^2$. Although jets of pulmonary valve insufficiency and blood flow across atrial or ventricular septal defects can be used in

the estimation of pulmonary arterial pressure (PAP), tricuspid valve regurgitant jets are the most ubiquitous and easily acquired haemodynamic phenomena used for this purpose in patients with PH (53). In the absence of pulmonary valve stenosis, systolic PAP can therefore be calculated as the tricuspid valve pressure gradient ($= 4(\text{Peak tricuspid valve jet velocity})^2$) + estimated right atrial pressure (RAP). RAP can be estimated by various methods including the Inferior Vena Cava Collapsibility Index and the extent of jugular venous pressure elevation detected clinically.

The reliability of these methods has been extensively investigated over the last twenty years (53-56). Impressive correlation has been demonstrated on numerous occasions with invasive measurements of systolic PAP ($r = 0.89-0.97$) (53-56). Doppler Echocardiography has, therefore, become established as the non-invasive screening investigation of choice in suspected cases of PH. Doppler Echocardiography studies do, however, also report relatively high standard errors of estimation (between 4.9 and 8 mmHg) (53, 56) making the accurate estimation of systolic PAP within a particular individual more unreliable. The Echo-Doppler method described is also subject to inevitable operator dependence and is particularly difficult to employ in obese patients and those with lung hyperinflation, e.g. patients with Chronic Obstructive Lung Disease (COPD) (in one cohort of COPD patients only 25% of examinations were successful (55)), who are at significant risk of developing PH.

1.3.1.2 Quantitative assessment of RV function

In patients in whom a diagnosis of PH has already been secured an accurate measurement of RV function is desirable, not least because of its powerful prognostic

influence. As we have discussed in earlier sections, RV function is the principal haemodynamic determinant of outcome in patients with PH (57), in whom RV failure remains the commonest mode of death (1, 58). Unfortunately, although echocardiography, being cheap and portable, is a convenient method for the assessment of RV function it is not a particularly accurate one. The geometric assumptions that echocardiography software employs to generate three dimensional ventricular volume measurements from data acquired in two-dimensions become increasingly flawed as the diseased RV dilates (59, 60) and fails. As we have discussed in Section 1.1.4, the RV is a complex structure and it is extremely difficult to model mathematically. Echocardiography is therefore an imprecise method of measuring RV dimensions and function in the setting of RV failure, limiting its usefulness in patients with established PH. RV ejection fraction (RVEF) can only be estimated indirectly from measurements acquired in two dimensions using echocardiography. Furthermore, variables derived from echocardiography that reflect RV function and provide useful prognostic information in PH are either complicated to define and therefore reliant upon an experienced operator (e.g. the Tei index) (61) or detected most frequently in patients in whom RV failure is already clinically overt (e.g. a pericardial effusion) (44).

1.3.2 Right heart catheterisation

Right heart catheterisation (RHC) is the current gold standard for haemodynamic assessment in patients with proven or suspected PH. Standard diagnostic algorithms require RHC for diagnosis (PH is defined as a mean PAP, which can only be measured at RHC, of > 25 mmHg at rest or > 30 mmHg on exercise). Since André

Cournand first demonstrated that PAP could be safely and accurately measured at RHC in humans in 1945 (62), simple techniques have been developed that allow the determination of additional important variables. These include:

1. Cardiac output (CO), which is most commonly measured using a thermodilution technique first described 1971 by Swan and Ganz (63)
2. Pulmonary artery occlusion pressure (PAOP) (and the related pulmonary capillary wedge pressure (PCWP) which provides an approximation of left atrial pressure by recording pressure measurements with a balloon-tipped pulmonary artery catheter wedged, with the balloon inflated, within a branch pulmonary artery (64)
3. Right atrial pressure (RAP)
4. Pulmonary artery (or mixed venous) oxygen saturation (PAOP or MVO₂)

Integration of Mean PAP, PAOP and CO allows the calculation of resistance to blood flow within the resistance vessels of pulmonary circulation (termed pulmonary vascular resistance (PVR)):

$$\text{PVR} = \frac{\text{Mean PAP-Pulmonary Artery Occlusion Pressure}}{\text{Cardiac Output}}$$

PVR provides a simple mathematical descriptor of the lung circulation that can be used to quantify pulmonary vascular disease. The computation of PVR from both pressure and flow makes this value a powerful index of disease severity. In health, the capacity for recruitment within the pulmonary circulation is large. On exercise, as

CO rises, PVR should therefore fall allowing the lung circulation to accommodate the increased CO with only a minimal rise in PAP. This feature of normal physiology is important as the earliest stages of pulmonary vascular remodelling are characterised by a relatively small reduction in the cross-sectional area of the pulmonary vascular bed, and therefore, a curtailed recruitable lung circulation. In this setting, PH may only be proven by either an abnormal rise in PVR and/or PAP on exercise. CO, RAP and PAOP have all been shown to predict a poor outcome in patients with Pulmonary Arterial Hypertension (65).

Acute Vasodilator testing can also be undertaken at RHC. Inhaled Nitric Oxide is the most commonly used vasodilator although alternative methods such as intravenous Prostacyclin and Adenosine have been successfully employed (65). A positive acute vasodilator test is defined as reduction of mean PAP of ≥ 10 mmHg to reach an absolute value of mean PAP ≤ 40 mmHg with an increased or unchanged cardiac output (65). In uncontrolled studies it has been shown that patients who demonstrate an acute vasodilator response at RHC derive sustained haemodynamic and survival benefit from long-term treatment with Calcium Channel Antagonists (66). Therefore, RHC provides important indices of pulmonary vascular disease. Nevertheless, the technique has significant limitations in PH patients, these include:

1. It is invasive
2. It is generally only performed at rest making the detection of early PH difficult and resulting in a loose correlation with symptoms in PH (67).
3. RHC does not seem to yield variables that correlate tightly with clinical improvement on therapy (67). Invasive haemodynamics (mean PAP, CO, and

PVR), although crucial to diagnosis, and usually responsive in terms of pure statistic significance, rarely improve in great physiological terms with apparently successful treatment (as defined by other means, e.g. exercise performance, symptom scores). This may reflect dissociation between the ‘cath. lab’ environment (lying supine, at rest) and ‘real life’ but also suggests that resting RHC is too simple a tool to adequately describe the physiological changes that occur in PH.

1.3.3 *The six-minute walk test*

An assessment of function, or exercise capacity, is important in the assessment of all patients with PH. This is because functional capacity, or WHO class correlates with survival in PH patients and exercise capacity is a useful surrogate of the day-to-day symptoms experienced by patients. The six-minute walk test (6MWT) is the most widely employed tool available for this purpose. If recorded at presentation and at subsequent clinic visits, six-minute walk test (6MWT) distance can be used to monitor patients on therapy and as a means of detecting clinical deterioration. 6MWT distance probably reflects RV function to some extent as it has been shown to correlate strongly with peak oxygen pulse measured by Cardiopulmonary Exercise Testing (46), which is a direct correlate of RV stroke volume. Furthermore, 6MWT distance at presentation has been shown to predict survival (46) in patients with idiopathic PAH and to correlate with clinical improvement with various therapies, including intravenous Epoprostenol (68-70). The 6MWT is easy to undertake, cheap and reproducible, it also the only measure of exercise capacity that has been approved

by the US Food and Drug Administration for use in clinical trials of therapy for PAH (67).

Nevertheless, the 6MWT is not specific to either the pulmonary circulation or RV. Deterioration in a patient's 6MWT performance can occur for reasons other than the progression of pulmonary vascular disease or the development of RV failure, e.g. arthralgia or muscle weakness. A recent study has also reported poor correlation between 6MWT and cardiopulmonary exercise test results in patients enrolled in clinical trials of therapy for PH (71). Therefore, an alternative means of assessing disease severity in PH at presentation and over a period of time is desired. Recent research conducted in patients with diseases of the systemic circulation has established a potential role for natriuretic peptide hormones in the detection and monitoring of RV dysfunction in PH patients.

1.3.4 *Natriuretic peptides*

The natriuretic peptides share a common 17-amino acid ring structure. Atrial Natriuretic Peptide (ANP) was discovered first, in the early 1980s (72), followed by Brain Natriuretic Peptide (BNP), now termed B-type natriuretic peptide and C-type Natriuretic Peptide (CNP). Both ANP and BNP bind to Natriuretic Peptide Receptor-A (NPR-A) and promote salt and water loss (natriuresis and diuresis) (73). CNP binds to NPR-B and is a potent vasodilator; however, it has no practical clinical role. ANP and BNP are synthesised within cardiac myocytes as high molecular weight precursor proteins which are then cleaved into an active hormone and an inactive N-terminal component. BNP, for example, is secreted as proBNP 1-108, which is

cleaved by enzymes such as Prohormone Convertase and Corin within cardiac myocytes into proBNP 1-76 (known as N terminal-pro Brain Natriuretic Peptide (NT-proBNP)), which is inactive and BNP 32 (known simply as BNP), which is the active hormone (74, 75).

BNP is secreted from both cardiac ventricles in response to raised chamber pressure or volume overload (76). In contrast, ANP release is dictated by atrial, rather than ventricular, filling pressures. The secretion of both ANP and BNP is influenced by other physiological factors, most notably blood pressure, salt intake and renal function. The secretory mechanisms of the two peptides dictate the effect these variables have on serum levels. ANP can be released rapidly in response to physiological stimuli because it is stored in secretory granules within atrial myocytes (77). In contrast, the secretion of BNP is constitutive because ventricular myocytes do not contain secretory granules (78). Therefore, serum ANP levels are more easily influenced by other physiological factors than BNP, making the former less attractive as a potential biomarker. The assay required to measure serum ANP levels is also extremely complex and expensive and so ANP is not used in clinical studies. Because the secretion of BNP is more predictable and its measurement is more straightforward, both BNP and NT-proBNP have become established as useful biomarkers in various cardiovascular diseases.

1.3.4.1 Natriuretic peptides and left heart disease

Elevated serum BNP levels have been reported in patients with LV systolic dysfunction (79), acute myocardial infarction (MI) (80), systemic hypertension (81)

and valvular heart disease (82). BNP and NT-proBNP concentrations below assay-specific thresholds have a powerful negative predictive value for a subsequent diagnosis of heart failure in patients presenting with symptoms suggestive of the diagnosis (83-85). In addition, serum BNP and NT-proBNP levels have proven useful as population-wide screening tests for LV systolic dysfunction in asymptomatic individuals (86). This diagnostic utility has led to the incorporation of natriuretic peptide testing into the standard diagnostic algorithms for heart failure recently published by both The National Institute for Clinical Excellence (NICE) (87) and the European Society of Cardiology (88). Furthermore, the provision of NT-proBNP results, in addition to clinical findings and the results of ECGs and echos resulted in a significant improvement in diagnostic accuracy in patients referred to their general practitioner with symptoms suggestive of heart failure (89).

1.3.4.2 Natriuretic peptides and Pulmonary Hypertension

The natriuretic peptide system is known to be up-regulated in PH patients (90, 91). For example, serum levels of BNP have been shown to correlate with invasive pulmonary haemodynamics and RV function (91, 92) in earlier studies. A close relationship has also been identified between NT-proBNP concentration and pulmonary haemodynamics (134), RV systolic function (163) and survival (135) in patients with PH. However, the diagnostic utility of NT-proBNP has yet to be tested in PH patients. In contrast to LV systolic dysfunction, where the large volume of data summarised above has been collected on the negative predictive value of NT-proBNP levels below certain thresholds, no attempt has yet been made to identify an NT-proBNP threshold indicates RV failure in PH. As a direct result, although high

NT-proBNP levels are considered a ‘bad sign’ in PH patients, conclusions regarding RV systolic function cannot yet be drawn from NT-proBNP measurements made in individual patients. Rather, clinicians remain reliant on invasive (right heart catheterisation) and potentially inaccurate (echocardiography) tools for an objective assessment of RV function. This makes the identification of ‘at risk’ patients with RV failure difficult and appears fertile ground for further study in PH patients. This topic is the subject of Chapter 3 of this thesis.

1.3.5 Summary

The methods used to assess RV function in PH have changed little over the last three decades. The significant limitations of these techniques reduce either their usefulness, their accuracy, or both in routine clinical practice. A novel alternative to the existing methods is now required. Such an alternative should be accurate, reproducible and, most importantly, non-invasive. A capacity to perform measurements during stress would be an additional, and considerable, advantage. The ability of Cardiovascular Magnetic Resonance (CMR) imaging to deliver these qualities in PH patients is tested throughout this thesis. In the next section, the evidence that has established CMR as the ‘gold standard’ for non-invasive RV assessment in PH is presented. This is preceded by a review of basic MR theory and the factors that dictate tissue contrast on CMR images.

1.4 Cardiovascular Magnetic Resonance (CMR) imaging

1.4.1 Magnetic resonance theory

1.4.1.1 Nuclear magnetic resonance fundamentals

Magnetic resonance imaging is based upon the principle of ‘nuclear magnetic resonance’ which was discovered in 1946 by Bloch and Purcell. Working independently in the US, they discovered that certain atoms absorbed and then released radiofrequency (RF) energy when moved in and out of a magnetic field. They demonstrated that individual atomic elements responded to RF energy of the same frequency that their own nuclei naturally spun at. The term ‘resonance’ was used to describe this effect as it is defined as ‘an amplified response to a stimulus of the same natural frequency’.

MR images are constructed using energy absorbed and then emitted by the spinning nuclei of hydrogen atoms. Hydrogen is a suitable element for this purpose because it absorbs energy within the RF range and is abundant in the human body. The average 70kg male contains 45 litres of water, comprised, of course, of two hydrogen atoms bound to a single atom of oxygen. Proteins and lipids contain even more hydrogen atoms, albeit within a different molecular environment. Each hydrogen atom is made up of a nucleus, containing a proton but no neutron, and an orbiting electron. Since the electron is redundant in this context and no proton exists, hydrogen nuclei will be referred to simply as protons in this thesis. Each proton has a positive charge, and therefore, spins naturally around its own tiny magnetic axis. The

orientation of proton spins is normally entirely random, see figure 1.3 overleaf. However, in the presence of a strong magnetic field protons will align themselves parallel to the direction of the field (identified by the symbol B_0), and are said to ‘precess’ at a characteristic frequency (the precession frequency). Precession frequency is dependent on the element, its environment and the strength of the surrounding magnetic field. This relationship is described by the Larmor equation:

$$\mu = \delta \times B$$

where μ is the precession frequency, δ is the gyromagnetic constant (a characteristic of a nucleus in a given environment) and B is the magnetic field strength. For example, hydrogen protons in water have a precession frequency of 63 megahertz in a 1.5 Tesla magnet. Under these conditions, the majority of protons spin, or precess, in the same direction as the magnetic field (B_0), while a slightly smaller number line up in the opposite direction to the field, see figure 1.4 on page 67. Those protons lined up with the magnetic field are said to be in a low energy state while those lined up against it are said to be in a high energy state. By applying a radiofrequency pulse at the precession frequency the low energy protons can be made to absorb energy and move to the high energy state (against the magnetic field). Then, when the RF pulse is switched off these protons will relax back to the low energy state (with the magnetic field) emitting detectable RF energy. Thus, the alignment of hydrogen protons spins, in hydrogen atom-rich tissue, placed within a strong magnetic field is a source of detectable RF energy. This is the basis of nuclear magnetic resonance, or magnetic resonance imaging (MRI) as it has come to be known.

Figure 1.3

Random natural orientation of hydrogen proton spins. Reproduced with the permission of Dr. John Foster

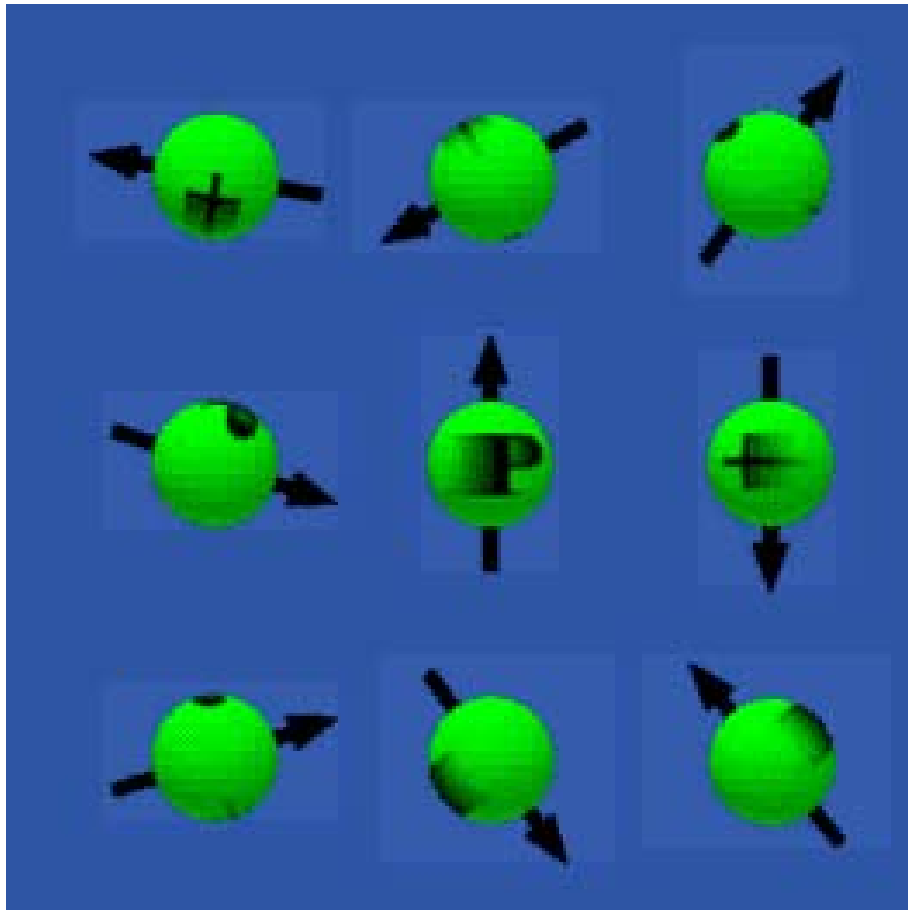
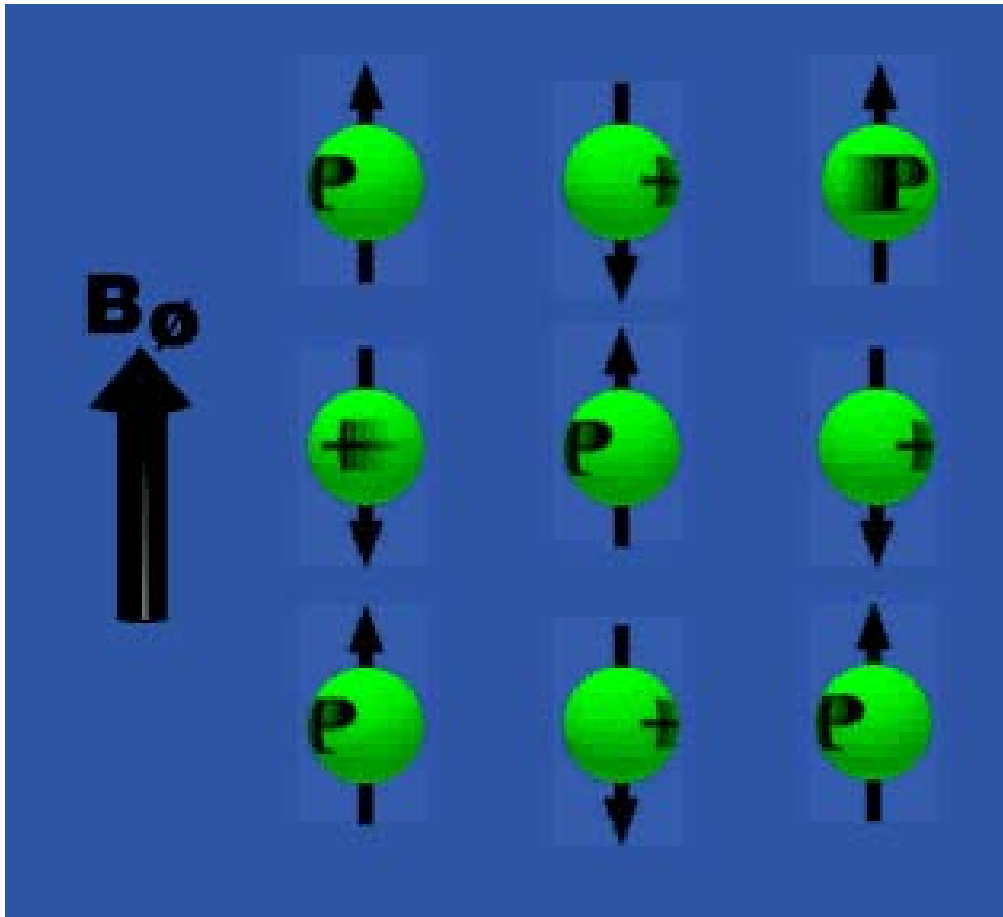


Figure 1.4

Precession of protons within a strong magnetic field (the direction of which is indicated by the standard nomenclature: B_0). The majority of protons line up parallel to the magnetic field. Reproduced with the permission of Dr. John Foster.



1.4.1.2 *Magnetic fields and magnets*

The purpose of the strong magnetic field in all diagnostic MRI systems is to produce precession of the protons within the target tissue. Although a minority of protons will line up anti-parallel to the magnetic field, the net alignment of protons under these conditions will always be in the direction of the magnetic field and arranged longitudinally. Therefore, the ‘overall’ effect of the magnet on the tissue, at equilibrium (i.e. before any RF pulse is applied to excite protons), is to generate a small secondary magnetic field, described as the net tissue magnetisation vector, see figure 1.5 overleaf.

Modern MRI systems use resistive electromagnets (as opposed to permanent magnets containing ferromagnetic material) to generate an electrical field perpendicular to an electrical current, flowing around a central coil. The orientation of the resulting magnetic field and its relationship to a patient is shown in figure 1.6 on page 70.

The magnetic field strength that a resistive magnet can generate greatly exceeds that of a permanent magnet but is limited by the resistance of the material in which the current flows. This can be reduced by the use of modern filaments to carry the current (e.g. Niobium) and by super-cooling the coil, e.g. by bathing it in pressurised, liquid Helium at approximately -250°C . Using these techniques contemporary MRI systems can generate field strengths of up to 7 T (Tesla) (70,000 times stronger than the earth’s magnetic field), although most clinical systems operate at 1.5 T.

Figure 1.5

The net magnetisation vector (in yellow) of protons within a strong magnetic field (B_0) is produced because the majority of protons line up parallel with the main field (i.e. pointing north; in red), while the rest of the protons line up anti-parallel (i.e. pointing south; in green)

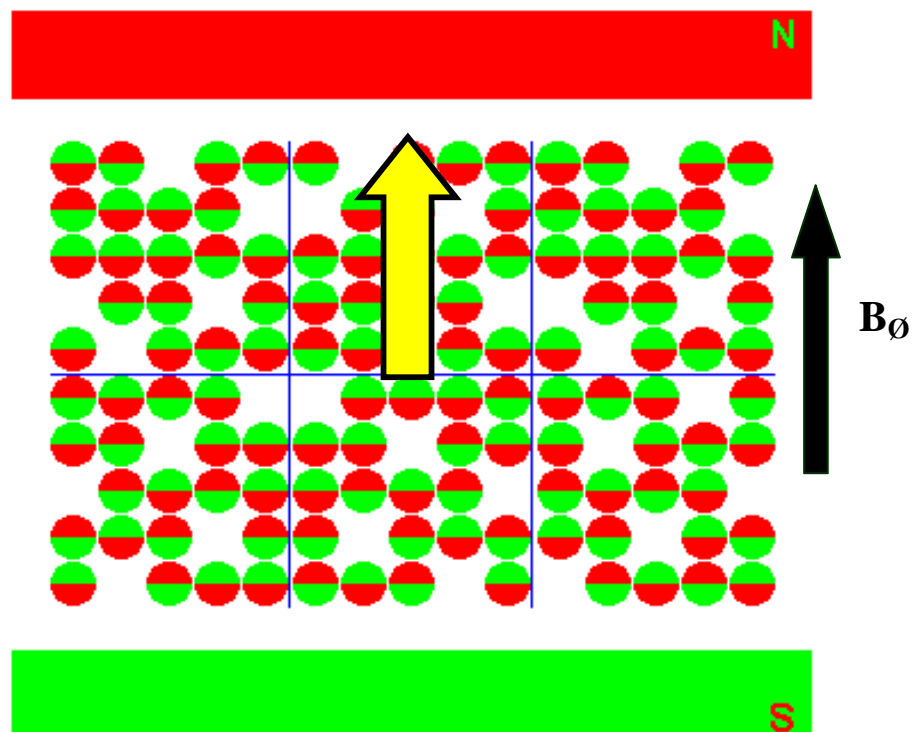
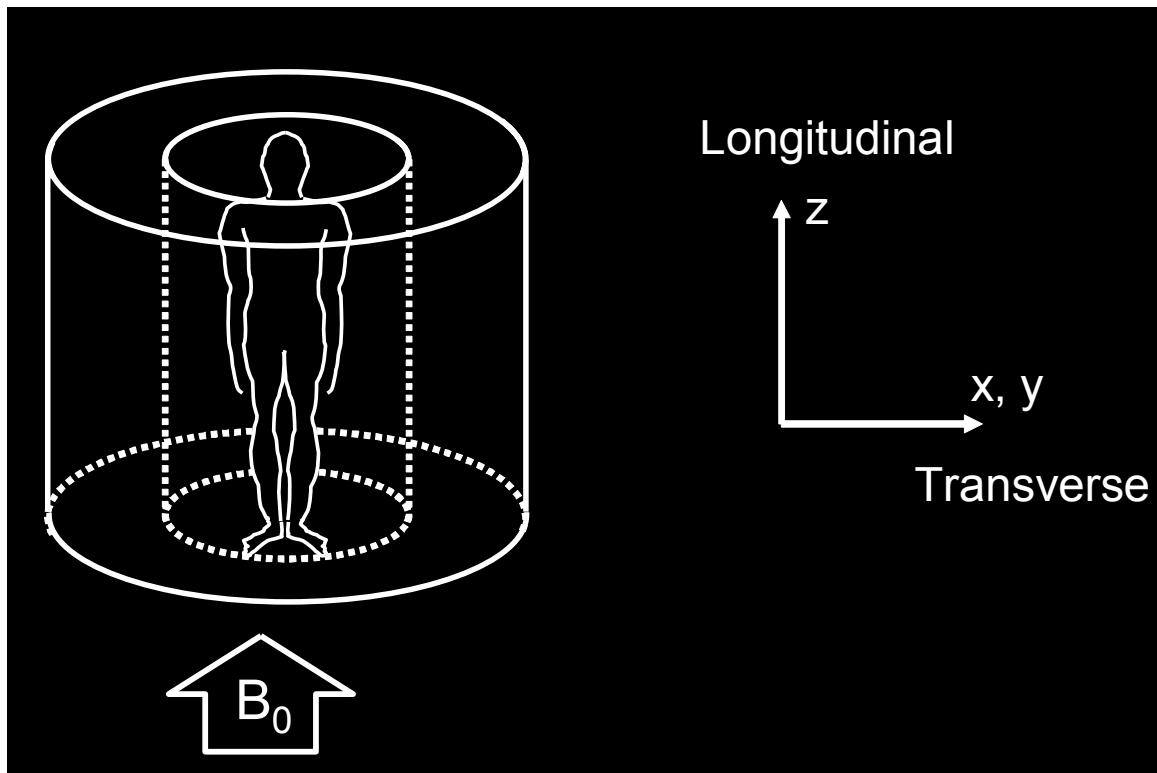


Figure 1.6

Magnetic field orientation (B_0) in a superconducting electromagnet. Note the orientation of the longitudinal and transverse magnetisation vectors relative to the patient (lying within the bore of the electromagnet).



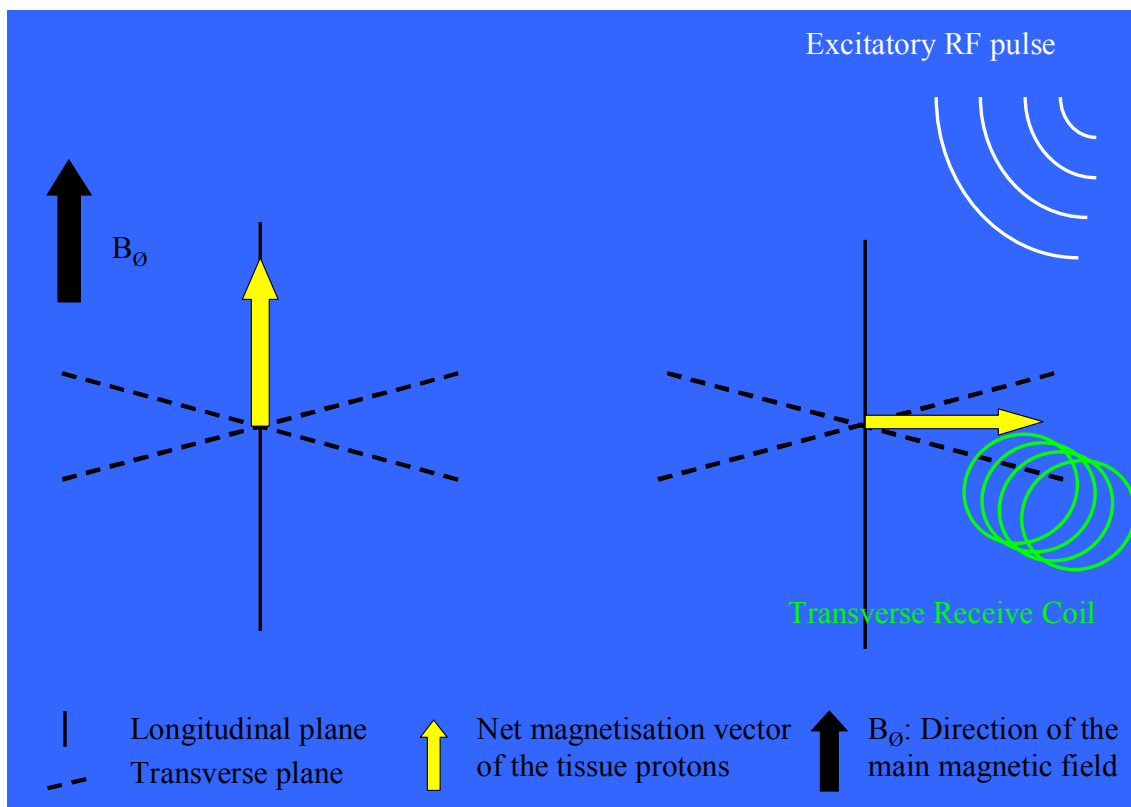
1.4.1.3 *Radiofrequency pulses and transverse magnetisation*

Radiofrequency pulses are used to stimulate tissue protons and alter net tissue magnetisation. This process is described as excitation. The RF energy released by the excited protons when the RF pulse is switched off can then be used to construct MR images. However, with the net tissue magnetisation vector in the longitudinal plane (i.e. aligned with the main magnetic field) changes in tissue proton alignment cannot be detected because they are dwarfed by the strength of the main magnetic field. MRI systems circumvent this problem by producing magnetisation in tissue protons in the *transverse* plane by the following method, which is presented graphically overleaf in figure 1.7.

An appropriate RF excitation pulse (delivered at the precession frequency of the tissue protons in that strength of MR field) causes the protons in the tissue to resonate and results in rotation of the axis around which they spin. This rotation out of the longitudinal plane has the effect of ‘tipping’ a component of the net magnetisation vector out of the longitudinal plane into the transverse plane. When the excitatory RF pulse is switched off, any RF energy released from the excited tissue protons in this transverse plane will produce a change in flux in a receiver coil in this orientation. This produces a voltage and thus a detectable signal from the tissue protons. This signal is relatively pure as it is unaffected by the background ‘noise’ of the main (longitudinal) magnetic field. The strength (or amplitude) of the RF pulse and the length of time it is applied for determine how far out of the longitudinal plane the net tissue vector is tipped. A 90° pulse will convert all longitudinal magnetisation into detectable transverse magnetisation, as shown in figure 1.7.

Figure 1.7

Schematic representation of a 90° excitation pulse which converts all longitudinal magnetisation in the imaged protons into transverse magnetisation. At equilibrium, shown on the left, the net magnetisation vector of the tissue protons is orientated in the same plane as the main magnetic field (B_0). Once a RF excitation pulse is applied, as shown on the right, the net magnetisation vector is tipped out of the longitudinal plane, into the transverse plane, in which the transverse receive coil is located.



1.4.1.4 *Relaxation*

Once the excitatory RF pulse is turned off, the tissue magnetisation vector drifts back from the transverse plane into the longitudinal plane, under the influence of the main magnetic field. This process is described as relaxation; during relaxation RF energy is released and results in a MR signal in the transverse receive coil. The rate of relaxation is an important determinant of tissue contrast in MR imaging and is dependent on the molecular environment of the water protons that were excited. Relaxation is rapid in highly cellular tissues containing a lot of ‘bound’ water. This is a term used to describe water molecules in close proximity to macromolecules (e.g. intracellular organelles, proteins, DNA). These larger molecules restrict the movement of the smaller water molecules. However their juxtaposition makes energy transfer more efficient in bound water compartments.

Conversely, relaxation of transverse magnetisation is slower in ‘free’ water solutions containing randomly orientated and rapidly tumbling water molecules because energy transfer is less efficient in this less structured environment. Thus, the molecular environment of water protons has a profound influence on the rate of RF energy release and therefore the MR signal received from different tissues. For example, free water solutions (e.g. cerebrospinal fluid, urine, glandular structures or cysts) look different to ‘bound’ water solutions (e.g. brain, liver) on MR images. This is, however, an oversimplification of the factors involved in MR tissue contrast. The return of tissue magnetisation from the transverse to the longitudinal plane, and the release of RF energy (and an MR signal) are dictated by two further characteristics of the imaged tissue. These are defined as T1 and T2 relaxation. T1 relaxation describes

the recovery of longitudinal magnetisation, while T2 relaxation describes the decay of transverse magnetisation. Clearly, these processes are related but they are not interchangeable and are completely independent.

1.4.1.4.1 T1 relaxation

T1 relaxation describes the recovery of longitudinal magnetisation after an excitatory RF pulse is switched off, see figure 1.8 overleaf. Therefore, it can also be described as T1 recovery or ‘longitudinal relaxation’. The time required for T1 relaxation is dependent on the efficiency with which RF energy can be dissipated from the excited protons to surrounding tissues, and the strength of the main magnetic field. The dependence of T1 upon the surrounding environment allows the alternative description of T1 relaxation as ‘spin-lattice’ interaction. *T1 relaxation time* is defined as the time taken for 63% of longitudinal magnetisation to recover to its original value; it is a constant for any given tissue, within a given MR field. Examples of T1 relaxation times for different tissues in a 0.5 T and a 1.5 T MR field are given in table 1.2.

Figure 1.8

Schematic representation of T1 relaxation. Once the excitatory RF pulse is switched off, the net magnetisation vector of the imaged protons relaxes back from the transverse plane, shown on the left, into the longitudinal plane, shown on the right. By this process, RF energy is released in the transverse plane and can be detected by the transverse receive coil. T1 relaxation time is defined as the time taken for 63% of longitudinal magnetisation to recover.

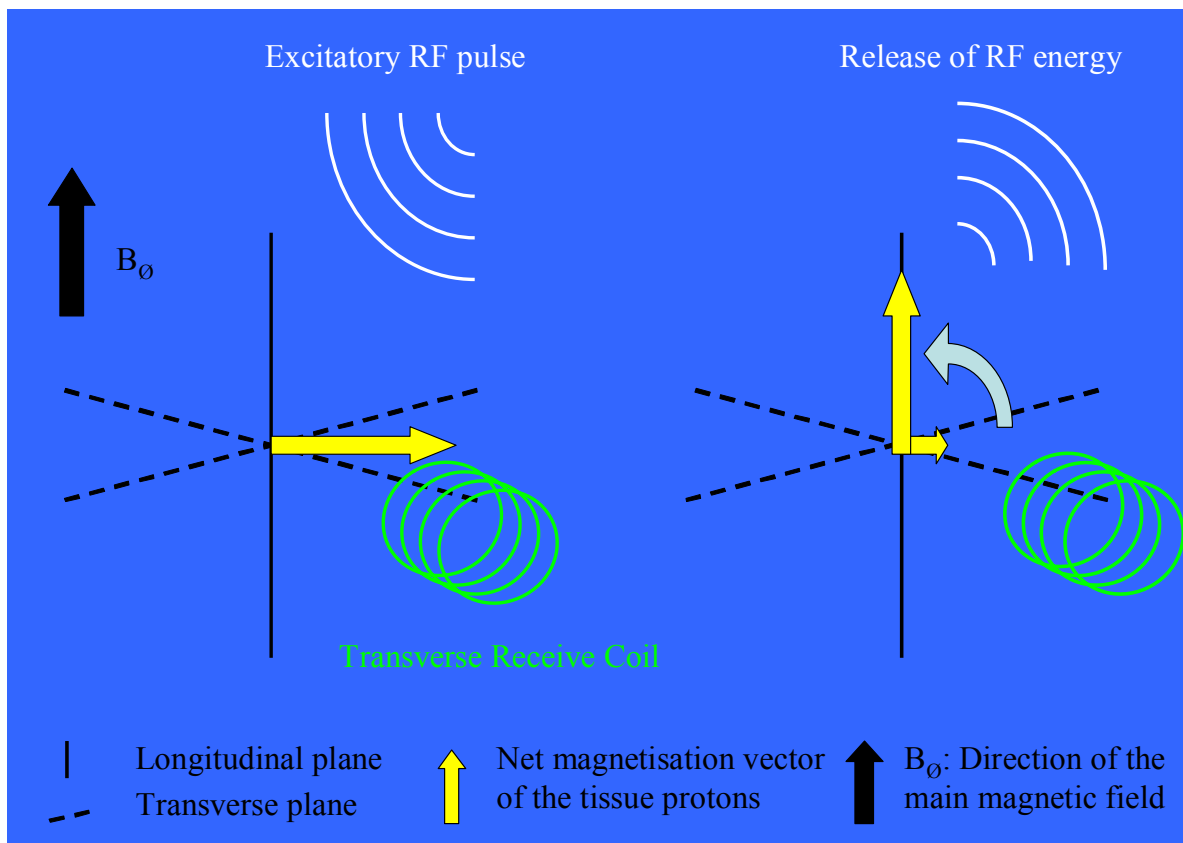


Table 1.2 T1 relaxation times (msecs) of commonly imaged tissues

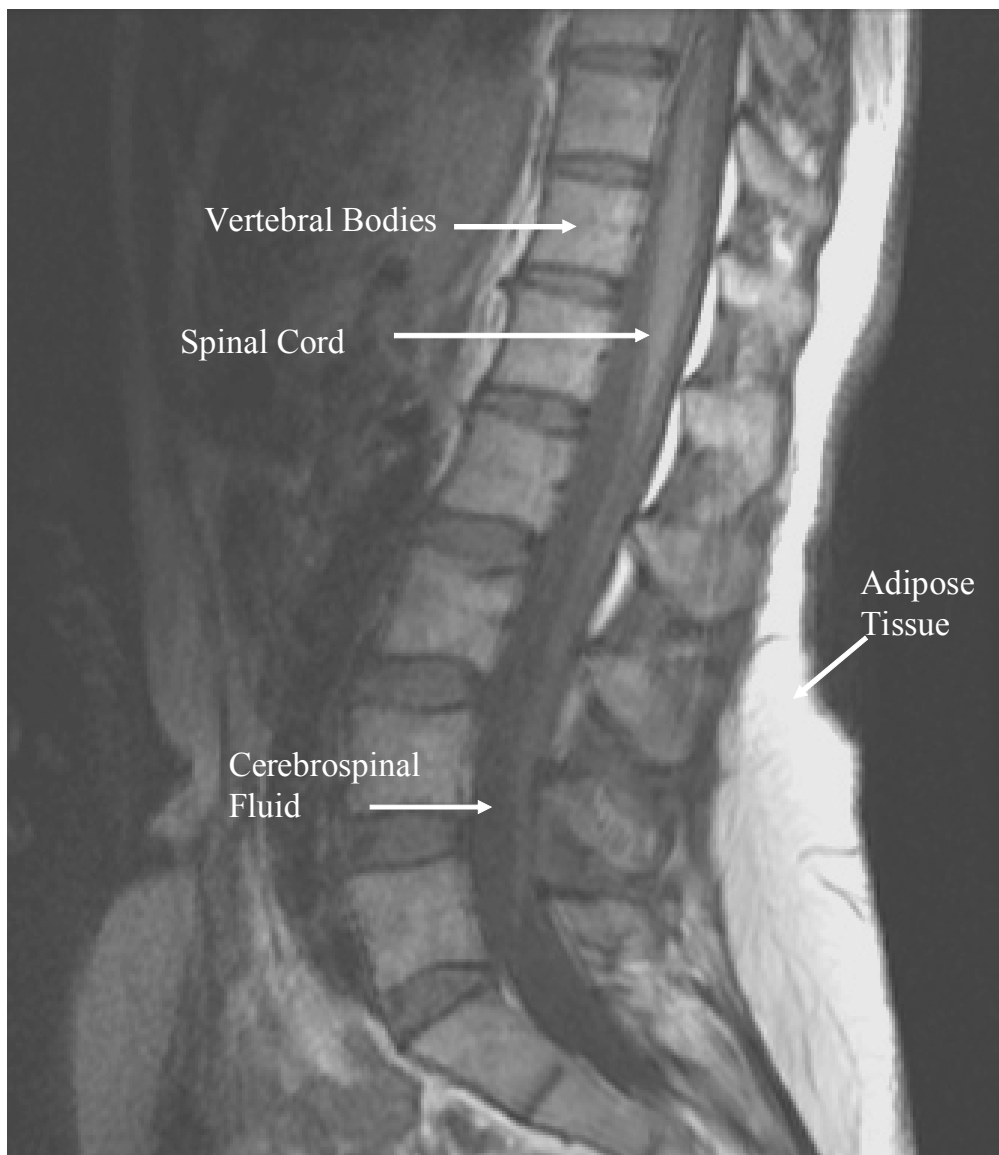
Tissue	T1 @ 0.5T	T1 @ 1.5T
Fat	215	260
Liver	323	490
Muscle	600	870
Grey Matter	656	920
CSF	>4000	>4000

Pure free water has the longest T1 relaxation time because it dissipates RF energy slowly (around 3 seconds, depending on magnetic field strength). Conversely, the T1 relaxation time of adipose tissue is extremely short. This reflects the restricted movement of fatty acids protons, which translates into extremely efficient energy transfer. Protons within protein macromolecules dissipate energy so quickly, because of their organised structure and size, that most MR scanners cannot detect signals *directly* from them. However, biological tissues are not comprised of pure protein and it is the effect of the protein content on water protons around them that determines the T1 relaxation times of tissues other than free water and fat. For example, viscous protein-rich solutions, e.g. pus, have a shorter T1 relaxation time than pure free water because of the increased amount of bound water protons (i.e. protons lying adjacent to protein macromolecules). Muscle, liver and brain contain variable proportions of free and bound water protons. This is reflected in the individual and characteristic T1 relaxation times of these, and all other tissues, which lie in the spectrum in between those of free water and adipose tissue.

In practice, this means that it will take a long time to receive an adequate signal back from a pure water solution. Since most MR sequences aim to detect a signal in less than a second, 'free' water solutions (e.g. cerebrospinal fluid) appear dark and adipose tissues (e.g. brain) appear bright on images that rely on T1 contrast, see figure 1.9 overleaf for an example. This type of image is known as a T1-weighted image which will be discussed in more detail in section 1.4.1.8.

Figure 1.9

T1 weighted sagittal image of the lumbar spine. Note that cerebrospinal fluid, which is a 'free' water solution, appears dark because of its long T1 relaxation time resulting in a low MR signal at the time of image acquisition. Adipose tissue, in contrast, appears bright reflecting its short T1 relaxation time.



1.4.1.4.2 *T2 relaxation*

T2 relaxation describes the decay (or dephasing) of transverse magnetisation produced by an excitatory RF pulse. Contrast this with T1 relaxation which describes the recovery of longitudinal magnetisation after the same event. If T2 relaxation (also described as T2 decay) was automatically translated into T1 recovery the use of individual terms to describe these processes would be unnecessary. However, the rate at which transverse magnetisation is lost (T2 decay) is greater than the rate at which longitudinal magnetisation returns (T1 recovery) in most tissues because of energy dissipation amongst individual protons (described as ‘spin-spin interaction’, contrast this with T1 relaxation, or ‘spin-lattice’ interaction, which is largely dependant on the dissipation of RF energy to surrounding tissues). A schematic representation of T2 relaxation is presented overleaf in figure 1.10. T2 relaxation rate is described by *T2 relaxation time*. Individual tissues have a characteristic T2 relaxation time, see Table 1.3 overleaf for examples.

Figure 1.10

Schematic representation of T2 relaxation which describes the dephasing of transverse magnetisation once the excitatory RF pulse is switched off. Note that this process results in the release of RF energy.

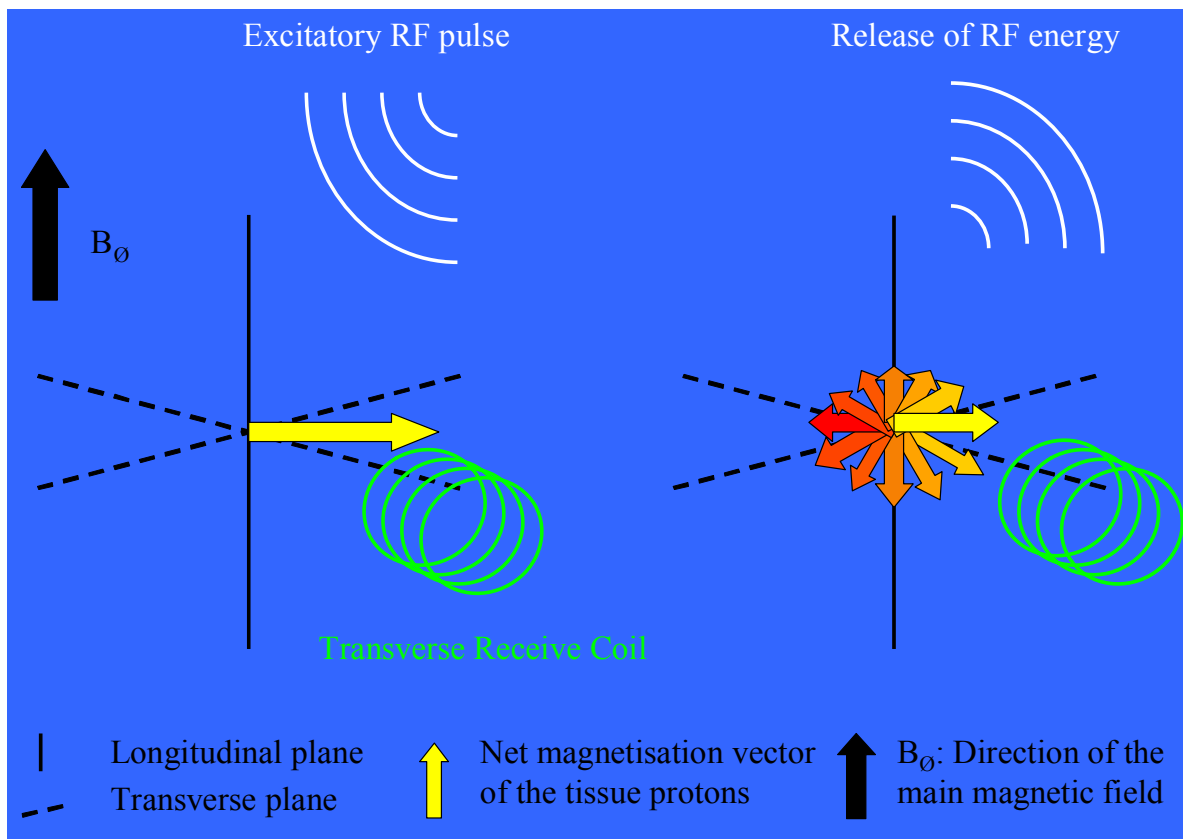


Table 1.3 T2 relaxation times (msecs) of commonly imaged tissues

Tissue	T2 @ 1.5T
Fat	85
Liver	43
Muscle	47
Grey Matter	100
CSF	1400

In contrast to T1 relaxation times, T2 times are relatively independent of magnetic field strength and influenced by different factors when compared with T1. T1 and T2 relaxation times are similar for pure free water and for adipose tissue because the unstructured arrangement of water protons in these environments makes energy transfer between individual protons (spin-spin interaction) inefficient. Therefore, the majority of transverse magnetisation decay is converted directly into longitudinal magnetisation recovery. In more organised molecular environments, particularly those containing a significant proportion of bound water (i.e. water molecules closely associated with protein macromolecules), spin-spin interaction is more efficient. This results in T2 relaxation times for tissues such as muscle and liver that are significantly shorter than their T1 relaxation times

Additional T2 decay occurs if there is any inhomogeneity in the magnetic field. In practice, tiny inconsistencies in the structure of the electromagnet are inevitable, even in modern superconducting systems, but also occur around paramagnetic material implanted in the imaged tissue. Common examples include ferrous metal joint replacements and foreign bodies. The term *T2* relaxation* is used to describe the total

decay of transverse relaxation as a result of both tissue relaxation and these local inhomogeneities.

Because significant T2 decay results in incomplete recovery of longitudinal magnetisation it is easy to consider T2 decay a form of 'energy loss'. This is not the case as a) RF energy is still released during T2 decay and is, therefore, detectable and b) longitudinal magnetisation never, in practice, recovers completely because the logarithmic scale on which it is plotted makes 100% recovery a theoretical impossibility. Rather, T1 and T2 decay should be considered independent processes of RF energy release following cessation of an excitatory RF pulse.

1.4.1.5 Tissue contrast

Contrast in MR imaging results from the different T1 and T2 characteristics of adjacent tissues. Detailed understanding of T1 and T2 relaxation and the effect on tissue magnetisation of different RF excitation pulses allows the design of sequences that optimise tissue contrast and maximise signal intensity. Before discussing these concepts it is useful to first review basic MRI sequence structure: Most MRI examinations require a repeating cycle of RF excitation pulses (producing multiple 'echoes' from tissue protons) to generate a data set rich enough for image construction. Each cycle is comprised of an excitation pulse, a time delay of varying length (during which precessing protons relax back into the longitudinal plane and release RF energy) and a period of data collection, immediately preceding a further excitatory pulse. Various parameters within this basic structure can be altered to

accentuate differences between the T1 (or T2) relaxation times of adjacent tissues, producing T1 (or T2) contrast and T1- (or T2-) 'weighted' images.

1.4.1.5.1 T1 contrast

T1 contrast results from differences between the T1 relaxation times of adjacent tissues. These differences can be accentuated, and T1 contrast increased, by reducing the '*Repetition Time*' (TR) of the excitatory RF pulse, which describes the time gap in between excitation pulses. When the TR is short, tissues which have a short T1 time will have recovered more longitudinal magnetisation than those with a long T1 time by the time data is collected (immediately before the next excitatory RF pulse). Thus, shortening the TR of a pulse sequence enhances contrast between tissues that have a difference in T1 relaxation time. However, shortening the TR of the pulse sequence reduces the time available for the recovery of longitudinal magnetisation, energy release and data collection. This has the effect of reduced overall signal intensity on images with a short TR. While this is helpful in producing T1 contrast it can result in poor image quality if compensations are not made in other aspects of the pulse sequence. The most important of these is the '*Flip Angle*', which describes how far out of the longitudinal plane the net tissue magnetisation vector is tipped (a 90° flip angle converts all longitudinal magnetisation to transverse magnetisation). The flip angle is a product of the strength and duration of the excitatory RF pulse. A lower flip angle tips less of the net magnetisation into the transverse plane. This has the effect of further lowering signal intensity on resulting MR images because energy can only be detected from protons precessing in the transverse plane. However, increasing the flip angle too much on a T1 weighted MR image can also be

detrimental. A large flip angle will convert a large proportion of longitudinal magnetisation into transverse magnetisation, e.g. a 90° pulse tips the net magnetisation vector completely into the transverse plane. While this produces a large amount of potential MR signal on the first RF pulse, it means that longitudinal magnetisation will only have time to partially recover if the TR is short. Therefore, there will be little longitudinal magnetisation for subsequent excitatory pulses to tip out into the transverse plane and signal intensity ultimately decays. Thus, there is an optimum flip angle for each tissue, based on its T1 time, which produces optimum signal intensity and compensates for the TR reduction necessary for T1 contrast. This is known as the *Ernst angle*. Ernst angles tend to be small for tissues with long T1 times (because any transverse magnetisation takes a long time to recover) and larger for those with short T1 times.

Therefore, for T1 weighted imaging, where contrast between tissues with different T1 times is the goal, a short TR and a small flip angle should be used. The flip angle should be above the (small) Ernst angle of the long T1 tissue and ideally around the Ernst angle of the short T1 tissue. This ensures high signal intensity from tissues with a short T1 time and low signal intensity from tissues with a long T1 time.

1.4.1.5.2 *T2 contrast*

For various reasons, transverse magnetisation cannot be measured immediately after its creation by an excitatory RF pulse. Rather, an echo must be produced of the original signal using magnetic field gradients (see next section). The resulting delay between the creation of transverse magnetisation and signal measurement is called the

Echo Time (TE). The TE is defined as the time from the RF excitation pulse to the resulting echoes used as the MR signal. It is an important determinant of tissue contrast, particularly, T2 contrast.

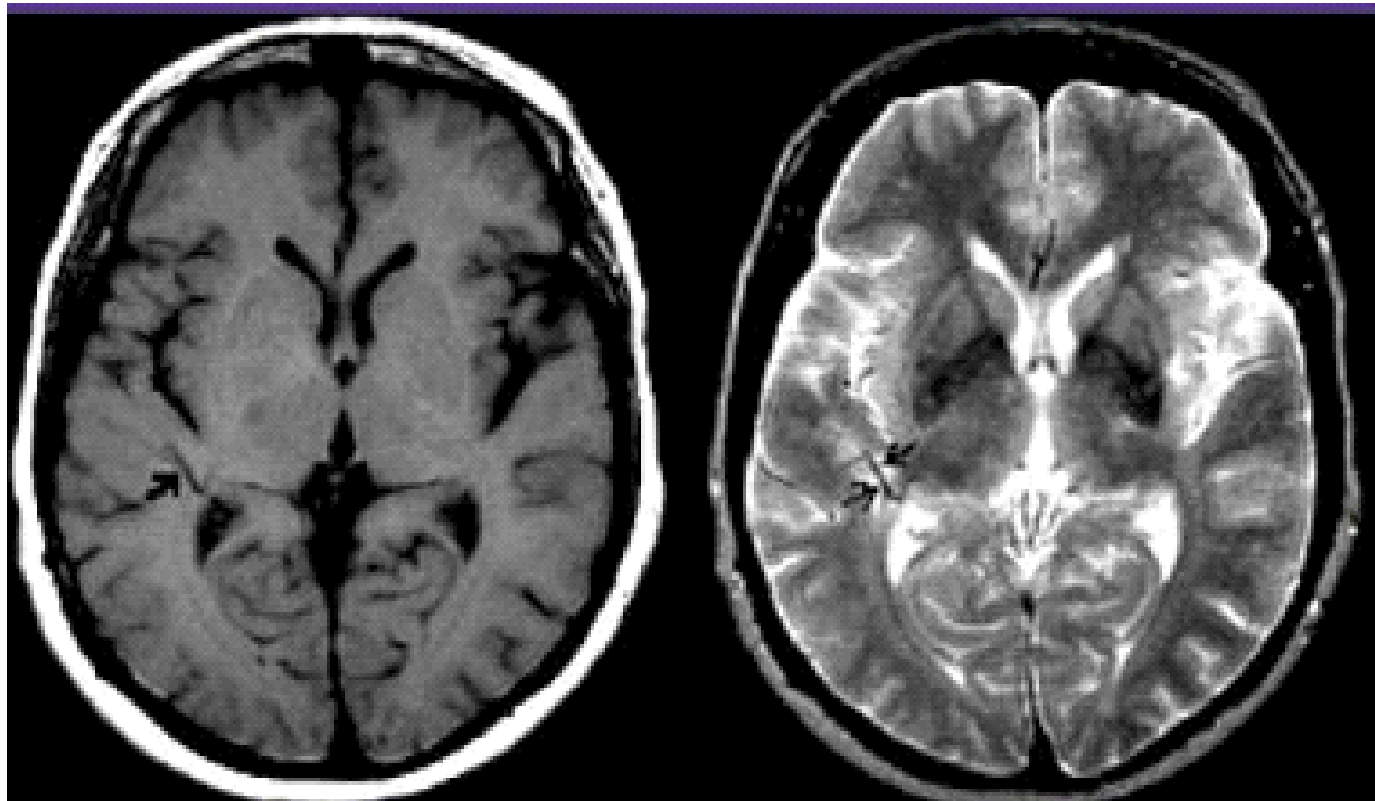
Inevitably, transverse magnetisation decays during this interval, at a rate defined by the T2 relaxation time of each tissue in the image block. This results in reduced signal intensity from tissues with short T2 times as a significant proportion of their RF energy potential is released before signal measurement. Sequences with TEs long enough to allow significant T2 decay from tissues with short T2 times, but short enough to minimise decay from tissues with long T2 times result in T2 contrast, or, T2-weighted images. TE is, however, constrained by the progressive nature of T2 decay; if TE is too long, little or no signal will remain when measurements are made and signal intensity will be low. Contrast on sequences with TEs shorter than the T2 of any of the tissues of interest will be determined by other factors, e.g. T1 contrast. T2 weighted images, therefore, tend to have a long TE. Since TR is a component of the TE, they also tend to have a long TR.

This concept of contrast weighted can be appreciated by comparison of T1- and T2-weighted images of the brain, presented overleaf in figure 1.11.

Figure 1.11, below

Comparative T1- and T2 -weighted images of the brain. The T1-weighted image, acquired using a short repetition time (TR), results in contrast between white (T1 = 780 msec at 1.5 T) and grey matter (T1 = 920 msec at 1.5 T) but no signal from the surrounding cerebrospinal fluid (T1 > 4000 msec at 1.5T). The T2-weighted image, acquired using a long TR and long echo time (TE) results in a bright signal from the cerebrospinal fluid (T2 = 500-1400 msec) but a lower signal from the white (T2 = 90 msec) and grey matter (T2 = 100 msec).

Figure 1.11



T1-weighted image of the brain

T2-weighted image of the brain

1.4.1.6 *Magnetic field gradients and spatial localisation of tissue*

So far we have discussed, in broad terms, how an MR signal is produced from different tissue samples and explored the basic reasons behind tissue contrast on MR images. The MRI signal used to form these images is, however, a radio-wave, which carries no directional information. A number of complicated techniques are therefore used to resolve the location of individual tissue protons and produce a useful MR image. The most important of these are the three *magnetic field gradients* or *imaging gradients*. These are weak supplementary magnets embedded in the inner core of the main electromagnet. Relative to the patient they are arranged in the sagittal, coronal and axial planes. They are used as a) *slice selection gradients*; to identify the block of tissue to be excited by the RF pulse and b) as *phase and frequency-encoding gradients*; to resolve the source of the MR signal detected and localise it to an individual voxel within the tissue block.

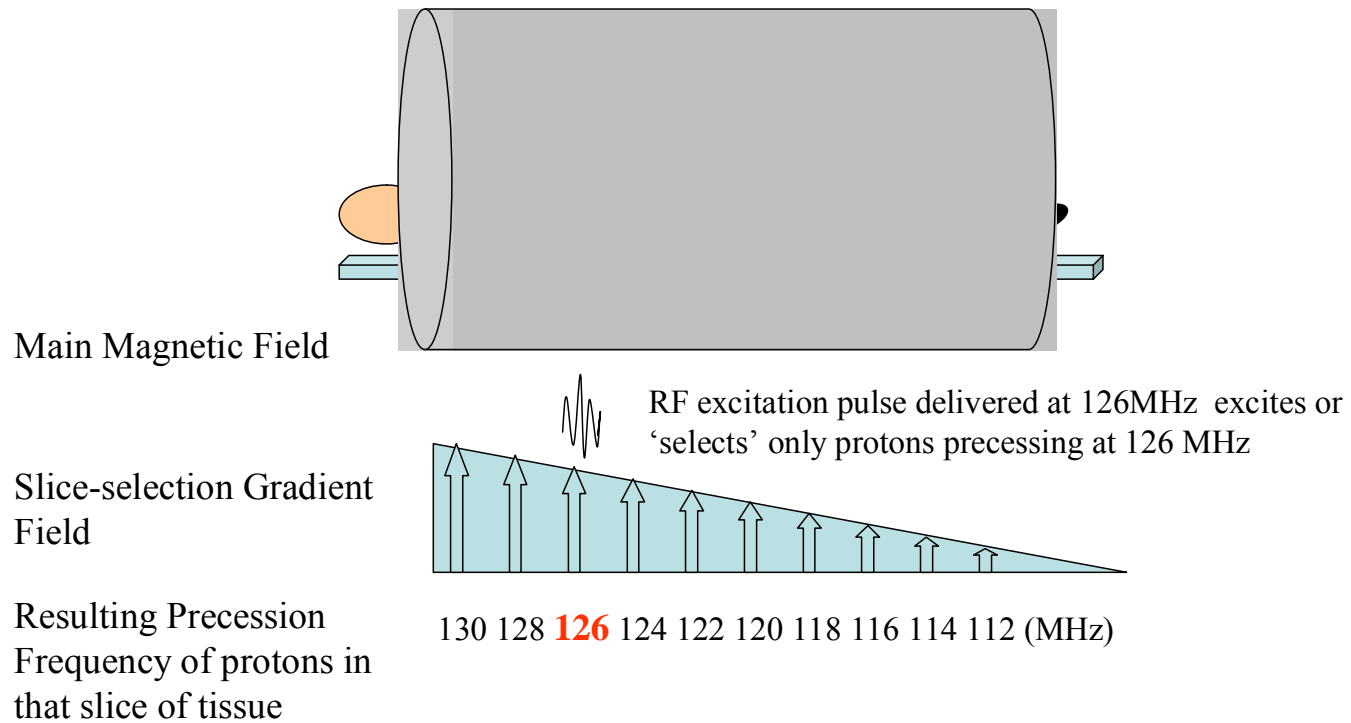
For the purpose of this discussion, we can assume that all of the tissue protons surrounded by the main magnetic field are spinning, or precessing, at the same frequency (since their precession frequency is directly proportional to the magnetic field strength they experience, as described earlier by the Larmor equation earlier, see section 1.4.1.1). If an additional, graded magnetic field is applied to these protons the total magnetic field they experience is altered; protons at the stronger end of the gradient field (which, therefore, experience the strongest total magnetic field) are made to spin faster than those at the weaker end. This effect of a gradient field can be used in two ways, as indicated above.

1.4.1.6.1 *Slice-selection gradients*

A magnetic field gradient can be applied at the same time as an excitation RF pulse to alter the precession frequency along a section of tissue protons. The excitation RF pulse will then only produce transverse magnetisation (and an MR image) in a small section of tissue protons which have been made to precess at exactly the right frequency, see figure 1.12 overleaf. Thus, a 'slice-selection' gradient is combined with the excitatory RF pulse to define the tissue to be imaged. This block can be selected in almost any plane using either, one of the gradients directly for axial imaging, or several of them in combination, for oblique imaging.

Figure 1.12

Diagrammatic representation of a slice-selection gradient. Protons at the stronger end of the gradient field precess at a higher frequency, proportional to the strength of gradient field. An excitation pulse frequency is chosen that matches the precession frequency of protons in the desired tissue slice (126 MHz in the example shown below) resulting an axial slice selection



1.4.1.6.2 *Frequency and phase encoding gradients*

Magnetic field gradients can also be used for the spatial localisation of tissue within the selected, one-dimensional, tissue slice. If a magnetic field gradient is applied along one axis of this tissue slice during MR signal measurement (contrast this with the slice-selection gradient which is applied during the excitation pulse) it will cause protons at the stronger end of the magnetic field to precess more rapidly than those at the weaker end. By this method the previously selected protons, which can already be localised in one-dimension via the slice-selection gradient, are 'encoded' in a second direction by their precession frequency during image measurement. This method is known as '*Frequency encoding*'.

For a useful MR image a means of localising tissue in a third dimension is required. The method used for this purpose is known as '*Phase encoding*'. It alters the phase (i.e. the position of individual protons as they spin around their axis at any one point, for example, 90°, 180°, 270°) of a portion of protons and uses this to identify their location within the tissue slice. The necessary alteration in phase is achieved by applying a brief gradient pulse in an axis perpendicular to the slice-selection and frequency encoding gradients. This produces a brief increase in the precession frequency of protons at the stronger end of the magnetic field and relative decrease in the precession frequency of those at the weaker end. Although these protons return back to a uniform precession frequency when the phase-encoding gradient is switched off, the phase of each one will be slightly different. The shift in phase produced is proportional to the strength of phase encoding gradient. Phase encoding pulses, or steps, are repeated for each column of tissue along this third dimensional plane to tag

each individual voxel of tissue. Strong frequency encoding gradients are a powerful method of resolving spatial differences between adjacent structures. Therefore, they play an important part in the production of the high fidelity, detailed images that MRI has become known for.

Thus, the combination of the slice selection (applied during the excitatory RF pulse), frequency encoding and phase encoding gradients (applied during MR signal measurement) provides a method uniquely tagging each proton in the imaged tissue block. This raw data that results must then be reconstructed to produce an actual MR image.

1.4.1.7 *K-space*

K-space can be described as temporary image space, in which digitalised data is deposited and stored during an MRI examination prior to image construction. K-space can be represented as a two-dimensional grid of points, on which the x-axis represents the frequency encoding gradient and y-axis is the phase encoding gradient see figure 1.13 on page 94-95. Although the two-dimensional K-space grid resembles a two-dimensional image of physical space it is essential to remember that K-space does not correspond directly to physical space. The analogue signal received during an MR examination is converted into digital information and encoded into grey scale blocks. Data is collected and deposited in K-space in horizontal lines, starting at the *centre* of the grid. Each line represents data collected during a single phase encoding step, or repetition time. As phase encoding steps are repeated with an alternating increases or decreases in the strength of the phase encoding gradient, a complete data

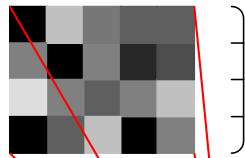
set is collected. Although the two-dimensional K-space grid resembles a two-dimensional MR image, individual data points in K-space do not correspond to individual image voxels. Rather, each data point in K-space contains information about every voxel of the tissue. Data points towards the periphery of K-space contain information on fine detail and edge detection, while those in the centre of K-space contain information on overall image intensity and tissue contrast. This reflects the fact that strong phase- and frequency-encoding gradients, which are represented at the extremes of the phase and frequency encoding axes in K-space are required to detect fine detail. Therefore, the data collected using these strong (positive or negative) phase encoding steps are laid down around the edges of K-space as data collection begins in the centre of the matrix and fans outwards. Once K-space has been 'filled', i.e. all of the required digital information has been collected, a detailed mathematical method known as Fourier Transform Image Reconstruction is used to convert the digitalised into a recognisable MR image.

The arrangement of data in K-space has implications for clinical MR imaging, particularly concerning spatial resolution and field of view (FoV). Higher spatial resolution requires an increased amount of data to be collected in the periphery of K-space. This is achieved by increasing the number of phase encoding steps and results in an increased size of K-space. Somewhat counter-intuitively, increasing the size of K-space does not result in an increased FoV. Rather, an increased FoV is achieved by filling K-space more densely, or reducing the space between data points. Since no data any further away from the centre of K-space are collected spatial resolution is unaffected.

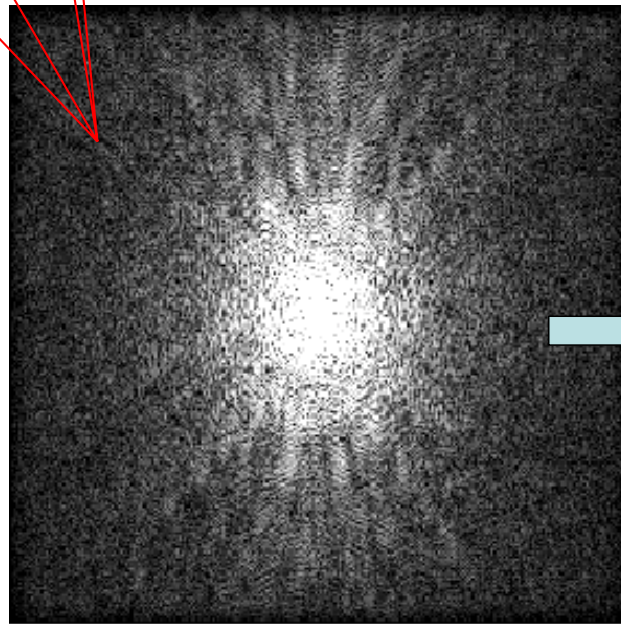
Figure 1.13, below

Diagrammatic representation of K-space. On the K-space grid, shown on the left, the x-axis represents the frequency encoding gradient and y-axis represents the phase encoding gradient. Data is deposited in K-space in horizontal lines, i.e. with consecutive phase encoding steps, starting the centre of the image. Fourier transform image reconstruction converts the digitalised data into a recognisable MR image.

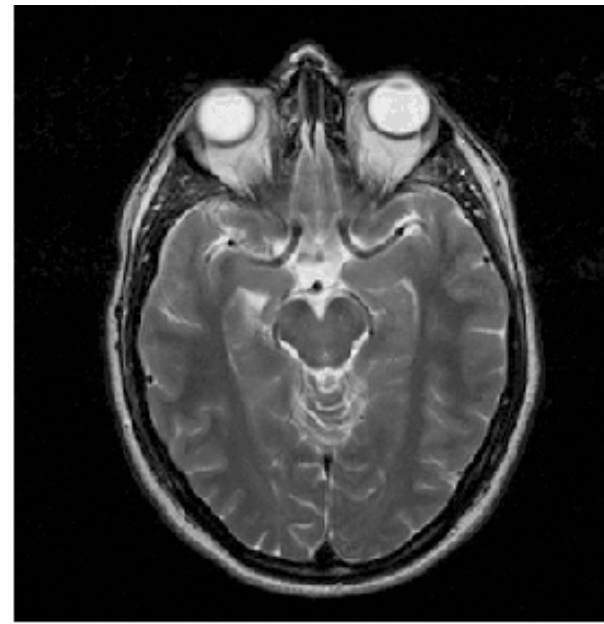
Figure 1.13



Grey-scale digital encoding of the analogue MR signal received during an MRI examination. Each line in K-space represents a different phase-encoding step



K-space formalism before Fourier Transform Image Reconstruction



Resulting MR image

1.4.1.8 *Pulse sequences*

So far, the basic components of the pulse sequences used to create MR images have been discussed. In the following sections the two most basic types of pulse sequences used in clinical MRI, and throughout this thesis, will be introduced.

1.4.1.8.1 *Gradient echo*

A gradient echo pulse sequence is comprised of an initial excitation RF pulse, executed in synchrony with a slice selection gradient, followed by measurement of an MRI signal or ‘echo’. The time between the creation of transverse magnetisation by the excitatory pulse and the measurement of this signal is known as the Echo time (TE) of the sequence. The MR signal is measured, within a receiver coil lying on the patient’s chest, immediately after a brief frequency encoding gradient and the signal is collected as the phase encoding gradient is pulsed repeatedly to localise the source of the signal. The time between two consecutive excitation pulse is known as the repetition time (TR).

Gradient echo techniques are able to achieve fast imaging times by using short TRs. They are, therefore, popular in CMR and are used in various forms in the experiments in this thesis. However, their short TR means that tissues retain transverse magnetisation (and thus produce a bright image) if either they have a short T1 or a T2 similar to, or longer than, the TR of the pulse sequence. Because T1 and T2 times of different tissues often run in parallel, simple gradient echo sequences, known as ‘unspoiled’ sequences result in images with both T1 and T2 contrast (known as T2/T1

weighting). All gradient echo sequences are sensitive to inhomogeneities in the main, and local, magnetic fields. They are therefore sensitive to $T2^*$, rather than true $T2$, contrast. Fluids and adipose tissue have the highest signal intensity on $T2/T1$ weighted images with all other tissues producing intermediate signal intensity. The Siemens unspoiled gradient echo sequence used in the experiments in this thesis is known as TrueFISP (Fast Imaging with Steady-state Precession).

If true $T1$ contrast is desired it is necessary to disrupt or 'spoil' any persisting transverse magnetisation prior to the next excitation RF pulse. Thus, 'spoiled' gradient echo sequences have been designed to incorporate an additional, 'spoiler', gradient pulse to dephase any residual transverse magnetisation and eradicate $T2$ contrast from the resulting image. The spoiler pulse is applied immediately after data collection and immediately before the next excitation pulse. The Siemens product used in the experiments in this thesis is known as TurboFLASH (Fast Low Angle Shot).

Gradient echo sequences are usually used for $T1$ contrast weighting. For this to be optimised TE should be kept as short as possible, to minimise $T2$ contrast from tissues with short $T2$. TR should also be short as it must be similar to, or shorter than, the $T1$ time of the tissues to be distinguished. However, as TR decreases, there is less time available to allow recovery of longitudinal magnetisation. Therefore, if signal intensity is to be maintained, the flip angle of the excitation pulse must also be reduced (to around the Ernst angle for that TR). Thus, gradient echo sequences tend to have short TRs and TEs and relatively low flip angles. This makes them ideally

suitable to CMR imaging which requires rapid pulse sequencing to allow acquisition of detailed cine images of the moving heart.

1.4.1.8.1 Spin Echo

Spin echo pulse sequences are very similar to simple unspoiled gradient echo sequences except for an additional 'refocusing' RF pulse which is applied in the middle of the TE. The purpose of this pulse is to reverse the phase difference in protons spins created by the slice selection gradient. This results in subsequent rephasing, or refocusing of protons spins. If signal measurement is timed to coincide with this event signal intensity can be maximised. Another advantage of spin echo is that it is more tolerant than gradient echo of main magnetic field inhomogeneity and that created by local imperfections (e.g. metal implants). Thus, spin echo is truly sensitive to T2 contrast, rather than T2*. The principal disadvantage of spin echo is the time required to incorporate the refocusing pulse. This tends to lengthen imaging times and limits the use of spin echo in cardiac MR. In other settings, the TR and TE of spin echo sequences can be adapted to produce T1 or T2 contrast.

1.4.2 Components of a modern CMR scanner

A detailed diagram of the components of a modern CMR scanner is provided in figure 1.14 (page 101) and the most relevant elements are summarised below. The scanner itself is comprised of a superconducting resistive electromagnet (made of Niobium, low resistance wire) bathed within supercooled liquid Helium (circulating at around -250°). The smaller gradient magnet coils are housed on the inner circumference of the

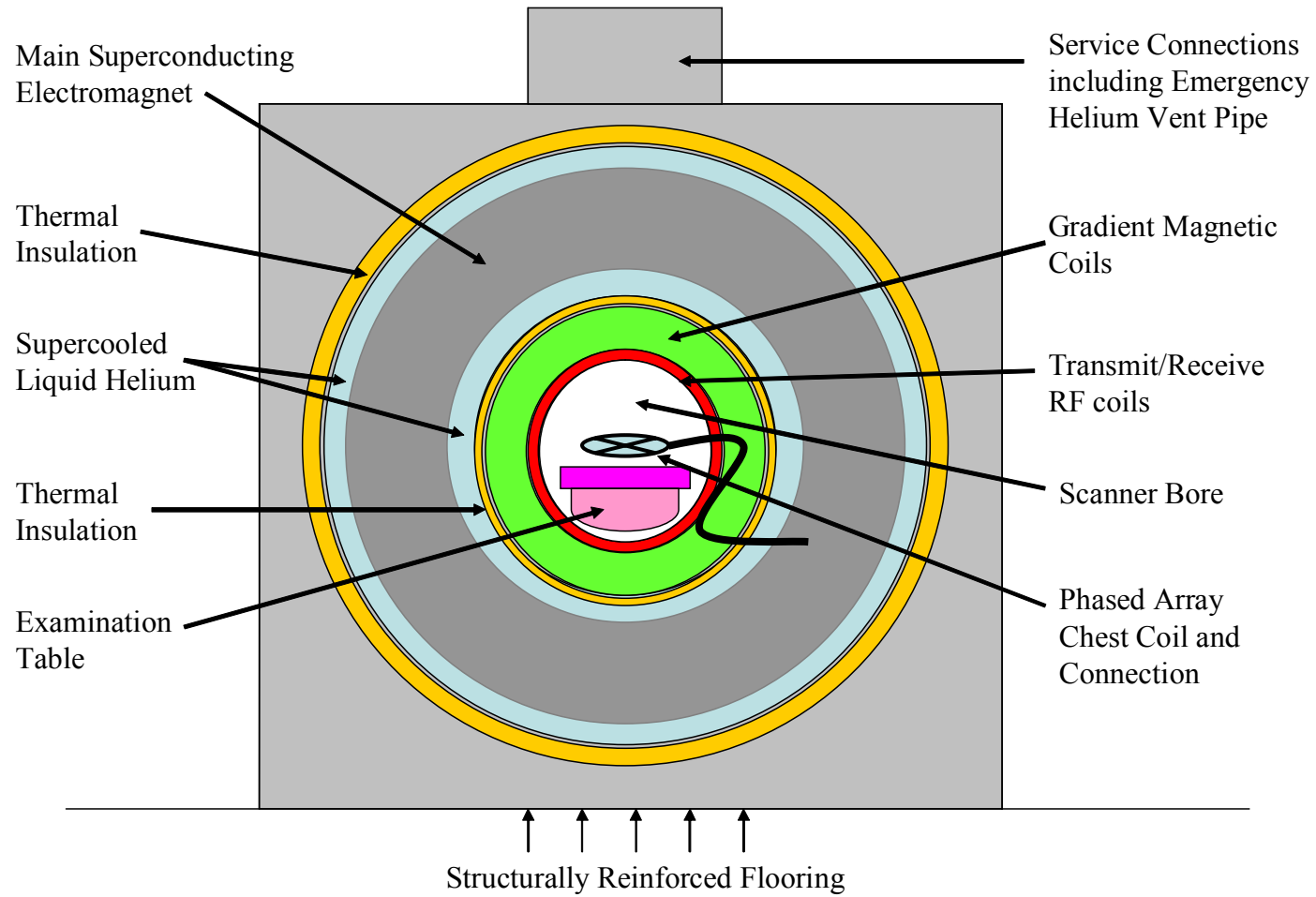
main magnet and the whole apparatus is enclosed within a copper lined room designed to deflect commercial radio waves that might interfere with its operation. Copper lined channels in one wall of this box allow transmission of tubing from infusion pumps in the control room and the delivery of drugs or oxygen to the patient during scanning. The floor beneath the MR scanner must be reinforced to accommodate the weight of the main electromagnet.

The MR signal is received by a phased array chest coil. This is a dedicated receiver coil that lies on top of the chest. It contains several component coils, the arrangement of which is designed to maximise MR signal strength but minimise interference from tissue movement and system noise (i.e. optimise the signal to noise ratio). ECG-gating is used to synchronise imaging cycles with the motion of the heart. The R wave of a 3-lead ECG, recorded continuously, is used to trigger the excitatory RF pulse. Gradient echo sequences, which have a short TR, can be used to generate video-quality cine loops. This capability has revolutionised cardiac imaging as end-diastolic and end-systolic phases can be defined on the resulting cine images and end-diastolic and end-systolic volumes can be accurately measured using methods that will be described in the sections that follow. Individual lines of K-space (representing individual phase encoding steps) are filled during consecutive heart beats; therefore each cine loop takes at least 5 cardiac cycles to complete, depending on the sequence being used. To minimise motion artefact on the resulting images, patients are asked to hold their breath in expiration during most gradient echo cine sequences. In longer pulse sequences this is not possible and the patient must be allowed to breathe freely, but they are asked to do so as smoothly as possible.

Once the predetermined K-space volume has been filled, the digital data is fed into a 'Reconstructor' computer which performs the Fourier Transform Image Reconstruction and generates pixelated grey-scale data that is presented to the user on a flat screen monitor as a completed MR image. During any MR examination the user can alter the operation of the gradient coils and select a variety of pulse sequences using a modified keyboard and mouse. Individual parameters within these sequences, e.g. TR, TE, flip angle, can be modified as the operator desires. Images can be saved to an internal database and to external compact disc and floppy disc drives. The same PC workstation can be used for image analysis using the necessary software.

Figure 1.14

Components of a modern MRI scanner



1.4.3 *Previous application of CMR in patients with PH*

Recent years have seen the publication of numerous studies demonstrating the capabilities of CMR imaging in the assessment of patients with PH.

1.4.3.1 *Right ventricular volumes, function and mass*

Using CMR, image acquisition is possible in almost any plane, at almost any angle. Rapidly acquired gradient echo sequences allow description of the complicated RV cavity by a series of short axis cine images extending from the atrioventricular valve plane to the cardiac apex. Planimetry of the end-diastolic and end-systolic images in these cine series, and summation of the resulting end-diastolic and end-systolic volumes allows direct, accurate and reproducible measurements of RV volume to be recorded (97, 98). RV end-diastolic (RVEDV) and end-systolic volumes (RVESV) can then be used to determine ejection fraction ($RVEF = \frac{RVEDV - RVESV}{RVEDV}$). These CMR measurements have been shown to be more accurate than similar values determined using echocardiography in patients with PH (99, 100). The superiority of CMR imaging reflects the flawed modelling assumptions regarding RV shape that echo relies on to extrapolate three-dimensional results from two-dimensional data.

RV mass can also be determined using CMR imaging with great accuracy. The high fidelity images generated by CMR allows the thin volume of tissue between the endocardial and epicardial surfaces of the RV to be defined and measured by a similar planimetric method used for ventricular volumes. The accuracy of CMR-derived RV mass has been verified against subsequently explanted bovine hearts (101). In

humans with PH, RV mass is increased (101), and correlates with mean pulmonary artery pressure measured invasively (102). Thus, CMR is the gold standard method of measuring RV volumes, ejection fraction (103) and mass (101) in patients with PH.

1.4.3.2 Contrast enhanced-CMR imaging

Studies conducted in the 1980s and 90s demonstrated that areas of myocardial injury (usually ischaemic injury in the models used) exhibited higher signal intensity on CMR images than regions of normal myocardium. This was true for T2-weighted images which did not require contrast enhancement and T1-weighted images after administration of a paramagnetic contrast agent such as Gadolinium. Gadolinium has the effect of shortening the T1 time of injured, or abnormal, myocardium, resulting in T1 contrast on appropriately timed T1-weighted gradient echo images.

The early non-contrast T2-weighted images used Spin Echo techniques and image quality was severely degraded by respiratory motion artefact which was unavoidable because the sequences took too long to acquire for the patient to breath-hold. Superior image quality and better contrast between areas of normal and injured myocardium was found when faster, gradient echo sequences were combined with Gadolinium contrast administration. Various contrast enhanced gradient echo sequences have been tested in patients with a variety of myocardial abnormalities. Most of the evidence has been collected in ischaemic injury models in which (in both animals and humans) the breath-hold segmented inversion recovery TurboFLASH (Fast Low Angle Shot) technique used in Chapter 4 of this thesis has performed best.

Using this technique, contrast enhanced images are acquired 5-10 minutes after the administration of intravenous Gadolinium to allow the contrast agent to perfuse the relevant tissues. Images are only acquired during diastole; minimising cardiac motion artefact. Importantly, an inversion pulse is applied before image acquisition to tip the net magnetisation vector of the myocardial tissue protons out of the longitudinal plane (where it resides at equilibrium) a full 180°, rotating the vector through the transverse plane (where signals can be detected, but are not sampled during this manoeuvre) back into the longitudinal plane ‘facing’ in the opposite direction. A variable time delay (known as the Inversion Time) is then allowed during which the net magnetisation vector rotates back into the transverse plane (T1 recovery) on it’s way back to equilibrium. A TI is chosen to produce nulling (i.e. minimum signal and, therefore minimum image intensity) within areas of normal myocardium, at which point as many K-space lines as possible are sampled before the onset of ventricular systole. The appropriate TI can be estimated from a series of test images acquired using a range of TIs. This process is repeated during consecutive heart beats until the required K-space volume is filled, hence the ‘segmented’ nature of the sequence. In most patients 8-12 heart beats, per breath-hold, are required to allow enough time for collection of the necessary K-space volume. Tissue contrast on the resulting images is determined by the T1 characteristics of the tissues being imaged and length of the TI. Gadolinium is avidly retained in abnormal myocardial regions resulting in a shortened T1 and increased signal intensity. The bright areas on the resulting images are described as areas of delayed contrast enhancement (DCE) (because of the time delay between contrast administration and image acquisition).

Delayed contrast enhancement (DCE) is not biologically specific and has been described in a variety of illnesses using similar CMR sequences to the one described above. Myocardial infarction, fibrosis and inflammation have all been shown to result in delayed contrast enhancement using Gadolinium as an intravenous CMR contrast agent (104-108). The physiological mechanism(s) responsible for DCE are the subject of much ongoing debate and investigation. Gadolinium (as Gadolinium-diethylene triaminepentaacetic acid (Gd-DTPA)) is a large molecule (> 800 kDa) and following intravenous injection it remains within the extracellular fluid compartment (109). DCE is therefore thought to result from delayed clearance of gadolinium from a relatively expanded extracellular volume within fibrotic or necrotic myocardial compartments (110, 111). This lack of biological contrast specificity necessitates histopathological correlation with areas of DCE at ce-CMR to be sure of the substrate within these areas. This has been achieved in Myocardial Infarction (112) and Hypertrophic Cardiomyopathy (113) (see the following sections for details) but in situations where such evidence is not available a hypothesis on the significance of DCE must be constructed based on other evidence.

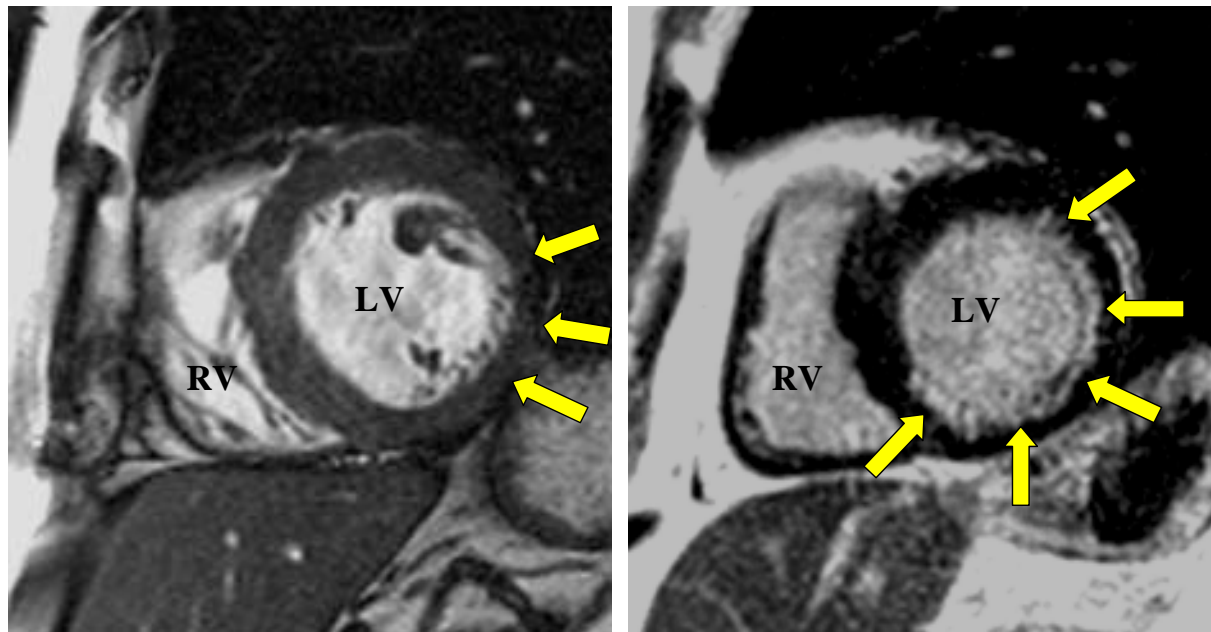
1.4.3.2.1 Myocardial infarction

DCE in acute myocardial infarction is usually localised to a coronary artery distribution and characteristically involves the subendocardial portion of the myocardium, extending transmurally depending on the size of the infarct (see figure 1.15 on page 107 for an example). The total volume of enhancing tissue corresponds closely to infarct size at autopsy (104, 108, 114), serum NT-proBNP (115) and Troponin concentrations (116), the extent of associated LV systolic dysfunction (116)

and the subsequent prognosis of the patient (107, 117). Recent research has demonstrated that DCE that extends to over 50% of the thickness of the ventricular wall is likely to be non-viable, i.e. it is unlikely to recover contractile function (118). The biological significance of DCE following myocardial infarction has been debated over recent years. Most researchers agree that DCE in this context reflects an increased volume of distribution for gadolinium as a result of disrupted cell membranes due to cellular necrosis (119). The intensity DCE tends to decrease following acute myocardial infarctions. Chronic myocardial infarction can be distinguished by associated thinning of the infarcted wall.

Figure 1.15

An example of sub-endocardial delayed contrast enhancement (DCE) in a patient with acute inferolateral myocardial infarction. The post contrast image on the right was acquired using a breath-held segmented inversion recovery TurboFLASH (Fast Low Angle Shot) technique similar to that used in Chapter 4 of this thesis.



Pre-contrast short axis CMR image showing thinning of the infarcted lateral LV wall (arrowed)

Post-contrast short axis image at the same slice position showing inferolateral sub-endocardial DCE (arrowed)

1.4.3.2.2 *Hypertrophic cardiomyopathy*

DCE has been described in several studies of patients with Hypertrophic Cardiomyopathy (HCM) using ce-CMR (106, 113, 120). These studies demonstrate typically patchy, mid-wall (as opposed to subendocardial) contrast enhancement in various areas throughout the heart. Common sites for DCE include the RV insertion points and the interventricular septum (120). These correlate with earlier autopsy findings in patients with HCM which reported gross muscle fibre disarray and destruction of the circumferential, mid-wall component of the ventricular myocardium at the RV insertion points (121). The biological significance of DCE has also been confirmed prospectively in patients with HCM by the comparison of ce-CMR images with histology from subsequently transplanted hearts. These studies confirm that DCE in HCM correlates with areas of increased myocardial collagen (113). An example of DCE in HCM is presented overleaf in figure 1.16.

1.4.3.2.3 *Myocarditis*

Myocarditis results from a variety of infectious or inflammatory insults, although the cause in individual patients is often unknown. Typically patients present with central chest pain, an abnormal ECG and, often, a rise in Troponin and/or evidence of ventricular dysfunction. As a result, differentiation between myocarditis and acute MI can be difficult on clinical grounds alone. Ce-CMR allows reliable discrimination between these two entities (105). Myocarditis typically produces diffuse, mid-wall DCE in a distribution not typical of a coronary artery territory. An example of DCE in a patient with acute myocarditis is presented in Figure 1.17 on page 110.

Figure 1.16

An example of patchy, mid-wall delayed contrast enhancement (DCE) in a patient with Hypertrophic Cardiomyopathy (HCM). The post contrast image on the right was acquired using a breath-held segmented inversion recovery TurboFLASH (Fast Low Angle Shot) technique similar to that used in Chapter 4 of this thesis.

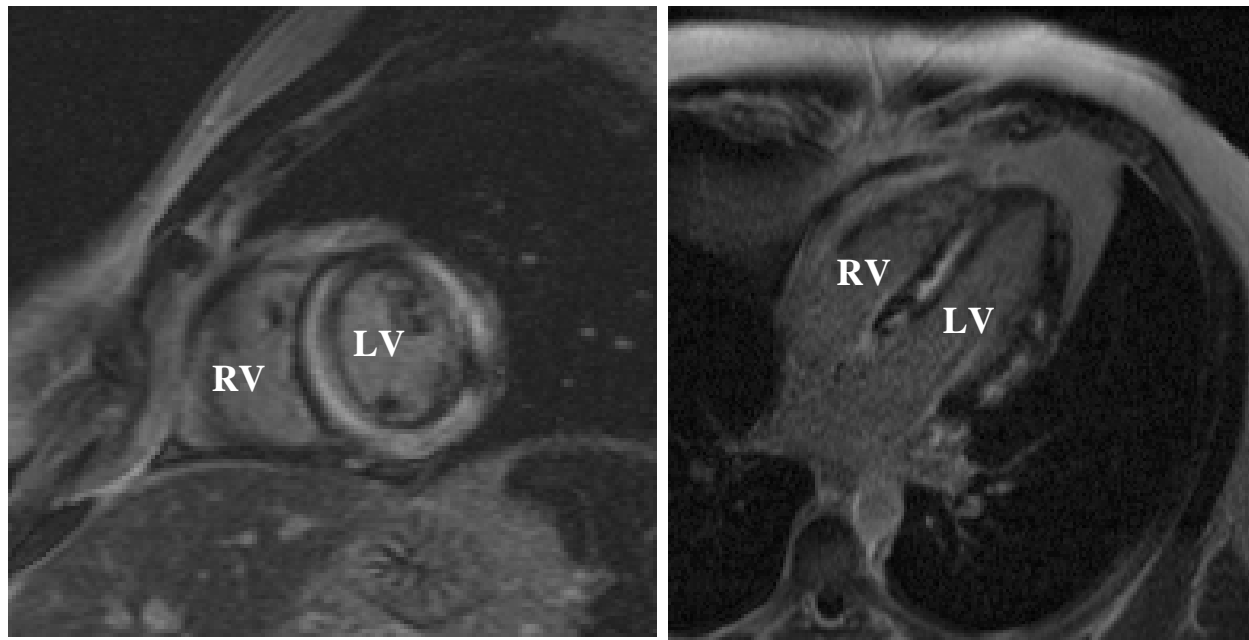


Pre-contrast short axis image showing hypertrophy of both RV and LV myocardium in a patient with HCM

Post-contrast image at the same slice position showing diffuse mid-wall DCE in various areas including the RV insertion points (arrowed)

Figure 1.17

An example of mid-wall delayed contrast enhancement (DCE) in a non-coronary artery distribution in a patient with acute myocarditis. These images were acquired using a breath-held segmented inversion recovery TurboFLASH (Fast Low Angle Shot) technique similar to that used in Chapter 4 of this thesis.



Post-contrast short axis image showing bright mid-wall DCE typical of acute myocarditis

Post-contrast horizontal long axis image showing further evidence of acute myocarditis in the same patient

1.4.3.3 *Right ventricular stroke volume and Pulmonary Artery Flow Mapping*

RV stroke volume can be determined using CMR imaging by simply subtracting RVESV from RVEDV. This technique can, however, result in overestimation of RVSV in patients with PH. This is because Tricuspid valve Regurgitation (TR) is common in PH and results in a significant proportion of the ejected blood volume travelling backwards through the incompetent tricuspid valve. Velocity encoded (or phase-contrast) flow mapping is a more precise means of measuring RVSV in PH patients. Protons within a moving column of blood acquire a difference in their phase of rotation as they move through a magnetic field gradient (because the strength of the magnetic field is higher at one end than it is at the other). The amount of the phase difference acquired is directly proportional to the velocity of blood flow. This principle can be used to encode moving protons within large vessels with velocity information which can be read using a phase-contrast MR sequence. Blood flow can be determined by integrating velocity within each tissue voxel and time. RV stroke volume can thus be computed by integrating blood flow data from the proximal main pulmonary artery with the area of the vessel. The necessary information is encoded within two sets of images, a set of 'velocity' images containing the phase-contrast data and a set of 'anatomical' cine images which are used to define the area of the target vessel using planimetry. This method has been shown to be accurate and reproducible in PH patients (122, 123). An identical flow map acquired across the proximal aorta can be used to quantify LVSV in the same patient. Velocity encoded flow mapping is used to precisely define right and left ventricular stroke volume

during dobutamine stress-CMR imaging in Chapter 5 of this thesis. The sequences used are discussed in more detail in the methods section.

1.4.3.4 Dobutamine stress-CMR imaging

Uniquely, CMR facilitates high quality imaging of right and left ventricles simultaneously. This capability provides an excellent opportunity to study cardiac physiology and the interaction between the two ventricles during exercise. However, true exercise-CMR images are degraded by movement artefact during physical activity, meaning that accurate images can only be acquired immediately following exercise. Dobutamine stress-CMR (ds-CMR) offers an alternative approach; it allows true stress measurements to be made and avoids potential errors relating to exercise recovery. Dobutamine approximates physiological conditions during exercise in PH patients by increasing cardiac output (124). It is a pure inotrope with no flow-independent effects on pulmonary vascular tone (125). In earlier studies, ds-CMR has been used successfully in patients with congenital heart disease (126-128) However, it has yet to be used in patients with PH due to other causes.

1.5 Hypotheses and aims of this thesis

The overriding aim of this thesis was to generate new and clinically relevant information regarding RV function in PH using CMR imaging. To this end, three separate, but related experiments were performed; see Chapters 3, 4 and 5. The hypothesis of each study is explained below.

Chapter 3: ‘Definition of an NT-proBNP threshold for the non-invasive detection of RV systolic dysfunction in pulmonary hypertension.’ A close correlation between BNP/NT-proBNP concentration and RV systolic function has been demonstrated before in patients with PH (91, 92, 135, 163). In earlier studies, a similar relationship with LV systolic function (79) was described in patients with left heart failure, in whom a threshold value for NT-proBNP, indicative of LV systolic function has been defined (83-85). As a result, NT-proBNP has been incorporated, as a simple, non-invasive test for heart failure in recent diagnostic algorithms (87, 88). The principal hypothesis of this study was that a similar NT-proBNP threshold could be identified for RV systolic dysfunction in patients with PH using CMR imaging as the reference method for RV systolic function.

Chapter 4: ‘Contrast enhanced-Cardiovascular Magnetic Resonance imaging in patients with severe Pulmonary Hypertension’. Delayed contrast enhancement (DCE), detected using contrast enhanced-CMR (ce-CMR), is a well established marker of myocardial abnormalities myocardial infarction, fibrosis and inflammation (104-108). The principal hypothesis of this study was that discrete myocardial abnormalities would exist in patients with PH and that this information might provide some new insight into the mechanisms of RV failure in this condition.

Chapter 5: ‘Dobutamine stress-Cardiovascular Magnetic Resonance imaging (ds-CMR) in patients with Pulmonary Hypertension’. Exercise limitation is common in patients with PH (129). Earlier studies clearly demonstrate that poor exercise tolerance in PH is related to an inability to increase cardiac stroke volumes (47, 130). However, the reasons for this are not well understood. The principal hypothesis of this

study was that ds-CMR imaging could be used to identify reason(s) for right and left ventricular stroke volume impairment during exercise in PH patients.

Chapter 2

Materials and Methods

2.1 Patient Recruitment

The patients involved in the studies in this thesis were recruited during the course of their routine diagnostic assessment for suspected PH at the Western Infirmary, Glasgow, UK. All patients had been assessed first in an out-patient pulmonary vascular clinic; those in whom a diagnosis of PH was suspected were offered a one-week elective admission for further assessment. All subjects were asked to participate in the studies reported in this thesis on the Monday of their admission and those who agreed, gave informed written consent to a study protocol that had been approved by the ethics committee of the West Glasgow Hospitals University NHS Trust, see figure 2.1 on pages 118-120. In total, 71 patients were recruited, although only 48 completed one or more of the experiments described herein. 8 patients did not undergo CMR imaging; either because they withdrew consent or because of technical problems with the scanner on the day of their examination. 15 patients were excluded before their MR images were analysed. This reflected the fact that patients were recruited and underwent MR imaging before a definitive diagnosis was made (after right heart catheterisation) and patients with a primary diagnosis other than PH were excluded. A flow chart describing patient recruitment and study completion is provided in Figure 2.2 on page 121. Thus, inclusion criteria included a diagnosis of PH reached by conventional diagnostic methods (57, 64) and informed written consent. Additional specific exclusion criteria were used for each experiment performed. These will be discussed in the relevant chapters and a demographic description of each study population will be provided. For all studies, CMR-related exclusion criteria were applied. These included an indwelling cardiac pacemaker, claustrophobia and pregnancy.

In all three of the experiments in this thesis, control subjects, with no history of any cardio-respiratory disease underwent CMR imaging to provide local control values for ventricular dimensions and function. All controls were staff of the Western Infirmary (Glasgow, UK) and were subject to the same exclusion criteria as the PH patients in each study. Controls were approached individually and asked to participate. All controls gave informed written consent but did not undergo right heart catheterisation or any other tests

Figure 2.1

Information sheet and consent form used in recruiting patients to the studies in this thesis

Brief Title of Project

The Non-invasive assessment of Pulmonary Hypertension using Cardiac MRI

Background

Pulmonary Hypertension is a rare and potentially serious condition. It is often difficult to diagnose and to treat. The major problem in Pulmonary Hypertension is high blood pressure in the lungs; this often leads to excessive stress being exerted on the right hand side of the heart. Sometimes, as a result of this, the right side of the heart becomes unable to pump blood into the lungs, as it should. This obviously can make the patient feel very unwell.

We usually make the diagnosis after a number of tests have been carried out; the most important of these currently is a **Right Heart Catheter**. This involves passing a plastic catheter into the heart through a vein in the neck or groin. Through this catheter we can measure the blood pressure in the lungs and assess how well the heart is pumping. We can also assess how likely that patient is to respond to treatment.

This test is very useful and generally safe, but some patients find it unpleasant and it there are some risks involved. We therefore do not tend to repeat it to see how well or badly a patient is doing unless it is absolutely necessary. Instead, we use a test that measures how far a patient can walk in six minutes. We then compare this measurement to the last one to say whether they are better or worse. This test is useful but can sometimes be misleading.

Because the catheter is done with you at rest it can also not pick up very early problems. Doing measurements whilst you are active makes the test more sensitive, but this is difficult to do accurately and safely with this procedure.

The Study

We are conducting a study looking at new ways to diagnose and monitor patients with Pulmonary Hypertension. We would like to invite you to take part. The study involves the use of a relatively new scanning technique called **MRI (Magnetic Resonance Imaging)**.

MRI allows us to get a lot of useful information about Pulmonary Hypertension. It does not use any X-rays or radiation, but instead uses magnets to acquire detailed images of the pulmonary blood vessels and the heart. It is therefore very safe. We can get a lot of the same information using MRI that we get at right heart catheterisation. We can combine the scan with a drug called **Dobutamine** that simulates conditions of exercise. This drug should help the scanner pick up early Pulmonary Hypertension. **Gadolinium** is a clear fluid like water. It is used in MRI scanning as it accumulates for a short time in abnormal tissue and lights up that area up so that the scanner can detect this part of the body. It is therefore useful in telling us

which part of the blood vessels and heart are affected. After a short while Gadolinium fades away and is removed from your body (within a few hours).

Compared with right heart catheterisation, MRI is safer, and patients tend to find it less unpleasant. This means not only could MRI be used in the diagnosis of Pulmonary Hypertension, we would be happier to repeat it in the future. This may allow us to better identify changes in the illness over time and so allow better tailoring of your treatment.

In addition to the MRI we would like to measure certain proteins in your bloodstream that we think may go up and down depending on how well you are.

What the study involves

During your 5-day stay at the Western Infirmary you will have a number of tests, including blood samples and x-rays. On the Thursday you will have your right heart catheterisation. We would propose doing an MRI scan at some time during this week. The scan would take around 1 1/2 hours and it would not prolong your stay in hospital. We will take some extra blood samples in addition (around one tablespoon in total). These samples will be taken off at the same time as your routine bloods and won't involve any extra needles.

What does the MRI involve?

On arrival at the **Clinical Research Initiative (CRI)** a radiographer will go through a safety checklist and make sure that all magnetic objects (e.g. jewellery and bankcards) have been removed. Following this you will be asked to sign the consent form. Once you have changed into a hospital gown you will then be asked to lie flat on the bed that will move into the scanner. The scanner is basically tunnel shaped, like a large "polo" mint. You are slid into the centre of the "polo" on an electric bed and the scans are acquired. Some people find it a little enclosing, but you can come out at any time.

Before you go into the scanner a small plastic cannula (similar to that used when putting up a drip) will be inserted into your vein. This allows us to give you a harmless dye called **Gadolinium** and a medicine called **Dobutamine**. A doctor will insert the cannula. During the scan we will inject some Gadolinium dye into the drip in your arm, this will help light up your blood vessels and heart muscle on the pictures. We will also run an infusion of the drug mentioned, Dobutamine; this will cause your heart to pump faster as if you were out walking. The initial dose of this drug is very small and we will only increase it slowly up if you are comfortable. This will allow us to assess how well the right side of your heart is pumping. After around 25 mins the Dobutamine will be stopped. A doctor will be in the control room throughout this procedure. When you are in the scanner you will need to wear a pair of headphones, allowing you to listen to music of your choice (you are welcome to bring your own CD) and to allow us to communicate with you throughout the scan. The headphones are also necessary because of the loud knocking noise that occurs when the pictures are being taken. You will be given an emergency buzzer and can very quickly be taken out of the scanner should you feel uncomfortable or if it is felt necessary. During the scan you will be asked to hold your breath at times to improve the quality of the pictures.

What are the risks?

- The MRI scanner is very safe as long as you have no metal implants in your body
- The side effects of Dobutamine tend to occur at higher doses than we are using. These include changes in your heart rhythm, light-headedness and nausea. Your heart rate and blood pressure will rise; this is the desired effect as this mimics exercise. You will be closely monitored throughout the procedure and a senior doctor will be present to ensure your safety
- The dye used is called Gadolinium. It is generally harmless and will be washed out of your system by your kidneys. Rarely it can cause headaches.

NB

- **You should not take part in this study if you are pregnant**
- **If you wish to take part in this study, your General Practitioner will be advised of your participation and the clinical management that you will undergo**
- **If you do not wish to participate in this study, or wish to withdraw at any time your care will in not, in any way, be affected**

If you have any questions regarding the study please contact Dr KEVIN BLYTH at 0141 211 1812

WEST ETHICS COMMITTEE

FORM OF CONSENT FOR PATIENTS/VOLUNTEERS IN CLINICAL RESEARCH PROJECT

Title of Project : The Assessment of Pulmonary Hypertension using Cardiac MRI

By signing this form you give consent to your participation in the project whose title is at the top of this page. You should have been given a complete explanation of the project to your satisfaction and have been given the opportunity to ask questions. You should have been given a copy of the patient information sheet approved by the West Ethics Committee to read and to keep. Even though you have agreed to take part in the research procedures you may withdraw this consent at any time without the need to explain why and without any prejudice to your care.

Consent:

I,.....(PRINT)

of.....

give my consent to the research procedures above, the nature, purpose and possible consequences of which have been described to me

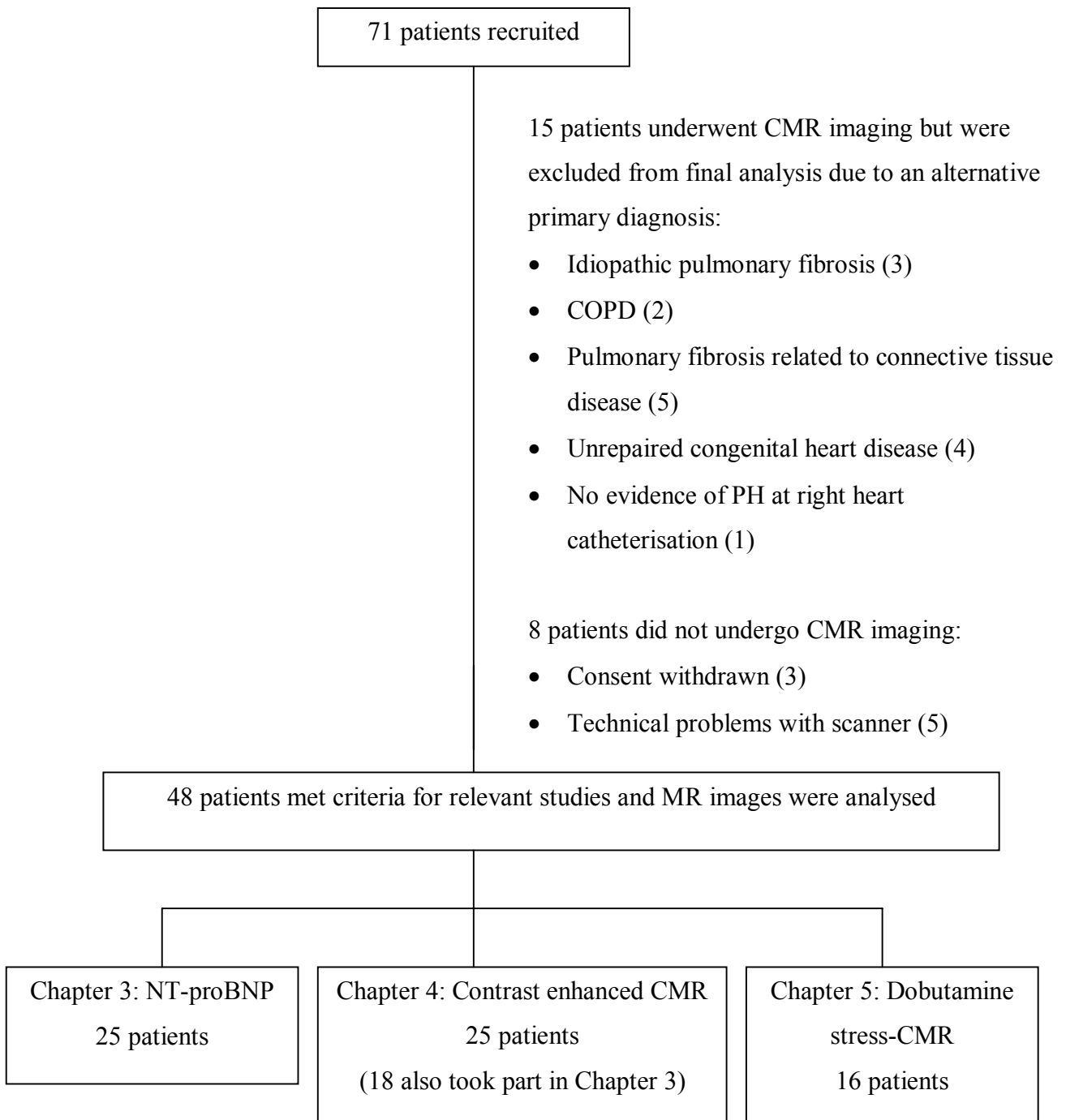
by.....

Patient's signature.....Date.....

Doctor's signature.....

Figure 2.2

Description of patient recruitment for the three experiments described in this thesis



2.2 Routine diagnostic assessment

2.2.1 Non-invasive assessment

During their one week stay, all patients underwent a series of tests following standard diagnostic algorithms for PH (57, 65). These included routine blood tests, 12-lead electrocardiogram, chest radiograph, transthoracic echocardiogram, lung function and six-minute walk tests, ventilation/perfusion (V/Q) scan, High Resolution CT scan and a CT Pulmonary Angiogram (CTPA). These investigations were performed using the facilities at the Western Infirmary and the adjacent Gartnavel General Hospital

2.2.2 Right heart catheterisation

Right heart catheterisation was performed in the laboratory at the Western Infirmary on the Thursday afternoon of the admission week. In patients who were prescribed diuretics or Calcium Channel Blockers, these were stopped the day before. On the Thursday morning an 8F introducer sheath was inserted into the right internal jugular vein under ultrasound guidance (Site-Rite 4, Bard Access Systems, Salt Lake City, USA). Anxious patients were occasionally prescribed a short acting Benzodiazepine, but in general, no pre-medication was used. Right heart catheterisation was performed using a 7F triple-channel thermodilution Swan Ganz catheter (Baxter Healthcare, Irvine, California, USA). All measurements were recorded with the patient in a supine position, at rest, breathing room air. These included mean right atrial pressure (RAP), right ventricular pressure and systolic and diastolic pulmonary artery pressures (PAP). Mean PAP was determined as the area under the PAP trace.

Pulmonary artery occlusion pressure was recorded with the catheter in the wedge position and the balloon inflated. Cardiac output (CO) was determined by thermodilution, allowing the determination of pulmonary vascular resistance (PVR) by the following: $(\text{mean PAP} - \text{PAOP})/\text{CO}$. Cardiac index was determined as $\text{CO}/\text{body surface area}$. If, after review of the V/Q scan and CTPA prior to catheterisation, suspicion remained regarding the presence of thromboembolic disease, selective pulmonary angiography was also performed in the catheterisation laboratory.

2.3 Cardiovascular Magnetic Resonance imaging

I performed all of the MR scans in this thesis after completing the Magnetic Resonance Imaging Basic Competencies course run by the Institute of Physics and Engineering in Medicine. The earlier scans were performed under the guidance Ms. Tracey Steedman, Cardiac MR Radiographer, Western Infirmary. All scans were performed a 1.5 T Siemens Sonata whole body MR scanner (see figure 2.3, overleaf).

Figure 2.3

Ms. Tracey Steedman (Cardiac MR Radiographer) positioning a patient before a scan using the Siemens Sonata 1.5 Tesla system at the Western Infirmary, Glasgow. The examination table is extended and the phased-array chest coil has been secured over the patient's chest using Velcro straps



2.3.1 *Patient preparation and positioning*

Before entry into the MR scanning room the patient was asked to complete and sign a safety questionnaire, see figure 2.4 overleaf. If they reported previous injuries involving metal fragments, especially any to the eyes, appropriate plain radiographs were requested to ensure that none remained. Patients were asked to change into surgical 'blues' and a 21 G intravenous cannula was placed in either the right or left antecubital fossa. This was used for contrast or dobutamine administration, depending on the study being performed.

The patient was asked to lie supine on the examination table, which had been remotely removed from inside the bore of the magnet, to a more accessible position, see figure 2.3. Adhesive monitoring pads for the 3-lead ECG were connected, and the phased array chest coil was placed on the patient's chest and secured in place with a loose fitting Velcro strap. The patient was then supplied with an emergency buzzer and protective ear-defenders. Immediately before movement of the patient inside the bore of the magnet, the centre of the chest coil, approximating the position of the heart, was defined by a laser pointer attached at the 12 o'clock position of the magnet's inner circumference. This point of reference was used to move the patient to a precise point within the bore of the magnet which ensured that their heart was at the centre of the main magnetic field. Once the patient was inside the bore of the magnet, the door of the scanning room was sealed and the staff performing the scan retreated to the control room. Proper functioning of the microphones and headphones that allow direct communication between patient and operator was verified before image acquisition was initiated

Figure 2.4

The safety questionnaire completed by all patients before entry into the scanner room

	<h2 style="margin: 0;">Glasgow Cardiac MR Unit</h2> <h3 style="margin: 0;">Safety Checklist: - <i>STAFF & VISITORS</i></h3>	
Name: _____		Date: ____/____/____
Reason for visit: _____		
<p>Have they ever:</p> <p>Had a cardiac pacemaker? YES NO</p> <p>Had any surgery to their heart? YES NO</p> <p style="padding-left: 20px;">• If yes, give details: _____</p> <p>Had any surgery on their head, brain or eyes? YES NO</p> <p style="padding-left: 20px;">• If yes, give details: _____</p> <p>Had any surgery involving the use of metal implants, plates, or clips? YES NO</p> <p style="padding-left: 20px;">• If yes, give details: _____</p> <p>Had any surgery involving the use of electronic, mechanical or magnetic implants? YES NO</p> <p style="padding-left: 20px;">• If yes, give details: _____</p> <p>Worked with metal or had metal fragments in their eyes? YES NO</p> <p>Had metal fragments in any other part of the body? YES NO</p> <p>Ladies only:</p> <p>Possibility of being pregnant? YES NO</p>		
<p>Before entry into the examination room all metal objects must be removed:</p> <p>Metal tools Scissors, keys Watches, pagers Credit Cards, coins Hair clips, hearing aid</p> <p>Have you removed all objects from your person? YES NO</p>		
<p>I confirm that the answers to the above safety questions are correct.</p> <p>Signature: _____ Date: ____/____/____</p>		
<p>Signature of Authorised Staff who has taken person through checklist</p>		

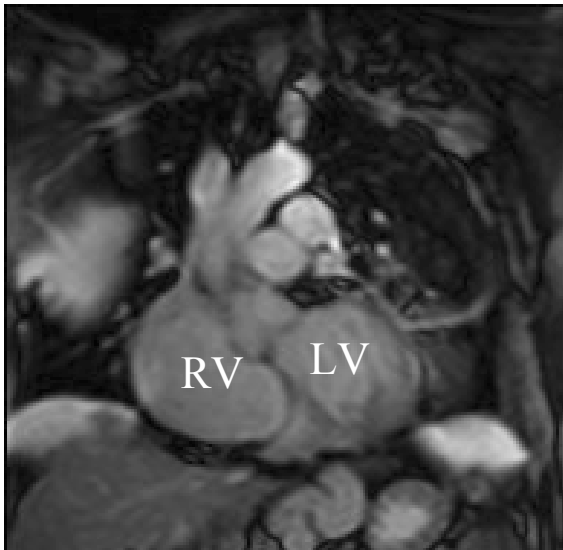
2.3.2 *CMR image acquisition*

2.3.2.1 *Standard imaging*

The following core imaging protocol was followed in all subjects. Fast imaging with steady state precession sequences (marketed as ‘TrueFISP’ by Siemens) were used to generate the initial axial scout images (see figure 2.5 overleaf) required to localise the heart within the thoracic cavity and all subsequent cine images. Vertical- and horizontal-long axis (VLA and HLA) cines (see figures 2.6 (page 129) and 2.7 (page 130), respectively) were planned and acquired based on the scout images. The first of a series of short axis (SA) cines (see figure 2.8 on 131) was then planned on image one of the HLA cine, intersecting the atrioventricular valve roots on this view. The SA imaging plane was then propagated apically, covering both ventricles with 8-mm SA imaging slices, separated by a 2-mm inter-slice gap, see figure 2.7. Methodological details which are specific to this thesis, or are of particular importance, include the use of a traditional left ventricle (LV) short axis cine stack for the acquisition of both RV and LV images. Imaging parameters, which were standardised for all subjects, included: TR/TE/flip angle/voxel size/FoV = 3.14 ms/1.6 ms/60°/2.2 x 1.3 x 8.0 mm/340 mm.

Figure 2.5

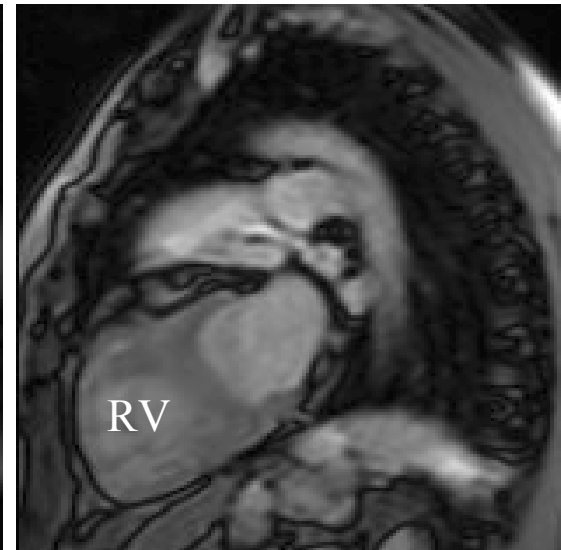
Typical axial scout images used to localise the heart within the thoracic cavity during CMR scanning of a patient with PH. Note the low definition images of these preliminary Fast imaging with steady state precession (TrueFISP) scout images



Coronal Scout Image



Transverse Scout Image



Sagittal Scout Image

Figure 2.6

Image 1 of a vertical long axis Fast imaging with steady state precession (TrueFISP) cine acquired in a patient with PH. The image was planned through the left ventricle (LV) as a standard LV protocol was used. This image was not used for analysis.

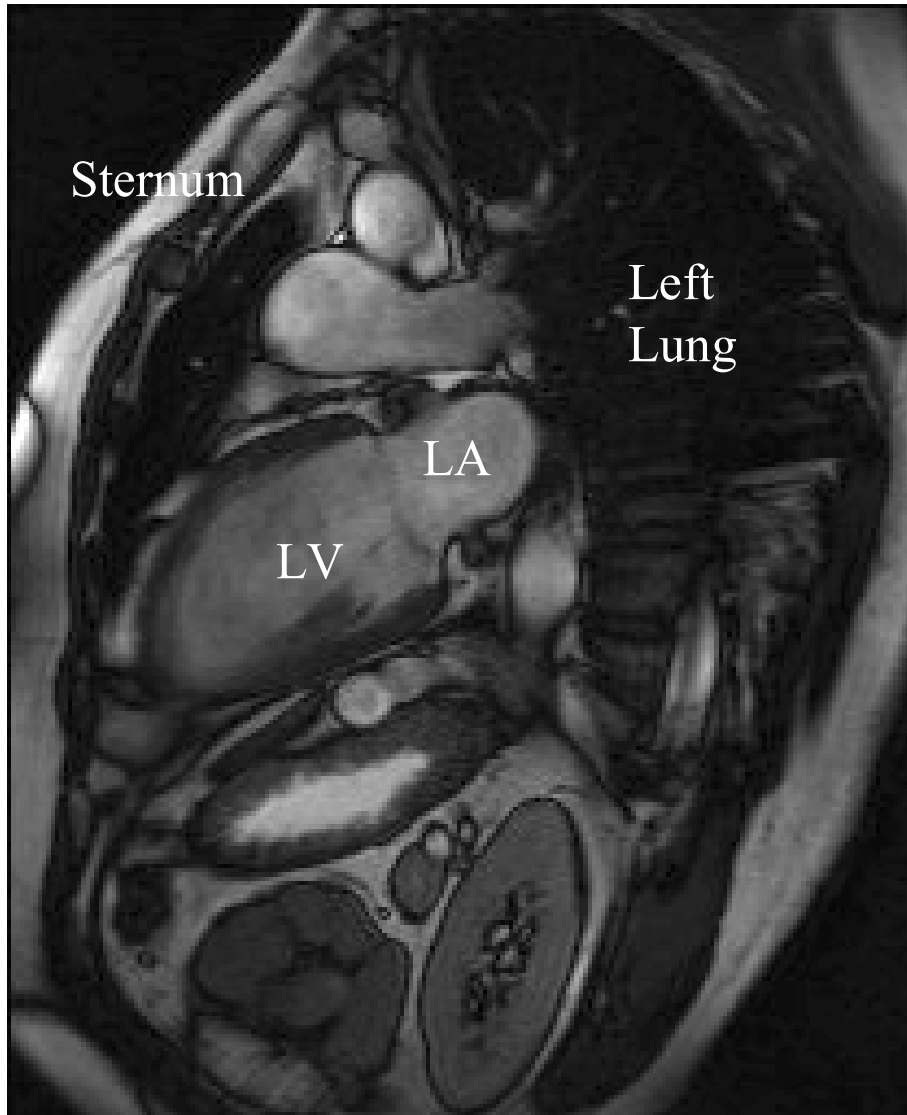


Figure 2.7

Image 1 of a horizontal long axis Fast imaging with steady state precession (TrueFISP) cine acquired in a patient with PH. This image was used to plan the first of a series of short axis (SA) cines, intersecting the atrioventricular valve roots as shown by the solid red line. The SA imaging plane was then propagated apically, covering both ventricles with 8-mm SA imaging slices (dashed red lines), separated by a 2-mm inter-slice gap. These images were not used for analysis.

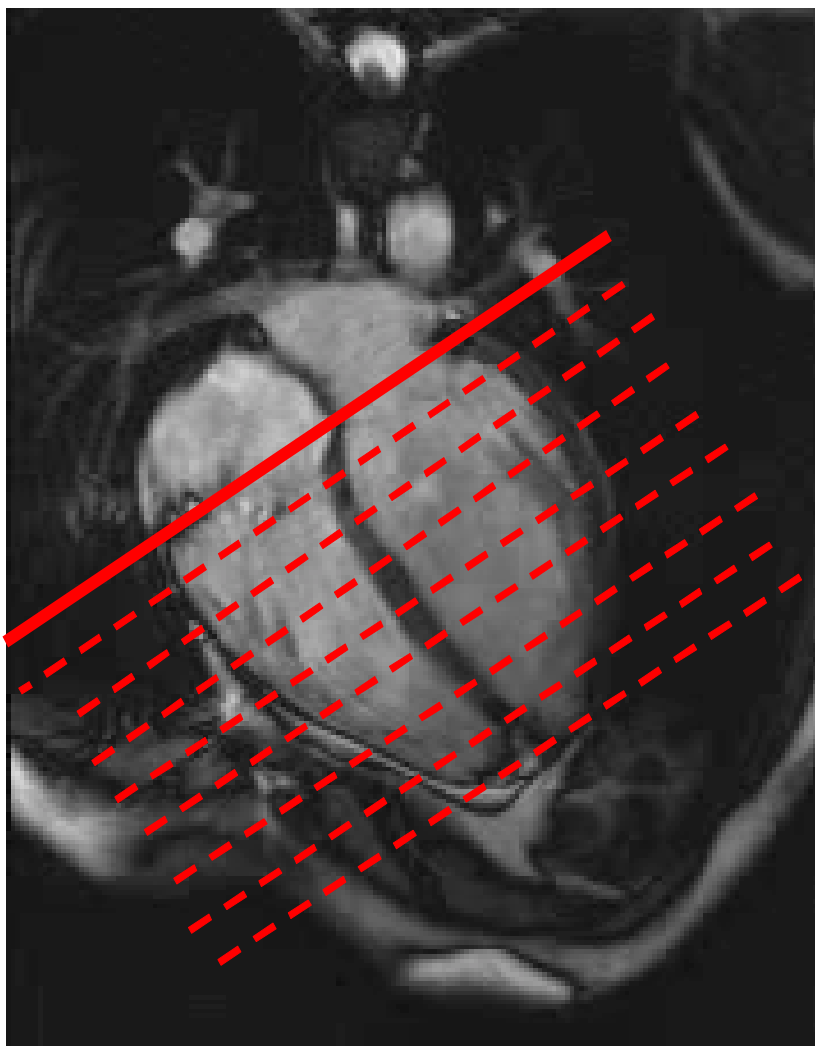
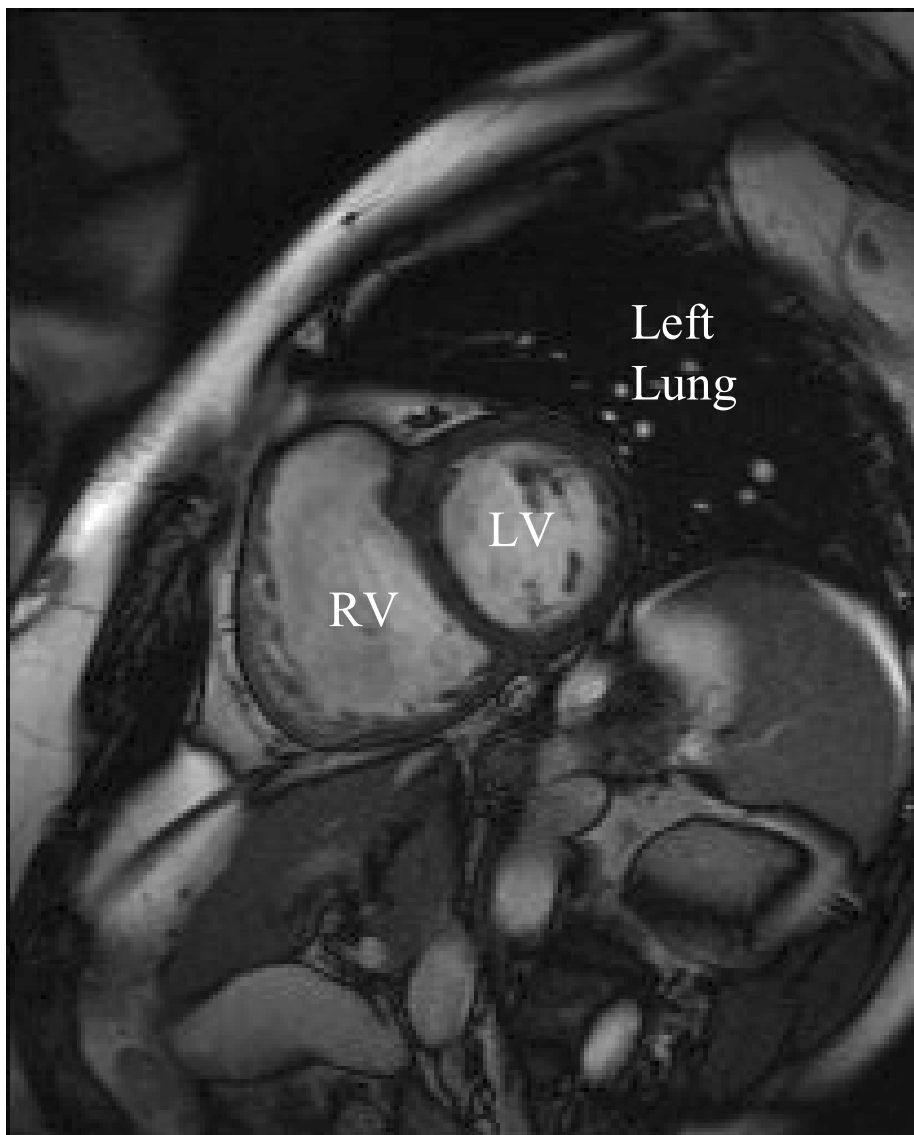


Figure 2.8

Image 1 of a basal short axis Fast imaging with steady state precession (TrueFISP) cine acquired in a patient with PH. A stack of these images were acquired covering both ventricles from base to apex. This stack of short axis images was used for the measurement of ventricular volume and mass using manual planimetry.



2.3.2.2 *Contrast enhanced-CMR imaging*

Following acquisition of a complete set of short axis cine images covering both ventricles, contrast enhanced imaging was performed in a cohort of PH patients as part of an experiment described in detail in Chapter 4.

Gadolinium-diethylene triaminepentaacetic acid (Gd-DTPA) was employed as an intravenous contrast agent. A dose of 0.2 mmol/kg was drawn up in the scanner room after completion of the above images and administered to the patient manually as a slow intravenous bolus via the intravenous cannula inserted during patient preparation and positioning (see Methods Section 2.3.1). A ten minute interval was then allowed before acquisition of a second complete set of short axis (SA) images. Importantly, this image set was acquired using slice positions copied directly from the pre-contrast cines but a different, contrast sensitive, ‘segmented inversion recovery’ pulse sequence (implemented by Siemens as an segmented inversion recovery Turbo FLASH (Fast Low Angle Shot)). This technique was introduced in Section 1.4.3.2.

Standardised scan settings were used for the contrast enhanced imaging in all subjects and specific parameters included TR/TE/flip angle/voxel size/FoV/number of segments = 11.6 ms/4.3 ms/20°/2.2 x 1.3 x 8.0 mm/23. The inversion time for the TurboFLASH sequence was optimised on an individual patient basis. Successful nulling of normal myocardium was deemed to have been achieved once the left ventricular myocardium appeared black and homogenous. Generally speaking an inversion time of between 240 and 280 msec was required to achieve this. Artefact on the contrast enhanced images was excluded by the acquisition of ‘swapped phase’

images through slice planes which appeared to demonstrate intramyocardial contrast enhancement. This technique involves the ‘swapping’ of the phase-encoding and frequency-encoding directions as the phase-encoding direction is particularly prone to artefacts caused by cardiac or chest wall movement. Only areas of contrast enhancement that persisted on these ‘swapped phase’ images were included in subsequent quantification of areas of contrast enhancement. Any areas of contrast enhancement were also compared directly with the pre-contrast cine image corresponding with the contrast enhanced image in terms of both slice position and time frame to further exclude artefact, especially that caused by partial volume effect and blood pool residing behind trabeculated myocardium. See figure 4.1 for examples.

2.3.2.3 *Dobutamine stress-CMR imaging*

Dobutamine stress-CMR imaging was utilised in Chapter 5 of this thesis. In the patients studied using this technique the standard imaging protocol described in Section 2.3.2.1 was used to acquire all resting measurements of right and left ventricular volumes. Since this study specifically required high fidelity measurements of RVSV, velocity encoded flow mapping was used to precisely measure right and left ventricular stroke volume from flow in the main pulmonary artery and ascending aorta, respectively. This methodology was introduced in Section 1.4.3.3. Flow maps were planned perpendicular to the target vessel in a double-oblique plane, at least 1.5 cm distal to the pulmonary or aortic valve. A velocity-encoded k-space segmented gradient-echo sequence was used (imaging parameters: TE/TR/flip angle/slice thickness/temporal resolution /image matrix/FoV/in-plane

resolution/velocity encoding range = 3.1ms /16 ms/ 15°/ 6 mm /limited by TR/256/380 mm/1.9 x 1.5 mm/150 cm per second) to generate 45 matched pairs of anatomical and velocity images.

Retrospective ECG-gating was used. This involves continuous data collection and the assignment of collected data to appropriate points in the cardiac cycle retrospectively. Although this means that a 'mean' cardiac cycle must be interpolated, because of natural variation in R-R interval, it ensures complete coverage of the cardiac cycle. Using prospective ECG-gating, late diastolic flow may not be measured correctly leading to inaccurate stroke volumes. Patients were instructed to breath freely throughout this section of the protocol and the average time of acquisition was 2-3 minutes depending on the patient's heart rate.

2.3.2.3.1 *Dobutamine infusion*

Dobutamine was administered using a digital syringe driver loaded with a 50 ml syringe containing 50 mg of dobutamine hydrochloride (Posiject, Boehringer Ingelheim) diluted in 0.9 % saline. The syringe driver was located in the control room and attached to the subject by a length of tubing fed through a wave-guide conduit. The infusion was started at 5 mcg/kg/min and increased in 5 mcg steps every 3 minutes to a maximum tolerated dose of 20 mcg/kg/min. A 3-lead ECG trace was monitored throughout and systemic BP was measured every 3 minutes. The following safety limits were set for each subject: a) rise in HR > 50 %, b) rise in systolic BP > 50 %, c) fall in systolic BP > 20 %, d) intolerable symptoms, e.g. excessive

breathlessness or chest pain. If any of these tolerances were exceeded the dobutamine dose was reduced.

2.3.2.3.2 *Stress imaging*

Stress CMR imaging was initiated 2 minutes after the maximum tolerated dose of dobutamine was reached. No specific alterations were made to the resting protocol for stress imaging. However, the velocity encoding gradient was modified to accommodate higher stroke volume velocities (maximum 300 cm per second) in approximately half of the PH patients and all of the controls.

2.3.2.4 *Common problems encountered during CMR imaging*

The commonest problems related to the three lead ECG trace used to trigger consecutive pulse sequences and to breath-holding. The former can be explained by the magnetohaemodynamic effect. This describes the altered ECG trace recorded in a strong magnetic field. It can be explained by the effect of the magnetic field on the ferrous metal component of red-blood cells and results in an increase in the amplitude of the T-wave on an ECG trace. The effect on the T-wave is proportional to the strength of the magnetic field. As a consequence, excitatory RF pulses can be triggered inappropriately by T-waves rather than R-waves resulting in poorly timed cine images and degraded image quality. The only solution to this problem was to remove the patient from the MR scanner, take off the chest coil and reposition the ECG electrodes. By trial and error a better ECG trace could usually be established and diagnostic quality images obtained. The second common problem was that some

patients could not hold their breath long enough to accommodate a complete pulse sequence. In extreme cases imaging was performed with the patient breathing freely. However, in most the TR of the sequences could be reduced by altering the flip angle and/or reducing the phase oversampling used as standard in the imaging sequences.

Recent studies have reported adverse effects of gadolinium contrast in patients with chronic renal impairment (nephrogenic systemic fibrosis) (131). This was not seen in any patient in my thesis, reflecting the largely normal renal function of the patients studied.

2.3.3 *Data storage*

On completion of each MR scan, the images were saved to the hard-drive of the scanner and backed up onto a compact disc (CD). Individual CDs were coded by number and stored in a locked filing cabinet until data analysis.

2.3.4 *Analysis of Cardiovascular Magnetic Resonance images*

All CMR images in this thesis were analysed on a satellite workstation attached to the main MR scanner using the Argus analysis software (Siemens, Erlangen, Germany). Individual CDs, which corresponded to individual patients, were retrieved and analysed in batches. At the time of analysis I was blinded to the haemodynamic results of any given patient. Although the name of the patient was visible in the corner of each MR image, each analysis was performed at least 6 months after their invasive assessment and I was unaware their haemodynamic results at the time of MR analysis.

2.3.4.1 *Standard imaging*

The images for each patient were loaded into the Argus program from each CD. Argus automatically identified the images within each SA cine loop that had the largest and smallest blood volumes and defined these as end-diastole and end-systole, respectively. An example of a complete image series with these images defined is provided in Figure 2.9 (page 139-140). The end-diastolic image was usually the first image acquired after R wave deflection. Using a trackball cursor the endocardial and epicardial borders of the end-diastolic and end-systolic images at each slice position within the SA stack were then defined by manual planimetry. These methods are standard in clinical MR practice and have been published before (97, 98). Particular points of note regarding the planimetry used herein include the deliberate inclusion of trabeculations and papillary muscles in all analyses. This has been shown by previous authors to be a more accurate, but more time consuming, method (98). By multiplying the individual slice areas by slice thickness (8 mm) plus the inter-slice gap (2mm) and applying Simpson's Rule, the Argus software automatically calculated RVEDV, RVESV, LV end-diastolic volume (LVEDV) and LV end-systolic volume (LVESV). Right and left ventricular stroke volumes (RVSV & LVSV) were determined as RV/LV EDV-ESV. Ejection fraction (RVEF and LVEF) was determined as a percentage (%) as $((RV/LV SV/EDV) \times 100)$ using this planimetry-derived stroke volume measurement in Chapters 3 and 4. In Chapter 5, velocity encoded flow mapping was used to determine precise, forward stroke volumes for each ventricle, as these were the primary measurements in this experiment and we developed the sequences for specific use in this study. The measurements of stroke volumes yielded by this technique were used to calculate RV and LV ejection fraction

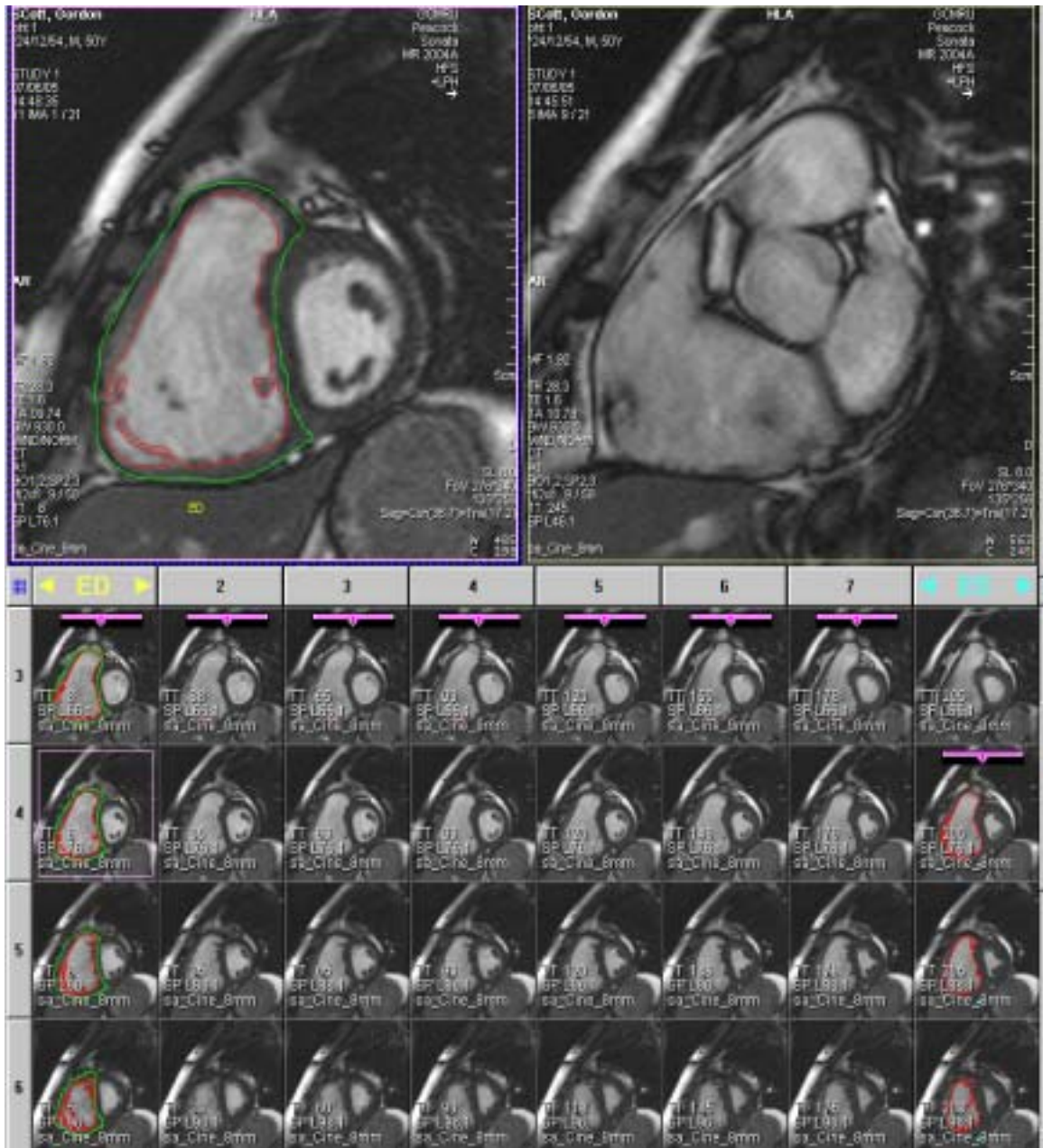
in Chapter 5. The flow mapping technique is described in detail in Section 2.3.4.3.2. It circumvents the predictable measurement error in planimetry-derived stroke volume resulting from tricuspid valve regurgitation (see Section 3.4.4), however both methods are established and commonly used tools for the assessment of stroke volume and ejection fraction in clinical practice.

RV and LV mass (RVM and LVM) were determined as the product of the difference between the end-diastolic and end-systolic volume for each ventricle and the quoted density of cardiac muscle (1.05 g/cm^3). RV mass was determined as RV free wall mass, with the Interventricular Septum (IVS) considered part of the LV. These methods are again, common in clinical CMR practice and have published before (97, 98). RVM Index (RVMI) was determined as RVM/LVM, as previously shown (102). Throughout this thesis, all ventricular volumes are corrected for Body Surface Area (BSA) and reported as indexed measurements: (RVEDV Index (RVEDVI), RVESV Index, (RVESVI), LVEDV Index (LVEDVI) and LVESV Index (LVESVI)).

Figure 2.9, opposite

An example of planimetry analysis of RV volumes and mass using the Argus analysis software. Each row of short axis images represents a loop of cine images acquired during one cardiac cycle at consecutive slice positions, beginning at the base of the heart, moving apically to cover both ventricles. The first images within each row (or slice position) were acquired immediately after R-wave deflection. They are therefore defined by the Argus software as the end-diastolic images (indicated by the yellow ED at the top of the left-hand column) and have the greatest total ventricular blood volume. The end-systolic images were defined automatically by the Argus software as the column of images with the smallest total ventricular blood volume and verified visually. A trackball mouse and cursor was used to define the endocardial (in red) and epicardial (in green) surfaces of the RV at end-diastole and the endocardial surface only at end-systole (in red). This allowed computation of RV end-diastolic and end-systolic volumes and RV mass.

Figure 2.9



2.3.4.2 *Contrast enhanced-CMR imaging*

The contrast-enhanced images for each patient were loaded into the Argus program from each CD. Areas of contrast enhancement were first identified visually. Mean signal intensities (\pm SD) for areas of contrast enhancement and for an adjacent reference area of non-enhancing myocardium were then determined using the Siemens Mean Curve software (Siemens, Erlangen, Germany). Delayed contrast enhancement (DCE) was defined as an area of visually identified contrast enhancement with a mean signal intensity that was $>$ two standard deviations higher than the mean signal intensity of an adjacent area of reference myocardium, which although nulled had a mean signal intensity significantly above zero. DCE volume was determined by planimetry of any areas of contrast enhancement meeting these criteria. An example of a set of contrast-enhanced images with areas of DCE defined is presented overleaf in figure 2.10. DCE mass was calculated by multiplying DCE volume by myocardial density (1.05g/cm^3) and is used in the subsequent correlations and discussion as the absolute measured value of contrast enhancing tissue seen.

Although DCE has previously been described within the RV insertion points in conditions such as Hypertrophic Cardiomyopathy, no universally accepted definition of the extent of the RV insertion points has been agreed for the purposes of CMR imaging. For the purpose of this study the boundaries of the RV insertion points were arbitrarily defined using a method described in detail and illustrated in figure 2.11, page 143.

Figure 2.10

An example of a set of contrast-enhanced images, acquired in a patient with PH, with areas of DCE defined using the Argus analysis software. Each image was acquired at a separate slice position, each of which was copied directly from the pre-contrast imaging protocol. Only visually identified areas of DCE with a mean signal intensity over two standard deviations higher than the mean signal intensity of an adjacent area of reference myocardium were included. DCE volume was determined by planimetry (shown in red). DCE mass was calculated by multiplying DCE volume by myocardial density (1.05g/cm^3)

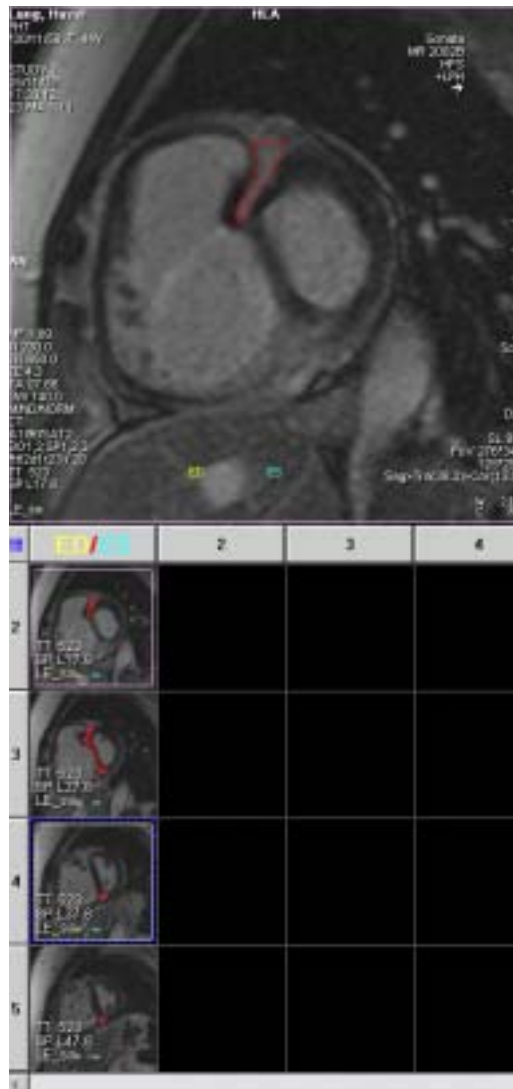
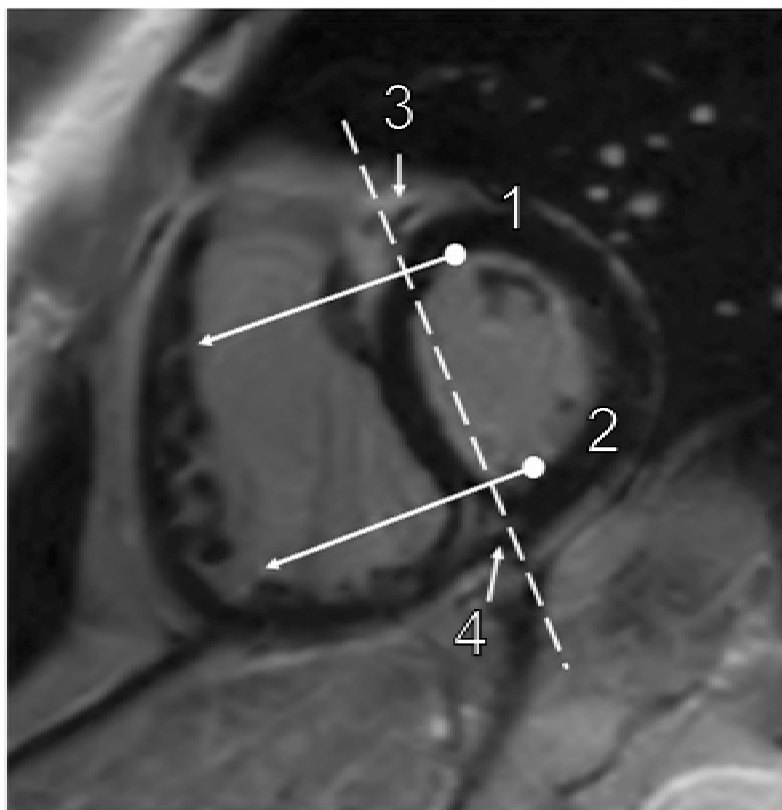


Figure 2.11

The following method was used to define the spatial boundaries of the RV insertion points (RVIPs): On a short axis ce-CMR image such as this, myocardial tissue found at the junctions of the RV free wall and IVS was defined as being within the RVIPs if it was located either above (for the anterior RVIP) or below (for the posterior RVIP) lines drawn across the IVS from the most superior (point 1) or inferior (point 2), respectively, endocardial borders of the LV cavity. These lines were orientated perpendicularly to a single (dashed) line joining the anterior and posterior interventricular grooves (points 3 and 4) on the same image. Myocardial tissue lying either below (for the anterior RVIP) or above (for the posterior RVIP) these two lines was considered part of the IVS.



2.3.4.3 *Dobutamine stress-CMR imaging*

2.3.4.3.1 *Right and left ventricular volumes*

Planimetry of selected short axis images was used to measure RV and LV volumes as described in Section 2.3.4.1.

2.3.4.3.2 *Right and left ventricular stroke volume and ejection fraction*

Velocity encoded flow maps were used to determine RVSV and LVSV at rest and during stress in Chapter 5; four flow maps were therefore analysed for each patient, each containing 90 images. Each image set was inspected to verify accurate depiction of the target vessel on the 45 anatomical images and the absence of artefacts including aliasing on the 45 velocity images.

A region of interest (ROI) was drawn around the interior surface of the target vessel on the first anatomical image. This ROI was propagated throughout the 45 anatomical images using a semi-automatic function within the Argus software. The propagated ROIs were then checked visually and modified using the ‘nudge’ function within Argus to approximate the interior surface of the target vessel throughout the set. These modifications were then copied onto the corresponding 45 velocity images. A second, reference, ROI was then drawn on the first anatomical image and copied directly onto all of the other images. This was defined within the soft tissue of the chest wall as close as possible to the target vessel and was used to correct for background movement of the thoracic contents through the imaging plane during

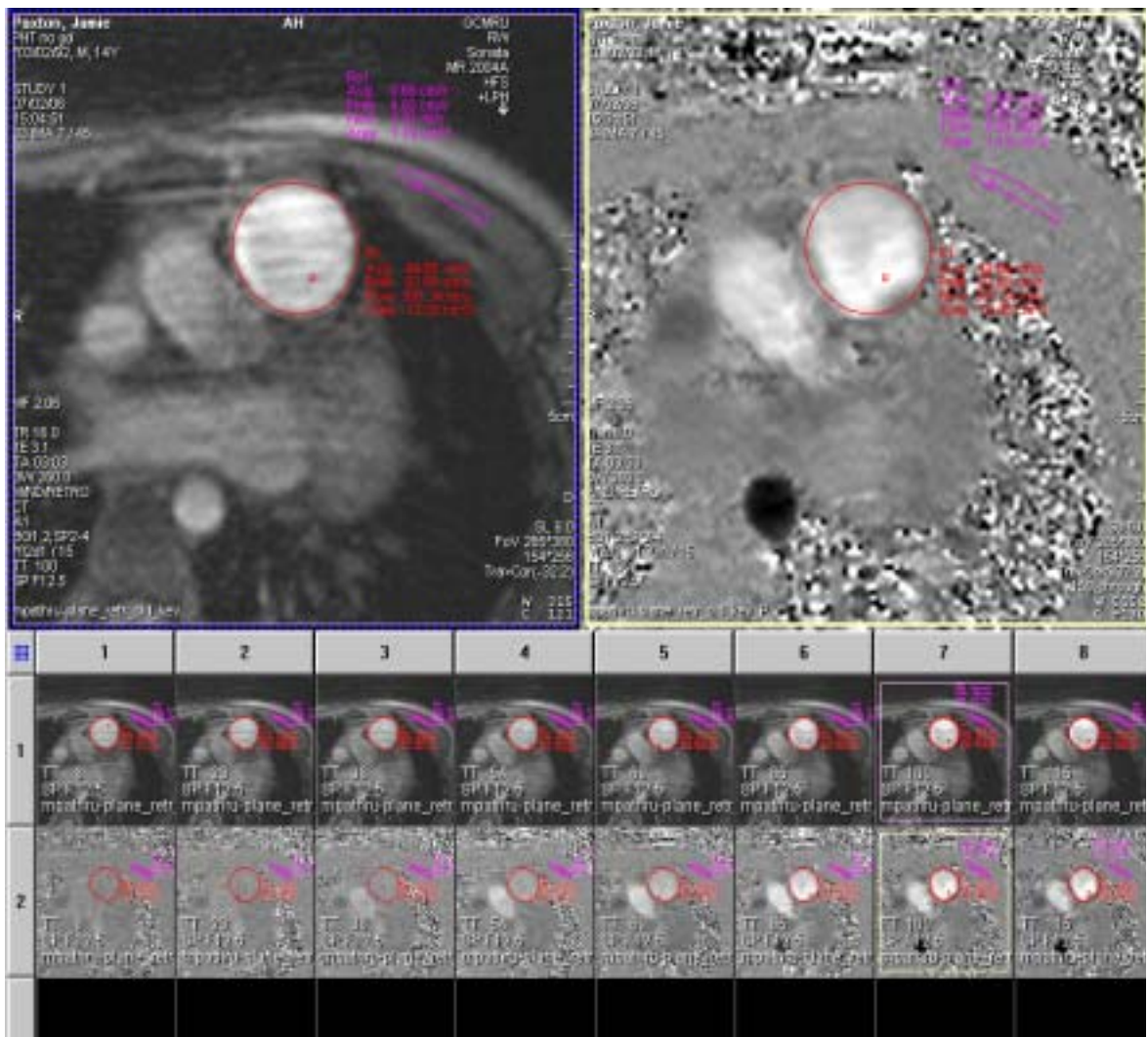
cardiac motion and normal respiration. An example of flow map analysis illustrating the appropriate contour definition is presented overleaf in figure 2.12. Four of these flow maps were used to define the four stroke volumes measured in each patient (RV rest, RV stress, LV rest, LV stress).

The software automatically computed the flow during each time point (ml/sec) within the target vessel ROI minus the reference flow values. These data were integrated with the area of the target vessel and the positive values summed to produce RSV and LSV; these values were corrected for Body Surface Area and are reported as RSVI and LSVI. Right and left ventricular ejection fraction (RVEF and LVEF) were determined as (stroke volume derived from flow mapping / end-diastolic volume) x 100, and expressed as a percentage (%). As described in Section 2.3.4.1 this is a different method of RVEF computation to that used in Chapters 3 and 4.

Figure 2.12, opposite

Velocity encoded flow maps were used to determine RVSV and LVSV at rest and during stress; four flow maps were therefore analysed for each patient, each containing 90 images. The resting main pulmonary artery flow map from a patient with PH is shown below. The anatomical image is shown on the left with the corresponding velocity-encoded image, from the same time point in the cardiac cycle on the right. A region of interest (ROI) was drawn around the interior surface of the target vessel on the first anatomical image. This ROI was propagated throughout the 45 anatomical images using a semi-automatic function within the Argus software. The propagated ROIs were then checked visually and modified using the ‘nudge’ function within Argus to approximate the interior surface of the target vessel throughout the set. These modifications were then copied onto the corresponding 45 velocity images. The final contours that resulted are shown overleaf in red. A second, reference ROI (shown in purple) was then drawn on the first anatomical image and copied directly onto all of the other images. This was defined within the soft tissue of the chest wall as close as possible to the target vessel and was used to correct for background movement of the thoracic contents through the imaging plane during cardiac motion and normal respiration.

Figure 2.12



2.3.4.4 *Common problems encountered during CMR image analysis*

Definition of the most basal ventricular slice to be included in the right and to a lesser extent the left ventricular analysis has proven difficult in the past. Erroneous definition can lead to significant errors because of the large volume of RV that is either excluded or included, inappropriately. To overcome this problem the most basal ventricular image (RV or LV), once identified visually, was cross-referenced with the horizontal long axis view before its inclusion in the final analysis to ensure this slice was indeed ventricular and not atrial.

Interventricular septal (IVS) bowing describes the paradoxical displacement of the IVS caused by the leftward trans-septal pressure gradient common in PH patients during early diastole. This phenomenon made definition of the end-diastolic and end-systolic images (based on blood volume) difficult for the Argus software because bowing tends to be most exaggerated in the mid-ventricle, and least prominent at the base and apex. The resulting mid-ventricular bulge tended to maximise RVEDV and minimise LVEDV at this position, relative to the base and apex, making consistent automatic definition difficult. The solution adopted for all scans in this thesis was to manually check that the maximum, and minimum, ventricular volumes (and thus the EDV and ESV) had been appropriately identified by Argus for each ventricle.

Chapter 3

Definition of an NT-proBNP threshold for the non-invasive detection of RV systolic dysfunction in pulmonary hypertension

3.1 Introduction

As has been discussed in earlier chapters, right ventricular systolic dysfunction (RVSD), at baseline (i.e. pre-treatment) in PH patients, has been associated with an increased mortality risk in earlier studies that identified RVSD either by invasive haemodynamic measurements (1, 3, 44, 58, 132) or by the detection of overt clinical signs of RV failure (i.e. patients within Class IV of the WHO classification of disease severity) (1). Accurate assessment of baseline RV function is therefore desirable in all patients with PH. This information may help identify individuals in whom prompt invasive assessment \pm the initiation of disease targeted therapy is appropriate. Because early RV dysfunction is difficult to detect on clinical examination, trans-thoracic echocardiography is often used for this purpose (65). Although inexpensive and widely available, RV ejection fraction (RVEF) can only be estimated indirectly from measurements acquired in two dimensions by this method. Furthermore, variables derived from echocardiography that reflect RV function and provide useful prognostic information in PH are either complicated to define and therefore reliant upon an experienced operator (e.g. the Tei index) (61) or detected most frequently in patients in whom RV failure is already clinically overt (e.g. a pericardial effusion) (44).

Cardiac Magnetic Resonance (CMR) imaging allows image acquisition in any plane and at almost any angle, allowing direct 'gold-standard' measurement of RV volumes and RVEF in patients with PH. At present, however, CMR imaging remains too expensive for routine clinical use and is not available in many PH centres. An alternative non-invasive method of identifying baseline RVSD in PH that was

objective, operator independent and widely available would, therefore, be clinically useful.

As indicated in Section 1.3.4, circulating natriuretic peptide levels have, as B-type natriuretic peptide (BNP), recently been shown to correlate with invasive pulmonary haemodynamics (91, 92), RVEF measured by computed tomography (CT) (91), survival (93, 94) and the response to therapy (95, 96) in PH patients. NT-proBNP, which is biologically inactive, is more stable *in vivo* and *in vitro* than BNP (133) and therefore is more suitable for use as cardiovascular biomarker.

In LV dysfunction an NT-proBNP threshold has been identified that can be used to identify patients with symptoms who are likely to have LV failure on subsequent tests (83-85). Although serum NT-proBNP concentration ([NT-proBNP]) has recently been shown to correlate with invasive pulmonary haemodynamics (134), survival and echocardiography derived measures of RV function in PH (135), a similar NT-proBNP threshold indicative of RVSD has yet to be determined. This may reflect insufficient precision in the previous reference method for RV systolic function: echocardiography. In this experiment I correlated serum [NT-proBNP] against RV systolic function measured directly by CMR imaging in patients with PH at baseline and hypothesised that an NT-proBNP threshold indicative of RVSD could be defined.

3.2 Methods

3.2.1 Patients

30 consecutive patients were recruited and clinically assessed as described in Methods Section 2.1-2.2. Specific inclusion and exclusion criteria for this experiment were used. The only specific inclusion criterion was a diagnosis of either Pulmonary Arterial Hypertension (PAH) or Chronic Thromboembolic PH (CTEPH) reached by conventional diagnostic methods (57, 65). Patients were excluded from this experiment (after review of their past medical history, admission blood tests and transthoracic echocardiogram and before CMR imaging and NT-proBNP measurement) if they met any of the following exclusion criteria:

1. Evidence of congenital heart disease (CHD), either at echocardiography or as a previous diagnosis. This was because differing patterns of natriuretic peptide release have been demonstrated in conditions that cause RV volume overload, such as CHD, in comparison to those that cause RV pressure overload (e.g. PAH and CTEPH) (136).

2. A history of any other condition that might cause elevation of [NT-proBNP].

These include:

- a. Ischaemic heart disease (137)
- b. Myocardial infarction (80)
- c. LV systolic dysfunction (79)
- d. Systemic hypertension (81)

- e. Left-sided valvular heart disease (82)
- f. Chronic renal impairment (138) or an abnormal serum creatinine on admission (normal was defined as $< 120 \mu\text{mol l}^{-1}$)
- g. Diabetes Mellitus (139) or a fasting blood glucose on admission to the SPVU of $> 6.1 \text{ mmol l}^{-1}$

On the basis of these criteria, 5/30 patients recruited were excluded from the final analysis (atrial septal defect (2/5), chronic renal impairment (1/5), significant mitral regurgitation (1/5) and systemic hypertension (1/5)). The remaining 25 subjects underwent CMR imaging and venous blood sampling for [NT-proBNP] within 24 hours of invasive assessment. The final diagnoses reached in these 25 patients were, idiopathic PAH (IPAH) in 11/25, CTEPH in 6/25 and PAH associated with connective tissue disease (PAH-CTD) in 8/25. At the time of the study no patient had received any disease-targeted therapy (i.e. Prostacyclin analogues, Bosentan, Sildenafil or calcium channel blockers) for PH.

Twelve control subjects were recruited as described in Method Section 2.1. Between PH patients and controls there were no significant differences in mean age (PH: $60 (\pm 12)$, Controls: $57 (\pm 12)$, $p = 0.455$) or mean systemic blood pressure (PH: $95 (\pm 13)$, Controls: $92 (\pm 17)$, $p = 0.536$). PH (17 ♀: 8 ♂) and control populations (8 ♀: 4 ♂) were well sex-matched.

3.2.2 *Venous blood sampling and measurement of NT-proBNP*

After at least 20 minutes of recumbent rest, 5 mls of venous blood was drawn from the antecubital fossa of all 25 PH patients immediately prior to CMR imaging. Blood samples were drawn into vacuum-sealed containers containing ethylenediamine tetraacetic acid and immediately centrifuged at 3000 rpm for 15 minutes using a PK110 centrifuge (ALC, Winchester, VA, USA). Supernatant was then removed and individual samples were coded, labelled and stored at -80°C until analysis.

NT-proBNP analysis was performed on an ELECSYS 2010 bench top analyser utilising a chemiluminescent assay with a Coefficient of Variation < 5 % (Roche Diagnostics, Lewes, UK). All biochemical analyses were performed by a single experienced clinical biochemist in the BHF Cardiovascular Research Centre (University of Glasgow, UK) who was blinded to haemodynamic, CMR and clinical results. NT-proBNP measurements are subsequently quoted as plasma concentration (ng/l).

3.2.3 *CMR image acquisition and analysis*

CMR imaging acquisition and analysis was as described in Method Section 2.3.

3.2.4 *Clinical assessment and right heart catheterisation*

Clinical assessment followed a standard diagnostic algorithm as described in Methods Section 2.2.

For all variables a normal distribution was verified using histograms and Kolmogorov-Smirnov tests. Non-normally distributed values ([NT-proBNP] and right atrial pressure) were logarithmically transformed and all correlation analyses were performed using Pearson's method. Comparisons between PH patients and controls (and between sub-groups of PH patients) were made using an independent samples (unpaired) t-test (using Welch's correction if appropriate). 2x2 contingency tables were used to calculate the sensitivity and specificity of various plasma concentrations of NT-proBNP as a means of detecting RVSD. RVSD was defined as an RVEF < 42 % (this constituted an RVEF > two standard deviations below the mean RVEF of the control population (66 (\pm 7) %)). The plasma [NT-proBNP] with the greatest diagnostic accuracy (that which produced the lowest number of false positive and false negative results) was chosen as a 'threshold' value for the detection of RVSD. Negative and positive predictive values ((NPV and PPV) for results either side of this NT-proBNP threshold were then calculated. The implications of an above threshold result were quantified by likelihood ratios and Fisher's exact test. To identify independent predictor(s) of circulating [NT-proBNP], variables significantly associated with [NT-proBNP] (RVEDVI, RVESVI, RVEF, RVMI, LVSVI, mean PAP, systolic PAP, diastolic PAP, cardiac index, pulmonary vascular resistance and mixed venous oxygen saturation (MVO₂)) (see table 3.3)) were entered into a multivariable stepwise linear regression model, in which NT-proBNP was the dependent variable. Co-variables with a correlation co-efficient ≥ 0.8 were tested within separate regression models to avoid the effects of co-linearity. All statistical analyses were performed using GraphPad Prism 4 for Windows (GraphPad Software

Inc., San Diego, USA), were two-sided and assumed a significance level of 5 %. All values are presented as mean (\pm 1SD) unless otherwise stated.

3.3 Results

3.3.1 *Clinical assessment and right heart catheterisation*

Invasive measurements acquired in the PH patients are summarised in Table 3.1.

Table 3.1 Results of right heart catheterisation in 25 patients with PH who underwent Cardiovascular Magnetic Resonance imaging

Variable	Mean (\pm SD)
PAP * (mmHg)	Systolic PAP 72 (\pm 20)
	Diastolic PAP 24 (\pm 9)
	Mean PAP 43 (\pm 12)
Cardiac Index (l/min/m ²)	2.4 (\pm 0.6)
PVR † (mmHg/l/min)	10 (\pm 6)
RAP ‡ (mmHg)	8 (\pm 8)
MV § O ₂ saturation (%)	65 (\pm 8)

* PAP: Pulmonary Arterial Pressure, † PVR: Pulmonary Vascular Resistance, ‡ RAP: Right Atrial Pressure, § MV: Mixed Venous

3.3.2 *CMR imaging*

Ventricular dimensions and systolic function of the 25 PH patients and 12 controls are presented in Table 3.2. In summary, RVEDV, RVESV, RV mass and RVMI were significantly increased, and RVEF significantly depressed in PH patients relative to control subjects. LVEDV and LVSV were significantly lower in PH patients compared with controls. All LV measurements, in both PH patients and controls, were within previously published normal limits (97, 140). Where available we have used CMR normal ranges determined by SSFP imaging sequences similar to those employed in our own study (140).

Table 3.2

Ventricular dimensions and function measured by Cardiovascular Magnetic Resonance imaging in 25 patients with Pulmonary Hypertension (PH) and 12 controls

	PH (n= 25)	Controls (n= 12)	p value
Right Ventricle			
EDV * (ml)	170 (± 57)	129 (± 46)	0.033
ESV † (ml)	99 (± 53)	45 (± 22)	< 0.0001
Stroke Volume (ml)	71 (± 19)	83 (± 29)	0.126
Ejection Fraction (%)	45 (± 14)	66 (± 7)	< 0.0001
Mass (g)	84 (± 34)	48 (± 18)	0.0002
RV Mass Index	0.87 (± 0.24)	0.41 (± 0.04)	< 0.0001
Left Ventricle			
EDV * (ml)	86 (± 25)	116 (± 36)	0.005
ESV † (ml)	28 (± 16)	31 (± 14)	0.579
Stroke Volume (ml)	60 (± 17)	85 (± 24)	0.0009
Ejection Fraction (%)	71 (± 9)	74 (± 7)	0.218
Mass (g)	94 (± 23)	120 (± 51)	0.117

* EDV; End-diastolic volume, † ESV; End-systolic Volume

3.3.3 *Correlation analyses*

[NT-proBNP] was non-normally distributed in the population studied. Median (interquartile range) [NT-proBNP] was 669 (94-2615) ng/l. After logarithmic transformation mean (\pm 1SD) \log_{10} [NT-proBNP] was 2.71 (\pm 0.77). A complete list of correlation co-efficients and accompanying p-values for variables compared with [NT-proBNP] is presented overleaf in Table 3.3. There was a powerful negative logarithmic correlation between [NT-proBNP] and RVEF (see figure 3.1). With the exception of LVSV, there was no significant correlation between [NT-proBNP] and LV measurements (see Section 3.4.4).

3.3.4 *Differences in \log_{10} [NT-proBNP] in subgroups of PH patients*

There were no statistically significant differences in [NT-proBNP] based on gender (mean \log_{10} [NT-proBNP] was 2.7 (\pm 0.6) in males and 2.7 (\pm 0.8) in females) or aetiology of PH (mean \log_{10} [NT-proBNP] was 2.6 (\pm 0.8) in PAH (2.4 (\pm 0.9) in IPH, 3.0 (\pm 0.7) in PAH-CTD) and 3.0 (\pm 0.5) in patients with CTEPH).

3.3.5 *RV systolic dysfunction*

RV systolic dysfunction (RVSD) was present in 9/25 PH patients (36 %). The distribution of [NT-proBNP] values for the 9 patients with RVSD and the 16 patients without RVSD were normal. Mean [NT-proBNP] was significantly higher in patients with RVSD (4127 (\pm 2951) ng/l) in comparison to those without RVSD (354 (\pm 435) ng/l) ($t= 3.813$, $df = 8$, $p = 0.005$).

Table 3.3

Correlation co-efficients between \log_{10} [NT-proBNP] (ng/l) and measurements acquired in 25 PH patients during Cardiovascular Magnetic Resonance imaging

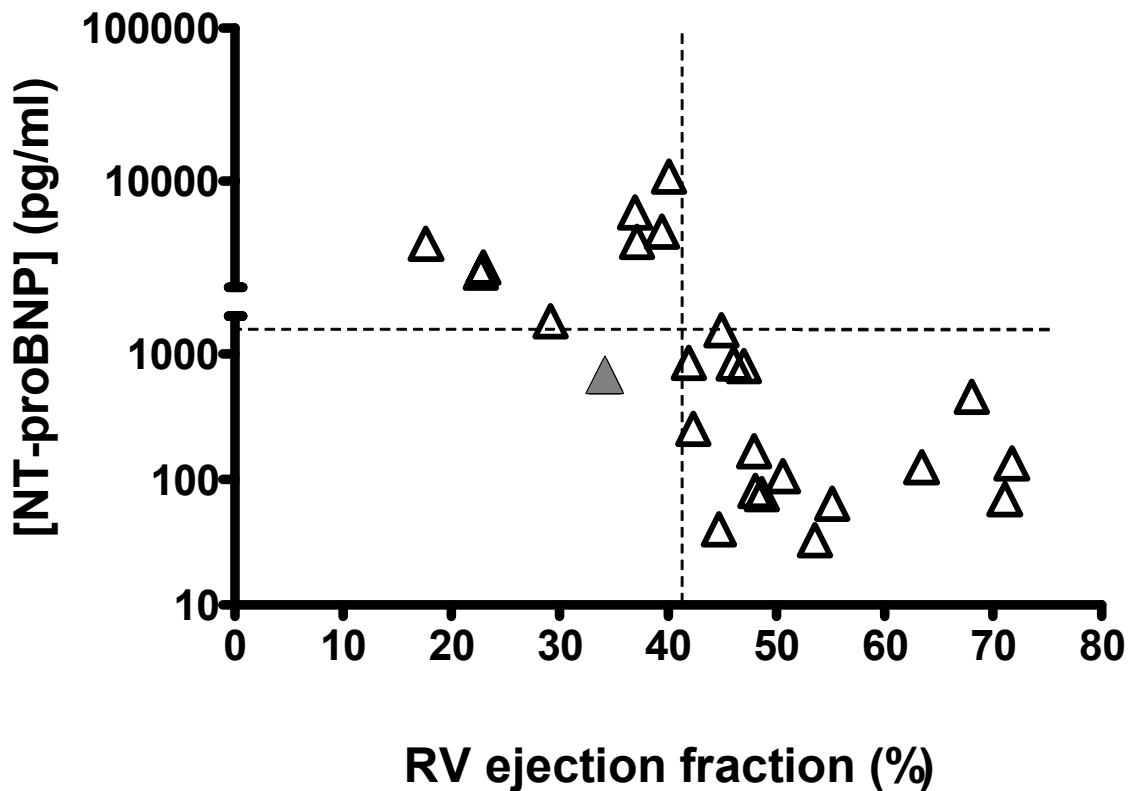
Variable	r co-efficient	p-value
Right Ventricle		
EDV * (ml)	0.556	0.004
ESV † (ml)	0.655	< 0.001
Stroke Volume (ml)	0.279	0.177
Ejection Fraction (%)	0.66	< 0.001
Mass (g)	0.613	0.001
RV Mass Index	0.713	< 0.001
Left Ventricle		
EDV * (ml)	0.376	0.064
ESV † (ml)	0.08	0.705
Stroke Volume (ml)	0.508	0.009
Ejection Fraction (%)	0.323	0.115
Mass (g)	0.196	0.349
Invasive Measurements		
Mean PAP ‡	0.501	0.011
Systolic PAP ‡	0.435	0.03
Diastolic PAP ‡	0.622	< 0.001
Cardiac Index	0.523	0.007
Pulmonary Vascular Resistance	0.566	0.003
Mixed Venous O ₂ Saturation	0.541	0.009

* EDV; End-diastolic volume, † ESV; End-systolic Volume, ‡ PAP;

Pulmonary Artery Pressure

Figure 3.1

CMR imaging and NT-proBNP measurements were acquired in 25 patients with Pulmonary Hypertension. [NT-proBNP], after logarithmic transformation correlated powerfully with RV ejection fraction (RVEF) ($r = -0.66$, $p < 0.001$). The horizontal line indicates the [NT-proBNP] threshold chosen (1685 ng/l) for the detection of RV systolic dysfunction (RVSD). The vertical line indicates the RVEF (42%) used to define RVSD. Only one false negative result (solid triangle) was returned.



3.3.6 *Diagnostic performance of NT-proBNP*

NT-proBNP performed best at a plasma concentration of 1685 ng/l, detecting RVSD with 100 Sensitivity % (95 % CI (63.0 % to 100 %)) and 94 % Specificity (95% CI (71.3 % to 99.9 %)). 1685 ng/l was therefore chosen as the threshold value for RVSD detection. 17/25 patients had an [NT-proBNP] below the 1685 ng/l threshold. 16/17 of these patients were true negatives (i.e. RVEF was normal (≥ 42 %)) and one was a false negative. In the false negative subject RVEF measured 34 % and [NT-proBNP] was 669 ng/l. The negative predictive value of a low [NT-proBNP] was, therefore, 94 %. 8/25 patients had an [NT-proBNP] > 1685 ng/l. RV systolic dysfunction was demonstrated by CMR imaging (RVEF < 42 %) in all of these individuals. Thus, the positive predictive value of a high [NT-proBNP] was 100 %. These results are presented graphically in figure 1. Based on likelihood ratio testing, individuals with an NT-proBNP above the 1685 ng/l threshold were 17 times more likely to have RVSD than those with below threshold results.

3.3.7 *Predictors of [NT-proBNP]*

Because RVEF correlated powerfully with RVMI ($r = -0.854$, $p < 0.001$) these variables were entered into two separate multivariable linear regression models in which [NT-proBNP] was the dependent variable. In these models, RVEF (Odds Ratio = -0.035, 95 % CI (-0.052 – -0.018, $p < 0.001$) and RVMI (Odds Ratio = 2.254, 95 % CI (1.403 – 3.106, $p < 0.001$) proved the only independent predictors of circulating [NT-proBNP].

3.4 Discussion

This chapter has identified a close correlation between RVEF, measured directly by CMR imaging and [NT-proBNP] in patients with PH, assessed prior to any treatment. A previous study, reported by Nagaya *et al*, demonstrated a similar relationship between RVEF, measured by electron beam CT imaging, and BNP concentration in a similar cohort of patients (91). The findings of this experiment reported herein are of additional interest to this previous report for three important and clinically relevant reasons.

1) In routine clinical practice most centres use NT-proBNP, not BNP, to aid clinical decision making in heart failure and a variety of other conditions. As previously discussed, this is because NT-proBNP is more stable *in vivo* and *in vitro* than the active BNP molecule itself (133).

2) The study by Nagaya *et al* used EBCT imaging to measure RVEF, while this study utilized CMR imaging as the reference method. Temporal resolution is better with CMR imaging (141) without the need for ionizing radiation or intravenous contrast (142). As a result, CMR has emerged over recent years as the gold standard for detailed study of the RV (143-146) and has become an established modality for the physiological assessment of PH patients in cross-sectional studies (102, 147, 148) longitudinal follow-up studies (149) and clinical trials of therapy (96). EBCT, in contrast, is not used routinely to assess PH patients. The current study is therefore useful as it defines the relationship between [NT-proBNP] and RV volumes and ejection fraction measured directly by CMR imaging.

3) In addition to a correlation between [NT-proBNP] and RVEF, this study has also demonstrated that an [NT-proBNP] > 1685 ng/l (detected in 8/25 patients) was a sensitive marker of RVSD (sensitivity 100 %). Below this threshold only one false negative result was returned, suggesting that RVSD is very unlikely when circulating [NT-proBNP] is less than 1685 ng/l, at least in patients assessed at baseline, before treatment initiation (negative predictive value 94 %). Stratifying patients either side of this NT-proBNP threshold may prove useful as an operator independent, objective means of classifying individuals at presentation based upon their probability of having RVSD and thus an increased risk of early death.

3.4.1 *Physiological determinants of NT-proBNP*

Several variables correlated closely with circulating [NT-proBNP] in this experiment (see Table 3.3). Of these variables only RVEF and RV mass index (RVMI), analysed within separate regression models to avoid the effects of co-linearity, proved independent predictors of [NT-proBNP]. Although it has previously been shown that RVMI relates linearly to mean PAP in PH (102), it has not been proven to predict early death in patients with this condition. For this reason we defined our primary goal as the detection of RVSD, not RV hypertrophy, using [NT-proBNP]. The influence of RV hypertrophy (as RVMI) should, however, be discussed and perhaps acknowledged as a potential confounder of our results. The vast majority (7/8 (88 %)) of patients in our study with above threshold NT-proBNP levels indicative of RVSD also had RV hypertrophy (defined as a RV mass > 84 g (> 2 SDs above mean RV mass of the control population (48 (\pm 18) g)) reflecting the co-variation between RVMI, RVEF and [NT-proBNP] that we found. Despite this, RVEF appeared to be

an important determinant of circulating [NT-proBNP] in our study. Interestingly, a recent study reported by Quaipe *et al* (150) has identified a close correlation between RVEF and RV wall stress. Since RV wall stress is the principal stimulus to NT-proBNP release in PH, this relationship may explain the usefulness of NT-proBNP as a means of detecting RVSD reported herein.

3.4.2 *Clinical implications*

Non-survivors in a recent PH study reported by Fijalkowska *et al* (135) were identified by an [NT-proBNP] > 1400 ng/l. Since non-survivors with PH are likely to die from RV failure, and [NT-proBNP] correlated powerfully with echocardiographic measures of RV systolic function in this study, it seems plausible that the 1400 ng/l threshold reported in the Fijalkowska study and our own 1685 ng/l threshold reflect genuine RV systolic dysfunction in the patients studied. However, the true clinical significance of the [NT-proBNP] threshold for RVSD (1685 ng/l) identified in our study can only be determined in a longitudinal survival analysis. For this reason it is difficult to justify detailed proposals for the future use of NT-proBNP in clinical practice at this time. The findings reported here indicate, however, that NT-proBNP, measured during a patient's first consultation at a specialist PH centre could, in conjunction with existing means of assessing RV function (i.e. clinical examination and echocardiography) help identify patients with prognostically significant RVSD. Assuming other reasons for a high NT-proBNP were excluded patients with a high [NT-proBNP] could then be invasively assessed at an early stage and treatment initiated if appropriate. Although there is no evidence yet that early treatment of PH alters prognosis *per se*, it is known that a history of overt RV failure before treatment

initiation is associated with an increased mortality risk (48). Prompt initiation of therapy in patients with high NT-proBNP levels and sub-clinical RVSD may, therefore, avoid the development of overt RV failure and reduce early mortality.

3.4.3 *RV ejection fraction*

In this chapter, RVEF was utilized to define RVSD. Although historical data have suggested that RVEF does not reflect RV systolic function alone (since it is also dependant upon right ventricular afterload) (151-153), RVEF determined by echocardiography and radionuclide ventriculography has recently been shown to predict adverse outcomes (cardiac death or deterioration) in patients with PH (154). Until longitudinal survival studies are reported in which CMR-derived variables are assessed the true prognostic significance of CMR-derived RVEF, and the cut-off value of 42 % used here to define RVSD cannot, however, be known.

3.4.4 *NT-proBNP and LV stroke volume*

In this experiment a statistically significant relationship between [NT-proBNP] and LV stroke volume (LVS_V), but no correlation between [NT-proBNP] and RV stroke volume (RVS_V) is reported. This apparent contradiction reflects the inaccuracy of CMR-planimetry in determining true (i.e. forward) stroke volume in patients with significant valvular regurgitation. CMR-planimetry of a dilated RV with significant tricuspid valve regurgitation will always overestimate true *forward* RVS_V because a proportion of the ejected blood volume will move backwards through the incompetent tricuspid valve. Since *forward* LVS_V and *forward* RVS_V will, over several heart

beats, be equivalent in the absence of any communicating shunt, and since no PHT patient in our study had any evidence of mitral regurgitation, the statistically significant relationship that we found between LVSV and [NT-proBNP] likely reflects an underlying correlation between [NT-proBNP] and true *forward* RVSV that is obscured by this predictable measurement error. Although CMR-planimetry may not always accurately determine forward RVSV in PH patients, RVEF still reflects the systolic contractile function of the ventricle, assessment of which was the primary aim of this study. An alternative confounder to the CMR-planimetry results might be the trabeculation of the RV. Despite this concern, we have found acceptable intra-observer variation for ventricular mass and ejection fraction (3.8-7.4 % and 3.4-4.4 %, respectively) measured by other researchers using the same method in the Glasgow Cardiac Magnetic Resonance Unit (unpublished data).

3.4.5 *Study limitations*

The relatively small number of patients involved in this experiment is of concern in the proposal of a specific cut-off level for use in the detection of RVSD in clinical practice. CMR imaging, however, represents an extremely accurate and reproducible gold standard of RVEF limiting the number of patients required for such studies. [NT-proBNP] can be affected by a number of factors including renal function, left-sided heart disease, age, gender (155) and recent exertion. In the current study patients who had other reasons for a high [NT-proBNP] were excluded and the timing and conditions surrounding NT-proBNP sampling were standardised. It should be emphasised that the results of this study should only be applied to selected PH patients assessed in this manner. In addition, it is not known whether therapies such

as Sildenafil, which acts directly upon the cardiac myocyte (156), will affect the relationship we report between RVEF and [NT-pro BNP] or whether any observed fall in [NT-pro BNP] during treatment will prove proportional to an improvement in RV systolic function. Further insight into these issues is necessary to understand the clinical significance of changes in [NT-proBNP] during treatment.

3.4.6 *Conclusion*

The study reported in this chapter is the first to utilise a specific NT-proBNP threshold (1685 ng/l) as a means of detecting RVSD in patients with PH. Classifying patients either side of such a threshold is simple, inexpensive and most importantly, non-invasive and may help to inform the largely subjective process of stratifying new patients for invasive assessment and the initiation of disease targeted therapy.

Chapter 4

Contrast enhanced-Cardiovascular Magnetic Resonance
imaging in patients with pulmonary hypertension

4.1 Introduction

In Chapter 3 it was shown that NT-proBNP can be used to detect RV systolic dysfunction non-invasively in patients with PH. Unfortunately, despite recent therapeutic advances, which have improved the short-to-medium term outlook for patients with PH, RV failure and early death remains inevitable in the majority (1, 58). In this chapter contrast enhanced-CMR (ce-CMR) imaging is used as a means of interrogating the right and left ventricular myocardium in patients with PH in a manner not possible using any other imaging technique. The purpose of this study was to gain some new insight into the mechanism(s) of RV failure in PH patients. Such information might facilitate better targeting of the treatments currently available and allow physicians to anticipate an individual's decline and the need for therapeutic intervention or referral for transplant. As discussed in section 1.4.3.2, delayed contrast enhancement (DCE) is well established as a marker of myocardial abnormalities in a variety of disease states. However, ce-CMR has yet to be utilised in patients with PH. The experiment in this chapter tested the specific hypothesis that discrete myocardial abnormalities might exist in patients with PH. It was hoped that the pattern of any DCE detected might provide new insight into the development of RV failure in patients with PH.

4.2 Methods

4.2.1 Patients

Twenty-five consecutive patients with PH were recruited and clinically assessed as described in Methods Section 2.1-2.2. Eighteen of these patients also took part in the NT-proBNP study reported in Chapter 3. No specific selection criteria were used, other than a diagnosis of either Pulmonary Arterial Hypertension (PAH) or Chronic Thromboembolic PH (CTEPH) reached by conventional diagnostic methods (57, 65). The final diagnoses reached in the 25 patients studied are summarised in Table 4.1.

Table 4.1

Final diagnoses reached in 25 patients with Pulmonary Hypertension who underwent contrast enhanced-Cardiovascular Magnetic Resonance imaging

Diagnosis	No. of Patients
Pulmonary Arterial Hypertension (PAH)	19
Idiopathic PAH	12
Associated PAH	7
Connective Tissue Disease	5
Repaired Congenital Left-to-Right shunt	2
Chronic Thromboembolic Pulmonary Hypertension	6

At the time of the study no patient had received any specific treatment (other than anticoagulation with warfarin) for PH. None of the patients had a previous diagnosis of ischaemic heart disease or a history of previous myocardial infarction. Twenty three out of the twenty five patients underwent ce-CMR within twenty four hours of right heart catheterisation. The other two patients underwent ce-CMR within four days of invasive assessment.

Twelve control subjects were recruited as described in Methods Section 2.1. Controls underwent CMR imaging, without contrast enhancement, to provide local control values for ventricular dimensions and function. Demographic data for the PH and control populations are summarised in Table 4.2.

Table 4.2

Group demographics for 25 patients with Pulmonary Hypertension and 12 control subjects who underwent contrast enhanced-Cardiovascular Magnetic Resonance imaging. Values are mean (\pm SD) unless stated

	PH	Controls	p value	
Age (years)	58 (\pm 14)	57 (12)	0.837	
Sex ($\text{\textcircled{f}}$; $\text{\textcircled{m}}$)	17;8	8;4		
Systemic BP(mmHg)	Systolic BP	125 (\pm 17)	129 (25)	0.635
	Diastolic BP	78 (\pm 9)	74 (13)	0.252
	Mean BP	96 (\pm 12)	92 (17)	0.403

4.2.2 *CMR image acquisition*

Pre-contrast CMR image acquisition, in PH patients and controls, was performed as described in Methods Section 2.3.2.1. Contrast enhanced imaging was performed in PH patients only as described in Methods Section 2.3.2.2.

4.2.3 *Pre-contrast CMR image analysis*

Pre-contrast CMR images analysis was performed as described in Methods Section 2.3.4.1.

4.2.4 *Contrast enhanced-CMR image analysis*

All post contrast CMR images were analysed as described in Methods Section 2.3.4.2.

4.2.5 *Clinical assessment and right heart catheterisation*

Clinical assessment followed a standard diagnostic algorithm as described in Methods Section 2.2.

4.2.6 *Statistical Analysis*

For all variables a normal distribution was verified using histograms and Kolmogorov-Smirnov tests. For demographic, haemodynamic and ce-CMR variables mean values \pm one standard deviation (\pm SD) were calculated. Correlations between

normally distributed CMR and haemodynamic variables were tested by Pearson's method, correlation involving non-normally distributed variables was assessed using Spearman's rho test; all tests were two-tailed. Mean signal intensity values for areas of DCE versus reference areas were compared by a paired t-test. An independent samples (unpaired) t-test (equal variances not assumed) was used to compare right and left ventricular measurements acquired in the twenty five PH patients studied with a) the twelve control subjects assessed in our own laboratory and b) previously published normal mean values. This method was also used to compare differences in mean DCE mass between sub-groups of patients with different aetiologies of PH and gender and to compare systemic blood pressure measurements in PH patients compared with controls. A significance level of 5 % was used in all tests. No adjustment was made to p-values to account for multiple testing. All statistical analyses were performed using SPSS 11.5 for Windows (SPSS Inc., Chicago, USA). All values are presented as mean (\pm 1SD) unless otherwise stated.

4.3 Results

4.3.1 Right heart catheterisation

Invasive measurements acquired in the PH patients are summarised overleaf in Table 4.3.

Table 4.3

Results of Right Heart Catheterisation in 25 patients with PH

	Mean (\pm SD)
PAP * (mmHg)	Systolic PAP 72 (\pm 20)
	Diastolic PAP 23 (\pm 9)
	Mean PAP 43 (\pm 12)
Cardiac Output (l/min)	4.3 (\pm 1.2)
PVR † (mmHg/l/min)	9 (\pm 5)
RAP ‡ (mmHg)	7 (\pm 5)
Mixed Venous Oxygen Saturation (%)	66 (\pm 8)

*PAP: Pulmonary Arterial Pressure, † PVR: Pulmonary Vascular Resistance, ‡ RAP: Right Atrial Pressure

4.3.2 *Pre-contrast CMR imaging*

Ventricular dimensions and systolic function of PH patients and control subjects are presented in Table 4.4 on page 174. In summary, LV measurements within PH patients were within previously published normal limits (97, 140); LVEDV and LVSV were, however significantly lower in the PH cohort compared with local controls. Within the control population both left and right ventricular measurements were within previously published normal limits (97, 140). In PH patients RV volumes and RV mass were significantly increased, and RVEF significantly depressed in

comparison with both control subjects and previously published normal ranges (97). For both left and right ventricular measurements in controls and PH patients we have compared our measurements with normal ranges acquired using a SSFP CMR technique where these ranges are available (140).

4.3.3 *Contrast enhanced CMR imaging*

Delayed contrast enhancement was demonstrated in twenty three out of twenty five patients. Median DCE mass for the population studied was 3.3g (range 0 – 22.2g). Contrast enhancement was confined to the RV insertion points (RVIPs) in seven out of twenty three patients. Further contrast enhancement was demonstrated outwith, but still contiguous with the RVIPs, within the Interventricular Septum (IVS), in sixteen out of twenty three patients (examples are shown in figure 4.1 on pages 175 and 176). Two patients showed no evidence of contrast enhancement.

Table 4.4

Ventricular dimensions and function in 25 patients with PH and 12 control subjects who underwent contrast enhanced-Cardiovascular Magnetic Resonance imaging.

Values are mean (\pm SD)

	PHT n = 25	Controls n = 12	p value
Right Ventricle			
EDV * (ml)	179 (\pm 60)	128 (\pm 46)	p = 0.009
ESV † (ml)	104 (\pm 58)	45 (\pm 22)	p < 0.001
Stroke Volume (ml)	75 (\pm 27)	83 (\pm 29)	p = 0.383
Ejection Fraction (%)	45 (\pm 17)	65 (\pm 7)	p < 0.001
Mass (g)	86 (\pm 34)	48 (\pm 18)	p < 0.001
RV Mass Index	0.88 (\pm 0.25)	0.41 (\pm 0.04)	p < 0.001
Left Ventricle			
EDV * (ml)	90 (\pm 25)	116 (\pm 36)	p = 0.01
ESV † (ml)	29 (\pm 17)	31 (\pm 14)	p = 0.601
Stroke Volume (ml)	63 (\pm 17)	85 (\pm 24)	p = 0.002
Ejection Fraction (%)	70 (\pm 11)	74 (\pm 7)	p = 0.457
Mass (g)	97 (\pm 27)	120 (\pm 51)	p = 0.178

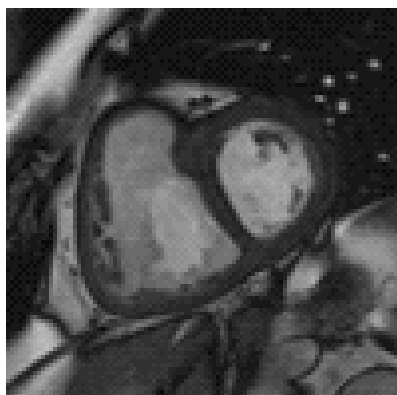
* EDV; End Diastolic Volume, † ESV; End Systolic Volume

Figure 4.1, opposite

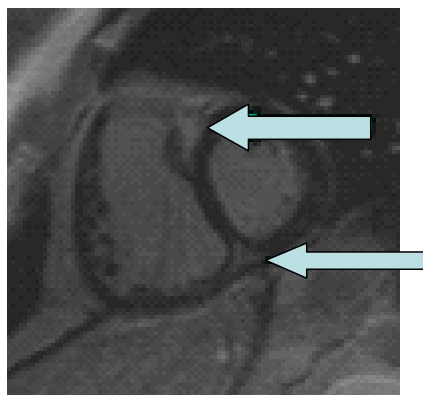
25 patients with Pulmonary Hypertension (PH) and 12 control subjects underwent contrast enhanced-Cardiovascular Magnetic Resonance imaging. Images series 1 and 2 were acquired at basal and mid-ventricular slice positions, respectively, in a patient with PH. Images 1(a) and 2 (a) are pre-contrast. Images 1(b) and 2(b) were acquired ten minutes after intravenous administration of Gadolinium. Images 1(c) and 2 (c) are ‘swapped phase images’, which were acquired to verify areas of delayed contrast enhancement (indicated by blue arrows).

Figure 4.1

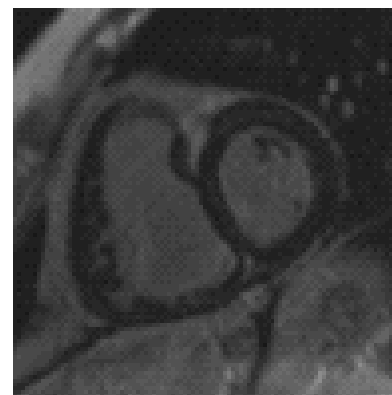
Image series 1



1(a)



1(b)

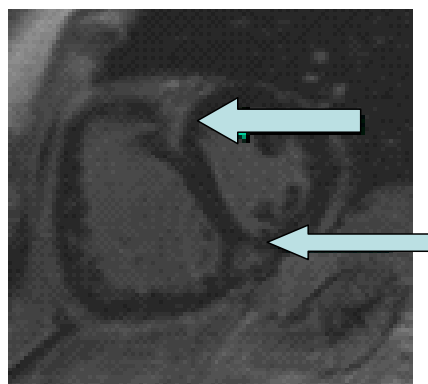


1(c)

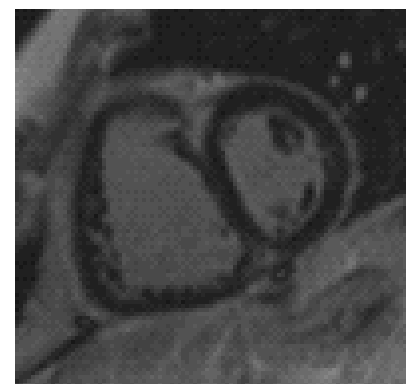
Image series 2



2(a)



2(b)



2(c)

The mean signal intensity (SI) of areas of contrast enhancement was significantly higher than that of reference areas (mean SI (contrast enhancement areas) = 31.6 (11.5), mean SI (reference areas) = 7.3 (1.8), $p < 0.001$). In all patients, contrast enhancement, whether it was localised to the RVIPs or extended into the IVS, was confined to the mid-wall region of the ventricular myocardium. No sub-endocardial contrast enhancement was seen. No contrast enhancement was seen within the RV free wall or the LV outwith the IVS. There were no significant differences in the DCE pattern or DCE mass in patients with different aetiologies of PH or different gender.

There were a number of statistically significant correlations between the extent of contrast enhancement seen (DCE mass) and both invasive pulmonary haemodynamics and RV dimensions and function at CMR (see figure 4.2 overleaf). Correlations not shown in this figure include DCE mass α RV mass/BSA ($r = 0.639$, $p = 0.001$), systolic pulmonary artery pressure (PAP) ($r = 0.589$, $p = 0.002$, diastolic PAP ($r = 0.538$, $p = 0.006$) and pulmonary vascular resistance (PVR) ($r = 0.459$, $p = 0.024$)

IVS bowing (displacement of the IVS towards the LV in early LV diastole) (148, 157) was observed in seventeen out of twenty five patients studied (see figure 4.3 on page 183). This phenomenon was observed in all sixteen patients in whom contrast enhancement was seen within the IVS. Only one patient with IVS bowing had contrast enhancement confined to the RVIPs.

Figure 4.2, below

25 patients with Pulmonary Hypertension (PH) underwent contrast enhanced-Cardiovascular Magnetic Resonance imaging. The extent of delayed contrast enhancement (DCE) within the RV insertion points and interventricular septum was quantified by manual planimetry and defined as DCE mass. DCE mass was correlated against various indices of RV structure, RV function and pulmonary haemodynamics

Figure 4.2

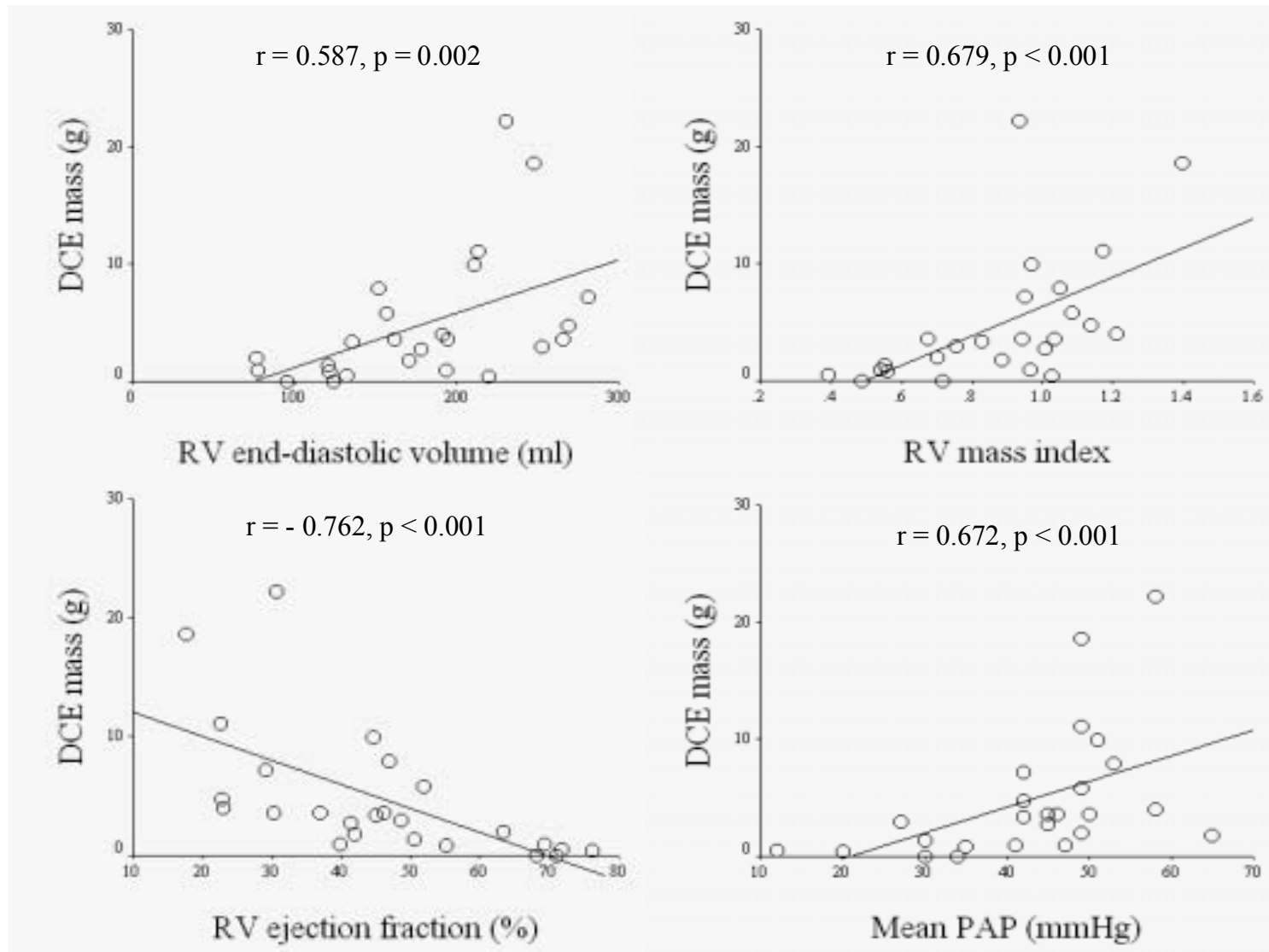
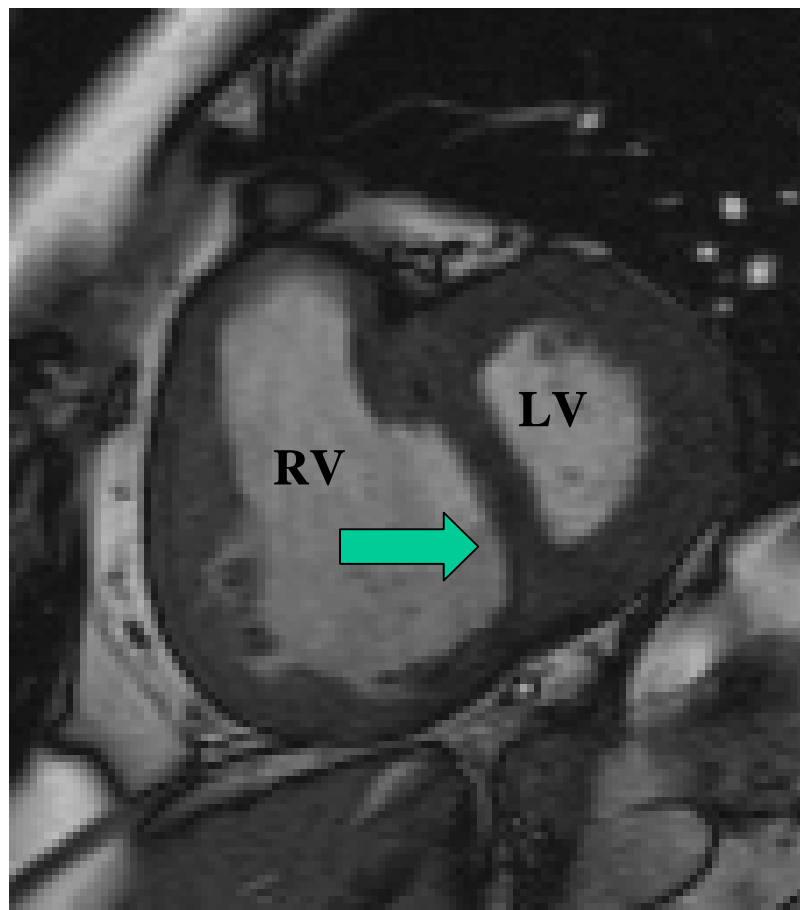


Figure 4.3

25 patients with Pulmonary Hypertension (PH) underwent contrast enhanced-Cardiovascular Magnetic Resonance imaging. A single pre contrast, short axis CMR image is presented. The image was acquired at a mid-ventricular level, in early diastole and clearly demonstrates interventricular septal (IVS) bowing (arrowed), i.e. leftward displacement of the IVS during diastole. This phenomenon was observed in 17/25 PH patients studied and all 16 patients in whom septal delayed contrast enhancement was detected. The image used was acquired in the same patient used in figure 4.1 for ease of comparison.



4.4 Discussion

The study described in this chapter was based upon the hypothesis that discrete, and detectable, myocardial abnormalities might exist in patients with PH. Delayed contrast enhancement (DCE), indicative of some form of myocardial damage, was demonstrated in the vast majority of patients in this experiment (twenty three out of twenty five subjects). The two subjects in whom DCE was not demonstrated both had low pulmonary artery pressures at invasive assessment (mean PAP 30 mmHg and 34 mmHg respectively) and normal RV anatomy and function at CMR (RV ejection fractions 68 % and 71% respectively). All areas of DCE detected were in the mid-wall of the ventricular myocardium at either the RV insertion points (RVIPs), in isolation (in seven patients), or both the RVIPs and the IVS (in the remaining sixteen patients). The extent of DCE, defined by DCE mass, correlated with various haemodynamic variables. Septal contrast enhancement was particularly associated with the presence of IVS bowing, i.e. in all sixteen patients in whom septal contrast enhancement was demonstrated, bowing of the IVS was also seen. Only one patient demonstrated IVS bowing without significant septal contrast enhancement (in this subject contrast enhancement was present but was confined to the RVIPs).

There were no significant differences in DCE mass in patients of different genders or different aetiologies. The numbers of patients in these sub-groups were, however, small making it difficult to draw significant conclusions from these results.

4.4.1 *Potential mechanisms of contrast enhancement*

The physiological mechanism(s) responsible for the contrast enhancement observed are unknown. In general, DCE is thought to result from delayed clearance of gadolinium from a relatively expanded extracellular volume within fibrotic or necrotic myocardial compartments (110, 111). Potential biological mechanisms for the contrast enhancement seen in this experiment are explored below.

4.4.1.1 *Myocardial ischaemia*

The exclusive and consistent mid-wall contrast enhancement pattern demonstrated is not typical of ischaemic injury. DCE in acute and chronic myocardial infarction characteristically involves the subendocardium and extends transmurally depending on the size of the infarct (104, 108). Furthermore, earlier studies found no evidence of reversible myocardial ischaemia within either the RVIPs or the IVS using stress myocardial scintigraphy in patients with PH (158).

4.4.1.2 *Myocardial fibrosis*

The mid-wall contrast enhancement pattern observed appears most similar to that recently described in several studies of patients with Hypertrophic Cardiomyopathy (HCM) using ce-CMR (106, 113, 120). These studies have demonstrated similar contrast enhancement to that seen in this experiment in both the RVIPs and other foci throughout the heart, including the IVS (120). Contrast enhancing foci in HCM have recently been shown to correlate histologically with areas of increased myocardial

collagen (113) and while autopsy studies of the hearts of patients with HCM had, in the past, demonstrated gross muscle fibre disarray and destruction of the circumferential, mid-wall component of the ventricular myocardium within the RVIPs (121) it is only since the publication of the more recent CMR studies referenced above that this distribution of fibrosis has become recognised as the pattern typical of HCM. Despite an extensive review of the literature we have, however, been unable to find any similar autopsy studies which describe the histopathological appearances seen within the RVIPs and IVS of human subjects with PH. This makes any speculation that similar mechanisms of delayed contrast enhancement might exist in patients with PH uncertain.

4.4.1.3 *Elevated RV afterload*

One possible precipitant for myocardial abnormalities in the setting of PH is elevated RV afterload. DCE mass in this experiment correlated positively with RV mass and RVMI; both variables which have been associated with the degree of RV hypertrophy present in patients with PH (101, 102). Pure *afterload-induced* myocardial hypertrophy seems, however, an unlikely cause of the fibrosis suggested by the contrast enhancement seen here. It is difficult to see how such a global insult to the RV myocardium could explain the consistent and exclusive deposition of contrast within the RVIPs and IVS. This localised contrast enhancement pattern suggests an additional precipitant of what appears most likely to be fibrotic change within the areas described.

4.4.1.4 *Mechanical wall stress*

The RVIPs are regions of a particular mechanical stress, even under normal physiological conditions. In severe PH, these mechanical stresses are amplified as elevation of RV chamber pressures results in the generation of a physiologically abnormal leftward trans-septal pressure gradient. This gradient is manifested physiologically as the paradoxical, leftward displacement of the IVS seen during early LV diastole (i.e. late RV systole) (148, 157) in a proportion of patients with PH (see figure 4.3). It is of note that in our study, all sixteen patients in whom there was evidence of septal contrast enhancement also showed clear evidence of IVS bowing. Furthermore, animal studies have shown that the middle, circumferential layer of the LV myocardium, which by conventional CMR terminology includes the areas identified within the RVIPs and IVS in this experiment, are subject to maximal hoop stress (defined as force generated per unit area of myocardium) during the course of normal ventricular contraction (159). Finally, in a rodent model of hypobaric-hypoxic PH the RVIPs (within three days of hypoxia) and later the IVS were identified by McKenzie and co-workers as the earliest sites of immunoreactive-Atrial Natriuretic Peptide expression. The authors concluded that these areas were subject to the earliest and most intense increases in mechanical wall stress as a result of developing PH and rising RV chamber pressures (160).

4.4.1.5 *Summary of potential mechanisms of DCE*

At the current time, it is only possible to speculate on the true reasons for the contrast enhancement pattern demonstrated in our study. However, based upon the evidence

available from earlier studies, it appears most likely to reflect altered contrast kinetics due to myocardial fibrosis (113) within the mid-wall, circumferential muscle compartment of the RVIPs and IVS. Elevated mechanical wall stress in these areas appears a likely precipitant of this fibrosis. Definitive proof will require correlation between areas of DCE at CMR and autopsy specimens from patients with PH.

4.4.2 *Study Limitations*

None of the patients in this study underwent coronary angiography to formally exclude ischaemic heart disease (IHD) which is an important cause of DCE. However, the contrast enhancement pattern observed is not typical of ischaemic myocyte injury and a diagnosis of IHD was not considered likely in any patient studied based on the presenting clinical picture.

4.4.3 *Clinical implications*

Contrast enhanced-CMR imaging provides a novel method of identifying and quantifying myocardial abnormalities in patients with PH, abnormalities which have thus far gone undetected. This study, in combination with the work of others (147, 148, 157) emphasises the importance of interventricular septal dysfunction in the evolution of RV failure in PH. Given the correlations of DCE mass with existing markers of disease severity in PH, this measure may prove useful in the prognostic classification of patients presenting with PH.

Chapter 5

Dobutamine stress-Cardiovascular Magnetic Resonance
imaging in patients with pulmonary hypertension

5.1 Introduction

In Chapter 4 it was shown that discrete myocardial abnormalities exist within the RV insertion points and interventricular septum of patients with PH. The nature of these could not be proven but the available evidence supports a hypothesis that they represent areas of myocardial fibrosis precipitated by mechanical wall stress associated with interventricular septum bowing. In this chapter the intimate relationship between the right and left ventricles of patients with PH is explored in more detail.

Exercise limitation is common in patients with PH (129) and appears related to an inability to appropriately increase cardiac output by increasing right and left ventricular stroke volumes during physical activity (47, 130). However, the reasons for stroke volume limitation in PH are not well understood, and are probably different for each ventricle. For example, the blunted LV stroke volume response seen in PH has been attributed to impaired LV filling as a result of low RVSV and low LV preload in some studies (161, 162), but related more to direct ventricular interaction, mediated by leftward displacement of the interventricular septum, in others (163-165).

Detailed study of cardiac physiology during exercise in PH patients is not easy. Ideally one would like to compare invasive cardiac filling pressures, during exercise, with accurate right and left ventricular volume measurements. However, the invasive nature of these studies makes them unattractive to both patients and investigators. An alternative, non-invasive approach is, therefore, preferable. As has been discussed in earlier chapters, CMR imaging can be used to directly and accurately measure

ventricular volumes and function and can also quantify right and left ventricular stroke volumes based on forward flow measured in the main pulmonary artery and aorta, respectively (166). Therefore, exercise-CMR imaging seems to offer obvious potential as a means of enhancing our understanding of the reasons for stroke volume limitation during exercise in PH. Unfortunately, true exercise-CMR images are degraded by movement artefact during physical activity, meaning that accurate images can only be acquired immediately following exercise. Dobutamine stress-CMR (ds-CMR) circumvents these difficulties and allows true stress measurements to be made, thus avoiding potential errors relating to exercise recovery. Dobutamine approximates physiological conditions during exercise in PH patients by increasing cardiac output. It is a pure inotrope with no flow-independent effects on pulmonary vascular tone (125). In earlier studies, ds-CMR has been used successfully in patients with congenital heart disease. However, it has yet to be used in patients with PH due to other causes. The primary hypothesis of the following experiment was that ds-CMR could be used to identify the reason(s) for right and left ventricular stroke volume impairment during exercise in PH patients.

5.2 Methods

5.2.1 Study participants and clinical assessment

Sixteen patients with PH were recruited and clinically assessed as described in Methods Section 2.1-2.2. None of these patients were recruited to the other studies in this thesis. Two specific exclusion criteria were used during recruitment for this study. Patients with PH due to congenital heart disease were excluded, after clinical

assessment and transthoracic echocardiography, because of their more complicated cardiac anatomy and physiology. Patients with contraindications to dobutamine were also excluded, e.g. aortic stenosis, hypokalaemia and dobutamine allergy. Six control subjects were recruited as described in Methods Section 2.1 and underwent dobutamine stress-CMR but no other tests. No study participant (PH patient or control) was taking chronotropic cardiac medication at the time of dobutamine stress-CMR.

5.2.2 *Dobutamine stress-CMR imaging*

Dobutamine stress-CMR was performed using the protocol described in Method Section 2.3.2.3 in PH patients and controls.

5.2.3 *Dobutamine stress-CMR image analysis*

All scans were coded by number and analysed using the Argus analysis software as described in Method Section 2.3.4.3.

5.2.4 *Statistics*

For all variables a normal distribution was verified using histograms and Kolmogorov-Smirnov tests. Comparisons between resting and stress CMR measurements were made using a paired t-test and quantified as percentage of the resting value (%). Comparisons between PH patients and controls and sub-groups of PH patients were made using an independent samples (unpaired) t-test (using Welch's correction if appropriate). Correlation between measurements was tested using

Pearson's method. All statistical analyses were performed using GraphPad Prism 4 for Windows (GraphPad Software Inc., San Diego, USA), were two-sided and assumed a significance level of 5 %. All values are presented as mean (\pm SD) unless otherwise stated.

5.3 Results

5.3.1 Clinical characteristics and demographics

The final diagnoses reached in the 16 PH patients were, Pulmonary Arterial Hypertension (PAH) in 12/16 (idiopathic PAH in 8, PAH related to connective tissue disease in 4) and Chronic Thromboembolic PH in 4/16. Invasive haemodynamic measurements are summarised overleaf in Table 5.1.

PH patients were older than controls (mean age PH: 55 (\pm 10), controls: 37 (\pm 10), $p = 0.001$) and 12/16 of the PH patients were female; all 6 controls were male. The two populations were well matched for systemic BP (systolic BP in PH: 123 (\pm 16), in controls: 114 (\pm 8), $p = 0.215$), diastolic BP in PH: 80 (\pm 12), in controls: 73 (\pm 6), $p = 0.1586$), mean arterial BP in PH: 98 (\pm 13), in controls: 87 (\pm 6), $p = 0.053$).

Table 5.1

Invasive haemodynamic measurements acquired in 16 patients with Pulmonary Hypertension who underwent dobutamine-stress Cardiovascular Magnetic Resonance imaging

Variable	mean (\pm 1SD)
Pulmonary artery pressure (mmHg)	
Systolic	84 (24)
Diastolic	27 (9)
Mean	50 (14)
Cardiac index (l/min/m ²)	2.3 (0.5)
Mean right atrial pressure (mmHg)	7 (5)
Pulmonary artery occlusion pressure (mmHg)	8 (2)
Pulmonary vascular resistance (mmHg/l/min)	12 (5)
Mixed venous oxygen saturation (%)	63 (6)

5.3.2 *Symptoms*

During dobutamine stress testing, 6/16 PH patients experienced breathlessness, 1/16 reported pounding in the chest, 1/16 reported light-headedness and 1/16 reported headache. None of these symptoms were intolerable or necessitated a reduction in dobutamine dose. However, 7/16 patients exceeded the safety tolerances set for the study (HR increment > 50 % in 5/16, fall in systolic BP > 20 % in 2/16). In these seven patients, the dobutamine infusion rate was reduced to 15 mcg/kg/min during stress CMR imaging. 5/7 of these patients experienced symptoms.

The average dose and total time spent on Dobutamine during measurement were similar in controls and PH patients (19.1 (1.4) vs. 18.1 (2.3) mcg/kg/min, ($p = 0.363$) and 26 (3) vs. 28 (7) minutes ($p = 0.450$), respectively).

5.3.3 *CMR results*

All PH patients and controls completed the CMR imaging protocol, which took an average of 35 minutes to complete. There was excellent internal agreement between RVSVI and LVSVI at rest and during stress in both PH patients and controls. Results are presented in detail below and are summarised overleaf in Table 5.2.

Table 5.2

Right and left ventricular measurements at rest and during dobutamine infusion in 16 patients with Pulmonary Hypertension and 6 controls who underwent dobutamine-stress Cardiovascular Magnetic Resonance imaging

	Controls			PH		
	Rest	Stress	% Change	Rest	Stress	% Change
Right Ventricle						
SVI (ml/m ²)	43 (± 8)	52 (± 13)*	+ 23	26 (± 10)†	29 (± 11)	
EDVI (ml/m ²)	75 (±14)	63 (± 13)		92 (± 24)†‡	86 (± 29)‡	
ESVI (ml/m ²)	32 (± 9)‡	14 (± 6)**‡	- 56	58 (± 24)†‡	48 (± 30)*‡	- 17
EF (%)	61 (± 19)	84 (± 10)*	+ 38	30 (± 13)†‡	38 (± 19)*‡	+ 27
Left Ventricle						
SVI (ml/m ²)	44 (± 9)	53 (± 15)*	+ 20	27 (± 10)†	30 (± 10)	
EDVI (ml/m ²)	78 (± 12)	67 (± 15)		48 (± 15)†	42 (± 12)*	- 13
ESVI (ml/m ²)	25 (± 6)	10 (± 4)**	- 60	16 (± 6)†	8 (± 5)**	- 50
EF (%)	57 (± 12)	79 (± 15)*	+ 39	57 (± 10)	72 (15)**	+ 26
Heart Rate (bpm)	62 (± 13)	97 (± 21)**	+ 56	75 (± 12)	105 (± 20)**	+ 41

SVI = stroke volume index, EDVI = end-diastolic volume index, ESVI = end-systolic volume index, EF = ejection fraction. * = p < 0.05, ** = p < 0.01 for stress vs. rest within groups, † p < 0.05 for PH patients vs. controls at rest, ‡ p < 0.05, right vs. left within groups

5.3.3.1 *Resting analyses*

RV volumes were larger and RSVI and RVEF were lower in PH patients compared to controls. 15/16 PH patients had RV systolic dysfunction based on previously published normal ranges. LV volumes and LSVI were also lower in PH patients; however LV systolic function was normal (140). All measurements were normal in controls (140).

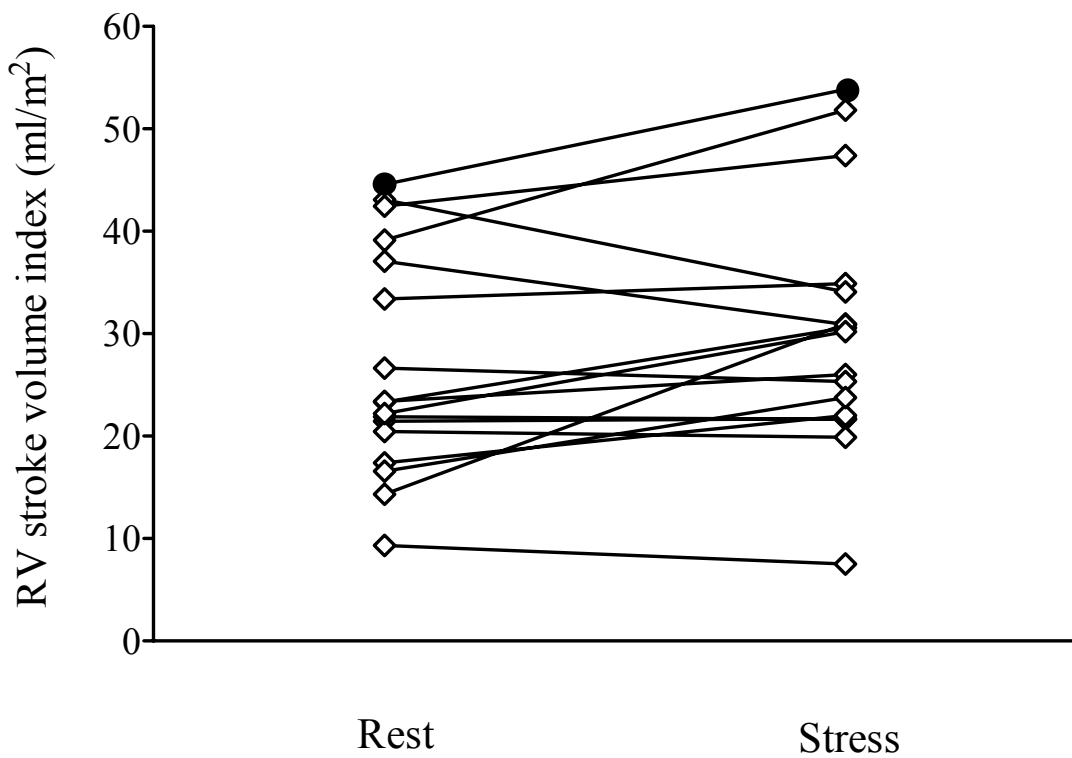
5.3.3.2 *Stress analyses*

In control subjects dobutamine resulted in statistically significant and matched increments in mean right and left ventricular stroke volume index (23 % and 20 %, respectively) and ejection fraction (38 % and 39 %, respectively). As a result, mean right and left ventricular end-systolic volume fell in a similar co-ordinated manner (by 56 % and 60 %). In controls, mean right and left ventricular end-diastolic volume was unchanged and heart rate rose significantly. These findings represent a normal physiological response to dobutamine as demonstrated in earlier studies (126, 167).

In PH patients, the co-ordinated response to dobutamine seen in controls was lost. RV stroke volume index did not increase overall and fell in 3/16 patients (see figure 5.1 overleaf). Although mean RV ejection fraction increased (by 27 %) and mean RV end-systolic volume fell (by 17 %) these changes were smaller in absolute terms than those observed in controls. Mean RV end-diastolic volume was unchanged in PH patients but LV end-diastolic volume fell significantly (by 13 %). HR rose by a similar amount in PH patients as it did in controls.

Figure 5.1

RV stroke volume index (RVSVI) was measured at rest and during dobutamine stress by Cardiovascular Magnetic Resonance imaging in 16 patients with Pulmonary Hypertension and 6 controls. Individual values are presented for PH patients (\diamond - \diamond); mean RVSVI did not change significantly overall (26 (10) ml vs. 29 (11) ml, $p = 0.1$) and RVSVI fell in three patients. RVSVI rose significantly in all controls, mean rest and stress RVSVI (\bullet - \bullet) (43 (8) vs. 52 (13), $p = 0.03$) are presented to summarise these data.



5.3.4 *Correlates of the right and left ventricular stroke volume response to dobutamine*

Right and left ventricular stroke volume responses to dobutamine were defined by Δ RVSVI and Δ LVSVI, respectively. These responses were correlated against changes in right and left ventricular dimensions during dobutamine infusion (identified in the text by the prefix Δ) and resting CMR measurements (see Table 5.3 overleaf). Δ RVSVI correlated closely with Δ RV ejection fraction ($r = 0.94$, $p < 0.001$) but did not relate to either resting or dynamic RV volumes or resting RV stroke volume index or ejection fraction.

Δ LVSVI correlated with Δ LV end-diastolic volume ($r = 0.547$, $p = 0.028$) and Δ LV ejection fraction ($r = 0.645$, $p = 0.007$) but was not related to resting LV volumes or ejection fraction. LV end-diastolic volume index correlated strongly with RV stroke volume index at rest ($r = 0.821$, $p < 0.001$) and stress ($r = 0.693$, $p = 0.003$) (see figures 5.2 (a) and (b), respectively, on page 201).

Table 5.3

Correlates of the effect of dobutamine on right and left ventricular stroke volumes measured using dobutamine stress-Cardiovascular Magnetic Resonance imaging in 16 patients with Pulmonary Hypertension

	Pearson r	p value
Δ RV stroke volume index		
Resting RV stroke volume index	-0.337	0.201
Resting RV ejection fraction	-0.219	0.416
Resting RV end-diastolic volume index	-0.022	0.936
Resting RV end-systolic volume index	0.012	0.657
Δ RV ejection fraction	0.94	< 0.001
Δ RV end-diastolic volume index	-0.436	0.092
Δ RV end-systolic volume index	-0.223	0.406
Δ LV stroke volume index		
Resting LV stroke volume index	-0.297	0.263
Resting LV ejection fraction	0.012	0.965
Resting LV end-diastolic volume index	-0.339	0.199
Resting LV end-systolic volume index	-0.142	0.599
Δ LV ejection fraction	0.645	0.007
Δ LV end-diastolic volume index	0.547	0.028
Δ LV end-systolic volume index	-0.142	0.599

Figure 5.2

RV stroke volume index (RVSVI) and LV end-diastolic volume index (LVEDVI) were measured at rest and during dobutamine stress-Cardiovascular Magnetic Resonance imaging in 16 patients with Pulmonary Hypertension. RVSVI was closely related to LVEDVI, both at rest (figure 5.3 (a), $r = 0.821$, $p < 0.001$) and during stress (figure 5.3 (b), $r = 0.693$, $p = 0.003$).

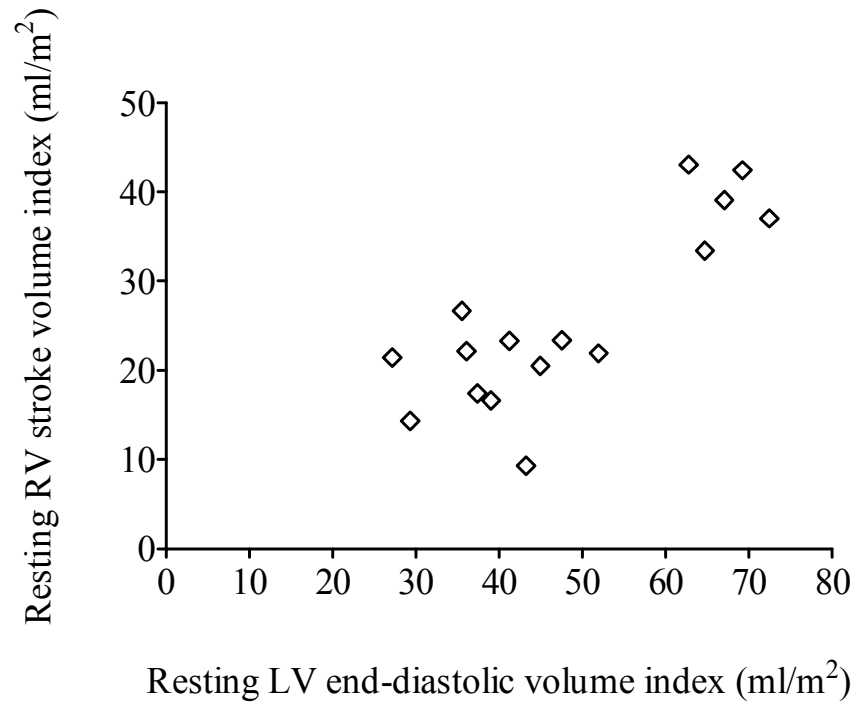


Figure 5.2 (a)

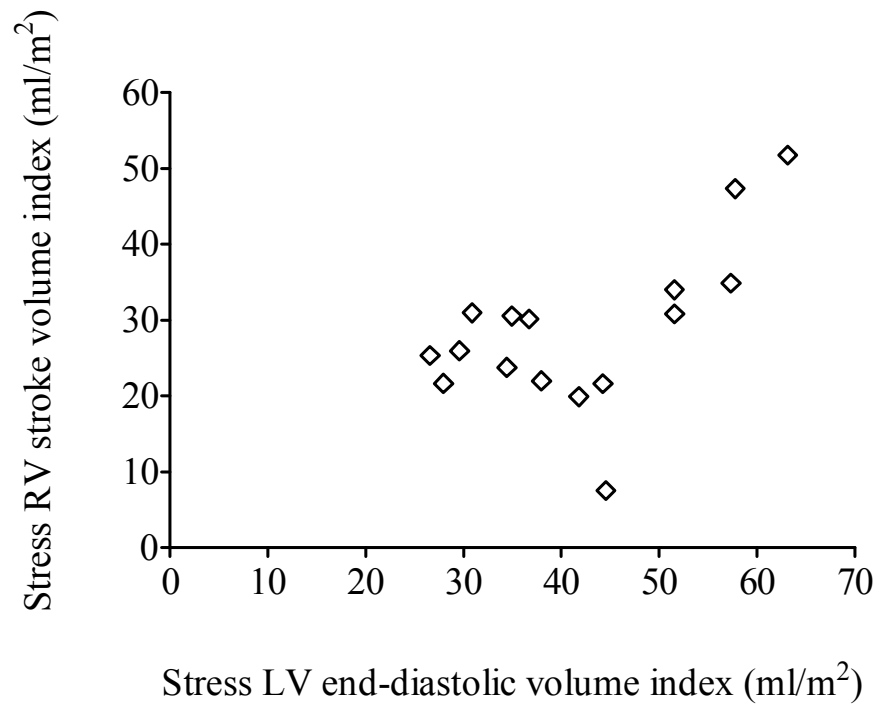


Figure 5.2 (b)

5.4 Discussion

In this Chapter, dobutamine stress-CMR imaging was performed successfully in all 16 PH patients and 6 controls. The protocol was well tolerated, with no serious adverse events. As expected there was good internal agreement between right and left ventricular stroke volumes both at rest and with stress in PH patients and controls. This provided quality assurance regarding the imaging performed.

The major results of this study are as follows. The normal, synchronised response to dobutamine was lost in PH patients who were unable to increase either right or left ventricular stroke volume. This has been shown before in earlier studies. (47, 168, 169) Interestingly, the reasons for stroke volume limitation were different for right and left ventricles. The principal reason for RSVV limitation appeared diminished RV contractile reserve. In contrast, LVSV was limited primarily by impaired LV filling, which, in turn, appeared due to low RSVV (i.e. preload) rather than LV compression due to displacement of the interventricular septum. These findings are discussed in more detail below.

5.4.1 *Right ventricle*

In PH patients, mean RV stroke volume did not rise in response to dobutamine and individual values actually fell in 3/16 patients, see figure 5.1. The increment seen in RV ejection fraction in PH patients (27 %), although statistically significant, was also smaller than that observed in controls (38 %). The extent of this change in RV ejection fraction (Δ RVEF) correlated strongly with the resulting change in RV stroke

volume (Δ RVSVI), which was not related to any other resting or stress CMR measurement. RV stroke volume is determined principally by RV end-diastolic volume and RV ejection fraction. However, RV end-diastolic volumes did not change during dobutamine infusion. These findings suggest that the principal factor limiting RV stroke volume augmentation in this experiment was the ability of the PH patients to increase RV ejection fraction appropriately.

The physiological significance of RV ejection fraction has been the subject of recent study. Although it reflects RV contractility, RV ejection fraction is also influenced by RV afterload (151-153). Interesting recent evidence has identified a close correlation between RV ejection fraction and RV wall stress in PH patients (150), indicating that RV ejection fraction is, in fact, a better reflection of the extent to which the RV has adapted to the afterload it faces (170). Thus, the intimate relationship between RV ejection fraction and the capacity to appropriately increase stroke volume in this experiment indicates a degree of RV maladaptation, or diminished contractile reserve. It is reasonable to presume that the rise in pulmonary artery pressure during physical activity previously demonstrated, using the ambulatory pulmonary artery catheter (171), mediates a rise in RV afterload and stroke work, exposing this maladaptation.

Previous studies have found similar evidence of RV stroke volume impairment in patients with PH, using exercise-CMR imaging (168), exercise-Electron Beam CT imaging (169) and cardiopulmonary exercise testing (47). RV ejection fraction fell in both of the earlier imaging studies (168, 169), in which stroke volume was measured post-exercise. These results support the conclusion that the RV contractile function, which reflects the level of adaptation of the RV to the afterload it faces, is the

principal determinant stroke volume during exercise in PH. However, the fall in RV ejection fraction demonstrated in these reports contrasts with the increment, albeit blunted, in RV ejection fraction seen in our patients, stressed using dobutamine. A similar difference between exercise-CMR and ds-CMR has been shown before in patients with congenital heart disease (126). It is unclear whether this difference reflects the fact that measurements can only be made post-exercise in exercise-CMR. Nevertheless results from the two techniques cannot be directly compared in PH patients.

5.4.2 *Left ventricle*

As indicated above, PH patients were unable to increase LV stroke volume in response to dobutamine. In contrast to the RV, the change seen in LV stroke volume (Δ LVSVI) correlated with both Δ LV ejection fraction and Δ LVEDV. While resting and stress LVEF was normal (161, 172) in PH patients, LV end-diastolic volumes were low at rest and fell further during stress testing in this experiment and in earlier studies (168, 169). Thus, reduced LV filling appeared the more important determinant of LV stroke volume than LVEF in the PH patients in this study. As indicated in Section 5.1, the mechanisms behind this are not well understood.

One potential explanation for reduced LV filling is compression of the LV within the enclosed pericardial sac. Earlier studies have demonstrated that the pressure overloaded RV causes leftward displacement of the interventricular septum during early diastole (163-165). Such a mechanism certainly seems plausible on inspection of CMR images in patients with PH showing an apparently squashed LV cavity.

Early animal studies by Elzinga and co-workers (173) first proposed that such pericardial ‘constriction’ played an important role in right-left ventricular interaction. More recently, Baker (174) and Belenkie (175), using similar canine models of acute RV pressure overload, demonstrated that opening of the pericardium facilitated improved LV filling and an increase in stroke volume. Evidence that direct ventricular interaction may be important in human subjects with PH has recently been reported by Gan *et al*, who correlated left atrial filling rate, derived from transoesophageal echocardiography, against cardiac dimensions measured at rest using CMR. In this study, LV filling rate correlated with the severity of leftward interventricular septal displacement and the authors concluded that septal displacement was directly impairing LV relaxation and, therefore, filling (163).

The alternative view is that impaired LV filling reflects low RV stroke volume and diminished LV preload (161, 162). Under these conditions, septal displacement would still occur, but would do so more as a consequence of reduced LV filling rather than as the cause of it. We found some evidence in support of this hypothesis in that we demonstrated a linear and consistent correlation between LV end-diastolic volume and RV stroke volume at rest and stress (see figures 3 (a) and (b), respectively). This indicates coupling between RV output and LV filling under both conditions.

This hypothesis is further supported by previous studies. Gurudevan *et al* demonstrated rapid resolution of mitral valve inflow abnormalities and normalisation of LV filling rates using echocardiography pre- and post-pulmonary thromboendarterectomy (PTE) in patients with chronic thromboembolic PH (161). These improvements were associated with a fall in pulmonary vascular resistance and

a rise in wedge pressure but no change in the M-mode appearance of the interventricular septum. Furthermore, Blanchard et al found, in patients with chronic RV pressure overload due to chronic thromboembolic PH (contrast this with the model of acute RV pressure overload used by Baker and Belenkie) that although the LV appears compressed by the RV, pericardiectomy results in no change in LV volume or diastolic filling (176). These studies suggest that the human pericardium may be able to adapt to pressure and shape changes over time and the role of 'direct' ventricular interaction due to pericardial constriction is unclear at this time.

Furthermore, earlier invasive exercise studies also support the conclusion that direct ventricular interaction is less important than reduced RV stroke volume in limiting LV filling: During Operation Everest II (OE II), normal subjects were exposed to chronic hypoxia and exercised during a simulated ascent of Everest. Pulmonary artery pressure and pulmonary vascular resistance rose in these subjects without any rise in pulmonary capillary wedge pressure (177), making them a reasonable haemodynamic model of established PH due to other diseases. In this study, LV stroke volume and end-diastolic volume also fell in all subjects during exercise, accompanied by a decrease in pulmonary capillary wedge pressure, but with preservation of LV systolic function (178, 179). These invasive measurements are consistent with my non-invasive observations. If septal displacement had played an important role in limiting LV end-diastolic volume in the OE II volunteers, a rise, rather than the observed fall in pulmonary capillary wedge pressure would have been expected.

In this chapter it has been shown that patients with PH are unable to increase right or left ventricular stroke volume when given the cardiac inotrope Dobutamine. The principal factor limiting RV stroke volume augmentation appears to be diminished RV contractile reserve, equivalent to maladaptation of the RV to the afterload it faces during exercise. In contrast, the principal cause of LV stroke volume limitation appeared to be impaired LV filling, as a result of low RVSV (i.e. preload) rather than LV compression due to interventricular septal displacement.

Chapter 6

General Discussion and Summary

Over the last fifteen years new and effective treatments for PAH and CTEPH have been developed. In patients with PAH, continuous intravenous Epoprostenol has been shown to improve survival in a randomised, controlled trial (180). Although this cumbersome, and potentially dangerous, treatment remains necessary in patients with WHO functional class IV disease, easier to manage oral alternatives, such as Bosentan, have proven as effective in patients with Class III disease in recent clinical trials (181). As a result, oral therapies are now accepted first-line treatment in patients with without overt evidence of RV failure (65). In a similar vein, pulmonary thromboendarterectomy (PTE) has revolutionised the outlook for patients with CTEPH. With increasing global experience and refinement of surgical techniques, post-operative care and pre-operative patient selection criteria, 5-year survival rates have reached almost 90% after successful PTE (182), in stark contrast to the 5-year survival rate of 10 % without surgery (183).

If this pace of clinical progress continues, even better therapies for PH may be developed in the years to come and treatment algorithms will have to evolve to accommodate them. In this dynamic clinical environment the development of a better means of quantifying and understanding RV function is essential. For the most part, RV function determines survival in PH patients and its precise and prompt measurement is likely to aid clinical decision-making in this context.

At present, PH physicians remain reliant on transthoracic echocardiography and right heart catheterisation for an assessment of RV function in their patients. As discussed in Sections 1.3.1 and 1.3.2 these tools are not ideal for this purpose. Echocardiography relies on flawed geometric assumptions to extrapolate three-dimensional RV volumes (and therefore function) from measurements acquired in two-dimensions and in a single plane. These assumptions become increasingly incorrect as the RV dilates and fails, as is inevitable in most PH patients. Right heart catheterisation is more accurate than echocardiography but it is so invasive that it cannot be justified in all patients. Furthermore, measurements are made during right heart catheterisation in a patient lying supine, at rest, in a catheterisation laboratory. This environment is far-removed from the patient's day-to-day activities and potentially distinct from their ability to exercise, on which the efficacy of subsequent treatments will be assessed. It is perhaps unsurprising, therefore, that resting invasive haemodynamics often change little despite apparently successful treatment of PH as assessed by improvement in symptom scores, exercise performance and survival (71, 184) since these values rarely reflect physiological conditions at the times that patients experience symptoms.

In Section 1.4.3 the advantages of CMR imaging in the assessment of the RV in PH patients were described. The principal strength of CMR is its ability to directly generate high fidelity measurements of right (and left) ventricular volume (97), mass

(101) and systolic function (97), in any plane and at almost any angle. These measurements can be made non-invasively, without the use of ionising radiation and are extremely reproducible, reducing the number of observations needed to test study hypotheses. Chapter 3 illustrates this final point clearly. In this experiment, CMR imaging was used to provide a gold-standard reference for RV systolic function. A close, logarithmic relationship between NT-proBNP and RV ejection fraction was found and the precision and reproducibility of the MR measurements allowed the identification of an NT-proBNP threshold for the detection of RV failure. As commented on by Groenning and co-authors in their paper on the NT-proBNP threshold for LV systolic function (79), the number of observations needed to define such a value using echocardiography would have been much greater due to the relative imprecision of the reference measurement

In Chapter 4, contrast-enhanced CMR was successfully used to identify occult myocardial abnormalities within the RV insertion points and interventricular septum (IVS) of patients with PH. These abnormalities, which probably reflect fibrosis related to IVS bowing, had gone undetected until this study. No other imaging modality has the ability that CMR imaging has to describe microscopic myocardial structure, in addition to macroscopic ventricular dimensions and function. The new information gleaned during this experiment emphasises the importance of IVS dysfunction in the evolution of RV failure in PH and is a potentially fertile area for future study (see Section 6.4).

In Chapter 5, Dobutamine stress-CMR (ds-CMR) was utilized to investigate and describe the reasons for right and left ventricular stroke volume impairment during

exercise in patients with PH. Ds-CMR was performed for the first time in PH patients in this experiment. Although stress echocardiography is a less expensive alternative to ds-CMR it is subject to the same errors as resting echocardiography described in Section 1.3.1. Stress echo is also extremely operator-dependant and pulmonary vascular units that do not specialise in echocardiography have had little success in replicating the results of the original publications by specialist stress-echocardiography units (185). Ds-CMR circumvents this operator dependency and allows high-fidelity imaging of both right and left ventricles during stress. Unlike physical exercise-CMR, which suffers from image degradation due to patient movement inside the scanner, ds-CMR also facilitates true stress imaging of PH patients, avoiding potential errors related to exercise recovery.

6.4 *Conclusions and future work*

This thesis has demonstrated that CMR imaging can be performed safely and yield high-quality images in patients with PH. Despite significant gas exchange problems the vast majority of patients studied were able to breath-hold adequately during the MR pulse sequences described herein.

The results of the experiments conducted in this thesis are novel and clinically relevant. The NT-proBNP threshold for RV failure defined in Chapter 3 has the potential to streamline the diagnostic pathway for patients with presenting with PH. In particular, the results of an NT-proBNP test may, in the future, help inform the largely subject process of stratifying new patients for invasive assessment and the initiation of disease targeted therapy. However, any incorporation of NT-proBNP

testing into diagnostic algorithms for PH must be combined with rigorous exclusion of patients with other reasons for a high NT-proBNP result. The strategy should be predated by prospective validation of the threshold identified in a larger cohort of patients. This is an obvious area for further study.

In Chapter 4, ce-CMR was used for the first time in PH patients. The occult, and previously unknown, myocardial abnormalities demonstrated in this study are a potentially fruitful area for further study. In patients with hypertrophic cardiomyopathy, areas of delayed contrast enhancement (DCE) within the septum and RV insertion points have recently been correlated with electrical instability on detailed ECG recordings and the incidence of life-threatening ventricular tachycardia (106). These areas have been proposed as arrhythmogenic foci, and thus, may prove to be the visible substrate for sudden arrhythmic death in patients with this condition. Since patients with PH are also prone to sudden arrhythmic death (58), it would be interesting to test the hypothesis that the DCE identified in similar areas in PH patients in Chapter 4, correlates with areas of similar electrical instability. This information might help identify patients with PH who are more likely to develop dangerous cardiac arrhythmias, and thus, benefit from prophylactic medication.

In Chapter 5, ds-CMR was performed successfully and safely in PH patients for the first time. In this study, both right and left ventricular stroke volumes failed to rise in PH patients during simulated exercise. The former appeared related solely to diminished RV contractile reserve, while the latter seemed to reflect diminished LV filling and the Frank-Starling mechanism. The data reported herein support the conclusion that LV filling is reduced during exercise in PH patients due to reduced

LV preload rather than extrinsic compression of the LV by septal bowing during diastole. This conclusion is in agreement with earlier invasive studies performed during Operation Everest II (178, 179) and a proportion of the latest relevant imaging studies performed in PH patients (161, 162). Nevertheless, contrary evidence has also been published (163) and the conclusion reached in this thesis cannot be considered absolute. Future studies combining ds-CMR and invasive cardiac pressure measurements may be able to definitively define the principal limitation to LV filling during exercise in PH patients. Nonetheless, the results of Chapter 5 add considerably to the knowledge base in this interesting area of study. Ds-CMR also provides a potentially useful assessment tool for patients with mild PH or those with risk factors for PH in whom a non-invasive screening test would be useful. Amplification of any abnormal signals from the pulmonary circulation in these patients may be possible using ds-CMR and further studies should be directed in this area.

Pulmonary vascular medicine is rapidly evolving clinical speciality in which huge progress has been made over recent years. 5-year survival has almost doubled for patients with PAH (from 34% in 1991 (1) to 61% in 2005 (3)) and new, and potentially more effective therapies, directed against well described intracellular targets, are the subject of ongoing clinical trials. Patients with proximal CTEPH can now be effectively treated by pulmonary thromboendarterectomy and even those with distal CTEPH can gain some benefit from medications previously reserved for patients with PAH (186). As the therapeutic armamentarium available to pulmonary vascular physicians grows treatment algorithms must evolve to reflect this increased complexity. Standard diagnostic aids such as echocardiography and right heart catheterisation are likely to remain essential components in these algorithms but CMR

imaging offers significant advantages over both. This thesis demonstrates that CMR imaging can be used to improve both the clinical management of PH patients and our understanding of the reasons for right and left ventricular dysfunction in this condition. It is hoped that over the next decade, as the availability of CMR imaging increases, the considerable advantages offered by CMR imaging can be experienced by patients unfortunate enough to develop PH.

References

REFERENCES

1. D'Alonzo GE, Barst RJ, Ayres SM, Bergofsky EH, Brundage BH, Detre KM, et al. Survival in patients with primary pulmonary hypertension. Results from a national prospective registry. *Ann Intern Med.* 1991;115(5):343-9.
2. McLaughlin VV, Presberg KW, Doyle RL, Abman SH, McCrory DC, Fortin T, et al. Prognosis of pulmonary arterial hypertension: ACCP evidence-based clinical practice guidelines. *Chest.* 2004;126(1 Suppl):78S-92S.
3. Kawut SM, Horn EM, Berekashvili KK, Garofano RP, Goldsmith RL, Widlitz AC, et al. New predictors of outcome in idiopathic pulmonary arterial hypertension. *Am J Cardiol.* 2005;95(2):199-203.
4. Howell JB, Permutt S, Proctor DF, Riley RL. Effect of inflation of the lung on different parts of pulmonary vascular bed. *J Appl Physiol.* 1961;16:71-6.
5. Weibel ER, Gil J. Structure function relationships of the alveolar level. In: West JB, editor. *Bioengineering aspects of the lung.* New York: Marcel Dekker; 1977.
6. Lai-Fook SJ. Mechanical factors in lung liquid distribution. *Annu Rev Physiol.* 1993;55:155-79.
7. Ciurea D, Gil J. Morphometry of capillaries in three zones of rabbit lungs fixed by vascular perfusion. *Anat Rec.* 1996;244(2):182-92.
8. Weibel ER. *Morphometry of the Human Lung.* Berlin/New York: Academic Press; 1963.
9. Sobin SS, Fung YC. Response to challenge to the Sobin-Fung approach to the study of pulmonary microcirculation. *Chest.* 1992;101(4):1135-43.
10. Sobin SS, Fung YC, Tremer HM, Rosenquist TH. Elasticity of the pulmonary alveolar microvascular sheet in the cat. *Circ Res.* 1972;30(4):440-50.

11. Fung YC, Yen RT. A new theory of pulmonary blood flow in zone 2 condition. *J Appl Physiol.* 1986;60(5):1638-50.
12. Gil J, Ciurea D. Functional anatomy of the pulmonary microcirculation. In: Peacock AJ, Rubin LJ, editors. *Pulmonary Circulation Diseases and their treatment.* Second ed. London: Arnold; 2004. p. 14-21.
13. MacLean MR. Endothelin-1: a mediator of pulmonary hypertension? *Pulm Pharmacol Ther.* 1998;11(2-3):125-32.
14. Naeije R. Pulmonary Vascular Function. In: AJ P, editor. *Pulmonary Circulation, A Handbook for Physicians.* London: Chapman & Hall Medical; 1996. p. 14-27.
15. West JB, Dollery CT, Naimark A. Distribution of Blood Flow in Isolated Lung; Relation to Vascular and Alveolar Pressures. *J Appl Physiol.* 1964;19:713-24.
16. von Euler US, Liljestrand G. Observations on the pulmonary arterial blood pressure in the cat. *Acta Physiologica Scandinavia.* 1946;12:301-20.
17. Warwick R, Williams P, editors. *Gray's Anatomy.* 35 ed. Edinburgh: Longman; 1973.
18. Sanchez-Quintana D, Garcia-Martinez V, Climent V, Hurle JM. Morphological changes in the normal pattern of ventricular myoarchitecture in the developing human heart. *Anat Rec.* 1995;243(4):483-95.
19. Sanchez-Quintana D, Climent V, Ho SY, Anderson RH. Myoarchitecture and connective tissue in hearts with tricuspid atresia. *Heart.* 1999;81(2):182-91.
20. Pearlman ES, Weber KT, Janicki JS, Pietra GG, Fishman AP. Muscle fiber orientation and connective tissue content in the hypertrophied human heart. *Lab Invest.* 1982;46(2):158-64.

21. Farrer-Brown G, Rowles PM. Vascular supply of interventricular septum of human heart. *Br Heart J.* 1969;31(6):727-34.
22. Cacoub P, Dorent R, Maistre G, Nataf P, Carayon A, Piette C, et al. Endothelin-1 in primary pulmonary hypertension and the Eisenmenger syndrome. *Am J Cardiol.* 1993;71(5):448-50.
23. Giaid A, Yanagisawa M, Langleben D, Michel RP, Levy R, Shennib H, et al. Expression of endothelin-1 in the lungs of patients with pulmonary hypertension. *N Engl J Med.* 1993;328(24):1732-9.
24. Giaid A, Saleh D. Reduced expression of endothelial nitric oxide synthase in the lungs of patients with pulmonary hypertension. *N Engl J Med.* 1995;333(4):214-21.
25. Tuder RM, Cool CD, Geraci MW, Wang J, Abman SH, Wright L, et al. Prostacyclin synthase expression is decreased in lungs from patients with severe pulmonary hypertension. *Am J Respir Crit Care Med.* 1999;159(6):1925-32.
26. MacLean MR, Herve P, Eddahibi S, Adnot S. 5-hydroxytryptamine and the pulmonary circulation: receptors, transporters and relevance to pulmonary arterial hypertension. *Br J Pharmacol.* 2000;131(2):161-8.
27. Eddahibi S, Humbert M, Fadel E, Raffestin B, Darmon M, Capron F, et al. Serotonin transporter overexpression is responsible for pulmonary artery smooth muscle hyperplasia in primary pulmonary hypertension. *J Clin Invest.* 2001;108(8):1141-50.
28. Yuan XJ, Wang J, Juhaszova M, Gaine SP, Rubin LJ. Attenuated K⁺ channel gene transcription in primary pulmonary hypertension. *Lancet.* 1998;351(9104):726-7.

29. Yuan XJ, Wang J, Juhaszova M, Golovina VA, Rubin LJ. Molecular basis and function of voltage-gated K⁺ channels in pulmonary arterial smooth muscle cells. *Am J Physiol.* 1998;274(4 Pt 1):L621-35.
30. Cowan KN, Jones PL, Rabinovitch M. Elastase and matrix metalloproteinase inhibitors induce regression, and tenascin-C antisense prevents progression, of vascular disease. *J Clin Invest.* 2000;105(1):21-34.
31. Cowan KN, Heilbut A, Humpl T, Lam C, Ito S, Rabinovitch M. Complete reversal of fatal pulmonary hypertension in rats by a serine elastase inhibitor. *Nat Med.* 2000;6(6):698-702.
32. Vieillard-Baron A, Frisdal E, Eddahibi S, Deprez I, Baker AH, Newby AC, et al. Inhibition of matrix metalloproteinases by lung TIMP-1 gene transfer or doxycycline aggravates pulmonary hypertension in rats. *Circ Res.* 2000;87(5):418-25.
33. Wagenvoort CA. The pathology of primary pulmonary hypertension. *J Pathol.* 1970;101(4):i.
34. Heath D, Edwards JE. The pathology of hypertensive pulmonary vascular disease; a description of six grades of structural changes in the pulmonary arteries with special reference to congenital cardiac septal defects. *Circulation.* 1958;18(4 Part 1):533-47.
35. Tuder RM, Groves B, Badesch DB, Voelkel NF. Exuberant endothelial cell growth and elements of inflammation are present in plexiform lesions of pulmonary hypertension. *Am J Pathol.* 1994;144(2):275-85.
36. Moser KM, Bloor CM. Pulmonary vascular lesions occurring in patients with chronic major vessel thromboembolic pulmonary hypertension. *Chest.* 1993;103(3):685-92.

37. Lee SD, Shroyer KR, Markham NE, Cool CD, Voelkel NF, Tuder RM. Monoclonal endothelial cell proliferation is present in primary but not secondary pulmonary hypertension. *J Clin Invest.* 1998;101(5):927-34.
38. Naeije D. Pathophysiology of Pulmonary Arterial Hypertension. In: M Demedts MD, R Verhaeghe, GM Verleden, editor. *ERS Respiratory Monograph - Pulmonary Vascular Pathology: A Clinical Update.* Huddersfield: The Charlesworth Group; 2004. p. 191-203.
39. Rubin LJ. Primary pulmonary hypertension. *N Engl J Med.* 1997;336(2):111-7.
40. Nichols WC, Koller DL, Slovis B, Foroud T, Terry VH, Arnold ND, et al. Localization of the gene for familial primary pulmonary hypertension to chromosome 2q31-32. *Nat Genet.* 1997;15(3):277-80.
41. Deng Z, Morse JH, Slager SL, Cuervo N, Moore KJ, Venetos G, et al. Familial primary pulmonary hypertension (gene PPH1) is caused by mutations in the bone morphogenetic protein receptor-II gene. *Am J Hum Genet.* 2000;67(3):737-44. Epub 2000 Jul 20.
42. Welsh CH, Hassell KL, Badesch DB, Kressin DC, Marlar RA. Coagulation and fibrinolytic profiles in patients with severe pulmonary hypertension. *Chest.* 1996;110(3):710-7.
43. Humbert M, Monti G, Brenot F, Sitbon O, Portier A, Grangeot-Keros L, et al. Increased interleukin-1 and interleukin-6 serum concentrations in severe primary pulmonary hypertension. *Am J Respir Crit Care Med.* 1995;151(5):1628-31.
44. Eysmann SB, Palevsky HI, Reichek N, Hackney K, Douglas PS. Two-dimensional and Doppler-echocardiographic and cardiac catheterization correlates of survival in primary pulmonary hypertension. *Circulation.* 1989;80(2):353-60.

45. Sandoval J, Bauerle O, Palomar A, Gomez A, Martinez-Guerra ML, Beltran M, et al. Survival in primary pulmonary hypertension. Validation of a prognostic equation. *Circulation*. 1994 Apr;89(4):1733-44.
46. Miyamoto S, Nagaya N, Satoh T, Kyotani S, Sakamaki F, Fujita M, et al. Clinical correlates and prognostic significance of six-minute walk test in patients with primary pulmonary hypertension. Comparison with cardiopulmonary exercise testing. *Am J Respir Crit Care Med*. 2000 Feb;161(2 Pt 1):487-92.
47. Sun XG, Hansen JE, Oudiz RJ, Wasserman K. Exercise pathophysiology in patients with primary pulmonary hypertension. *Circulation*. 2001 Jul 24;104(4):429-35.
48. Sitbon O, Humbert M, Nunes H, Parent F, Garcia G, Herve P, et al. Long-term intravenous epoprostenol infusion in primary pulmonary hypertension: prognostic factors and survival. *J Am Coll Cardiol*. 2002 Aug 21;40(4):780-8.
49. Dartevelle P, Fadel E, Mussot S, Chapelier A, Herve P, de Perrot M, et al. Chronic thromboembolic pulmonary hypertension. *Eur Respir J*. 2004;23(4):637-48.
50. Moser KM, Auger WR, Fedullo PF. Chronic major-vessel thromboembolic pulmonary hypertension. *Circulation*. 1990 Jun;81(6):1735-43.
51. Gowda RM, Khan IA, Vasavada BC, Sacchi TJ, Patel R. History of the evolution of echocardiography. *Int J Cardiol*. 2004;97(1):1-6.
52. Edler I, Hertz CH. The use of ultrasonic reflectoscope for the continuous recording of the movements of heart walls. 1954. *Clin Physiol Funct Imaging*. 2004;24(3):118-36.
53. Yock PG, Popp RL. Noninvasive estimation of right ventricular systolic pressure by Doppler ultrasound in patients with tricuspid regurgitation. *Circulation*. 1984;70(4):657-62.

54. Currie PJ, Seward JB, Chan KL, Fyfe DA, Hagler DJ, Mair DD, et al. Continuous wave Doppler determination of right ventricular pressure: a simultaneous Doppler-catheterization study in 127 patients. *J Am Coll Cardiol.* 1985;6(4):750-6.
55. Torbicki A, Skwarski K, Hawrylkiewicz I, Pasierski T, Miskiewicz Z, Zielinski J. Attempts at measuring pulmonary arterial pressure by means of Doppler echocardiography in patients with chronic lung disease. *Eur Respir J.* 1989;2(9):856-60.
56. Berger M, Haimowitz A, Van Tosh A, Berdoff RL, Goldberg E. Quantitative assessment of pulmonary hypertension in patients with tricuspid regurgitation using continuous wave Doppler ultrasound. *J Am Coll Cardiol.* 1985;6(2):359-65.
57. Recommendations on the management of pulmonary hypertension in clinical practice. *Heart.* 2001;86(Suppl 1):I1-13.
58. Kanemoto N. Natural history of pulmonary hemodynamics in primary pulmonary hypertension. *Am Heart J.* 1987;114(2):407-13.
59. Foale R, Nihoyannopoulos P, McKenna W, Kleinebenne A, Nadazdin A, Rowland E, et al. Echocardiographic measurement of the normal adult right ventricle. *Br Heart J.* 1986;56(1):33-44.
60. Levine RA, Gibson TC, Aretz T, Gillam LD, Guyer DE, King ME, et al. Echocardiographic measurement of right ventricular volume. *Circulation.* 1984;69(3):497-505.
61. Yeo TC, Dujardin KS, Tei C, Mahoney DW, McGoon MD, Seward JB. Value of a Doppler-derived index combining systolic and diastolic time intervals in predicting outcome in primary pulmonary hypertension. *Am J Cardiol.* 1998 May 1;81(9):1157-61.

62. Cournand A, Bloomfield R, Lauson D. Double lumen catheter for intravenous and intracardiac blood sampling and pressure recording. *Proceedings of the Society of Experimental Biology and Medicine*. 1945;60:73-5.
63. Ganz W, Donoso R, Marcus HS, Forrester JS, Swan HJ. A new technique for measurement of cardiac output by thermodilution in man. *Am J Cardiol*. 1971;27(4):392-6.
64. Werko L, Varnauskas E, Thomasson B. The influence of the pulmonary arterial pressure on the pulmonary capillary venous pressure in man. *Circ Res*. 1953;1(4):340-4.
65. Galie N, Torbicki A, Barst R, Darteville P, Haworth S, Higenbottam T, et al. Guidelines on diagnosis and treatment of pulmonary arterial hypertension. The Task Force on Diagnosis and Treatment of Pulmonary Arterial Hypertension of the European Society of Cardiology. *Eur Heart J*. 2004 Dec;25(24):2243-78.
66. Sitbon M, Humbert M, Ios V. Who benefits from long-term calcium-channel blocker therapy in primary pulmonary hypertension? [abstract]. *American Journal of Respiratory and Critical Care Medicine*. 2003;167:A440.
67. Hoeper MM, Oudiz RJ, Peacock A, Tapson VF, Haworth SG, Frost AE, et al. End points and clinical trial designs in pulmonary arterial hypertension: clinical and regulatory perspectives. *J Am Coll Cardiol*. 2004 Jun 16;43(12 Suppl S):48S-55S.
68. Badesch DB, Tapson VF, McGoon MD, Brundage BH, Rubin LJ, Wigley FM, et al. Continuous intravenous epoprostenol for pulmonary hypertension due to the scleroderma spectrum of disease. A randomized, controlled trial. *Ann Intern Med*. 2000 Mar 21;132(6):425-34.
69. Galie N, Humbert M, Vachiery JL, Vizza CD, Kneussl M, Manes A, et al. Effects of beraprost sodium, an oral prostacyclin analogue, in patients with pulmonary

arterial hypertension: a randomized, double-blind, placebo-controlled trial. *J Am Coll Cardiol.* 2002;39(9):1496-502.

70. Simonneau G, Barst RJ, Galie N, Naeije R, Rich S, Bourge RC, et al. Continuous subcutaneous infusion of treprostinil, a prostacyclin analogue, in patients with pulmonary arterial hypertension: a double-blind, randomized, placebo-controlled trial. *Am J Respir Crit Care Med.* 2002;165(6):800-4.

71. Oudiz RJ, Barst RJ, Hansen JE, Sun XG, Garofano R, Wu X, et al. Cardiopulmonary exercise testing and six-minute walk correlations in pulmonary arterial hypertension. *Am J Cardiol.* 2006 Jan 1;97(1):123-6.

72. de Bold AJ. Atrial natriuretic factor: a hormone produced by the heart. *Science.* 1985 Nov 15;230(4727):767-70.

73. Marin-Grez M, Fleming JT, Steinhausen M. Atrial natriuretic peptide causes pre-glomerular vasodilatation and post-glomerular vasoconstriction in rat kidney. *Nature.* 1986 Dec 4-10;324(6096):473-6.

74. Wu F, Yan W, Pan J, Morser J, Wu Q. Processing of pro-atrial natriuretic peptide by corin in cardiac myocytes. *J Biol Chem.* 2002 May 10;277(19):16900-5.

75. Yan W, Wu F, Morser J, Wu Q. Corin, a transmembrane cardiac serine protease, acts as a pro-atrial natriuretic peptide-converting enzyme. *Proc Natl Acad Sci U S A.* 2000 Jul 18;97(15):8525-9.

76. King L, Wilkins MR. Natriuretic peptide receptors and the heart. *Heart.* 2002 Apr;87(4):314-5.

77. Hasegawa K, Fujiwara H, Itoh H, Nakao K, Fujiwara T, Imura H, et al. Light and electron microscopic localization of brain natriuretic peptide in relation to atrial natriuretic peptide in porcine atrium. Immunohistochemical study using specific monoclonal antibodies. *Circulation.* 1991 Sep;84(3):1203-9.

78. de Bold AJ, Ma KK, Zhang Y, de Bold ML, Bensimon M, Khoshbaten A. The physiological and pathophysiological modulation of the endocrine function of the heart. *Can J Physiol Pharmacol*. 2001 Aug;79(8):705-14.
79. Groenning BA, Nilsson JC, Sondergaard L, Pedersen F, Trawinski J, Baumann M, et al. Detection of left ventricular enlargement and impaired systolic function with plasma N-terminal pro brain natriuretic peptide concentrations. *Am Heart J*. 2002 May;143(5):923-9.
80. Arakawa N, Nakamura M, Aoki H, Hiramori K. Plasma brain natriuretic peptide concentrations predict survival after acute myocardial infarction. *J Am Coll Cardiol*. 1996 Jun;27(7):1656-61.
81. Pedersen F, Raymond I, Kistorp C, Sandgaard N, Jacobsen P, Hildebrandt P. N-terminal pro-brain natriuretic peptide in arterial hypertension: a valuable prognostic marker of cardiovascular events. *J Card Fail*. 2005 Jun;11(5 Suppl):S70-5.
82. Golbasy Z, Ucar O, Yuksel AG, Gulel O, Aydogdu S, Ulusoy V. Plasma brain natriuretic peptide levels in patients with rheumatic heart disease. *Eur J Heart Fail*. 2004 Oct;6(6):757-60.
83. Cowie MR, Struthers AD, Wood DA, Coats AJ, Thompson SG, Poole-Wilson PA, et al. Value of natriuretic peptides in assessment of patients with possible new heart failure in primary care. *Lancet*. 1997 Nov 8;350(9088):1349-53.
84. Maisel AS, McCord J, Nowak RM, Hollander JE, Wu AH, Duc P, et al. Bedside B-Type natriuretic peptide in the emergency diagnosis of heart failure with reduced or preserved ejection fraction. Results from the Breathing Not Properly Multinational Study. *J Am Coll Cardiol*. 2003 Jun 4;41(11):2010-7.
85. Zaphiriou A, Robb S, Murray-Thomas T, Mendez G, Fox K, McDonagh T, et al. The diagnostic accuracy of plasma BNP and NTproBNP in patients referred from

primary care with suspected heart failure: results of the UK natriuretic peptide study. *Eur J Heart Fail.* 2005 Jun;7(4):537-41.

86. McDonagh TA, Robb SD, Murdoch DR, Morton JJ, Ford I, Morrison CE, et al. Biochemical detection of left-ventricular systolic dysfunction. *Lancet.* 1998 Jan 3;351(9095):9-13.

87. NICE. Chronic heart failure: management of chronic heart failure in adults in primary and secondary care. London: National Institute for Clinical Excellence; 2003.

88. Task Force for the Diagnosis and Treatment of Chronic Heart Failure ESoC, Remme WJ, Swedberg K. Guidelines for the diagnosis and treatment of chronic heart failure. *Eur Heart J.* 2001 September 1, 2001;22(17):1527-60.

89. Wright SP, Doughty RN, Pearl A, Gamble GD, Whalley GA, Walsh HJ, et al. Plasma amino-terminal pro-brain natriuretic peptide and accuracy of heart-failure diagnosis in primary care: a randomized, controlled trial. *J Am Coll Cardiol.* 2003 Nov 19;42(10):1793-800.

90. Hill NS, Klinger JR, Warburton RR, Pietras L, Wrenn DS. Brain natriuretic peptide: possible role in the modulation of hypoxic pulmonary hypertension. *Am J Physiol.* 1994 Mar;266(3 Pt 1):L308-15.

91. Nagaya N, Nishikimi T, Okano Y, Uematsu M, Satoh T, Kyotani S, et al. Plasma brain natriuretic peptide levels increase in proportion to the extent of right ventricular dysfunction in pulmonary hypertension. *J Am Coll Cardiol.* 1998 Jan;31(1):202-8.

92. Leuchte HH, Holzapfel M, Baumgartner RA, Ding I, Neurohr C, Vogeser M, et al. Clinical significance of brain natriuretic peptide in primary pulmonary hypertension. *J Am Coll Cardiol.* 2004;43(5):764-70.

93. Nagaya N, Nishikimi T, Uematsu M, Satoh T, Kyotani S, Sakamaki F, et al. Plasma brain natriuretic peptide as a prognostic indicator in patients with primary pulmonary hypertension. *Circulation*. 2000 Aug 22;102(8):865-70.
94. Park MH, Scott RL, Uber PA, Ventura HO, Mehra MR. Usefulness of B-type natriuretic Peptide as a predictor of treatment outcome in pulmonary arterial hypertension. *Congest Heart Fail*. 2004;10(5):221-5.
95. Nagaya N, Ando M, Oya H, Ohkita Y, Kyotani S, Sakamaki F, et al. Plasma brain natriuretic peptide as a noninvasive marker for efficacy of pulmonary thromboendarterectomy. *Ann Thorac Surg*. 2002 Jul;74(1):180-4; discussion 4.
96. Wilkins MR, Paul GA, Strange JW, Tunariu N, Gin-Sing W, Banya WA, et al. Sildenafil versus Endothelin Receptor Antagonist for Pulmonary Hypertension (SERAPH) study. *Am J Respir Crit Care Med*. 2005 Jun 1;171(11):1292-7.
97. Lorenz CH, Walker ES, Morgan VL, Klein SS, Graham TP, Jr. Normal human right and left ventricular mass, systolic function, and gender differences by cine magnetic resonance imaging. *J Cardiovasc Magn Reson*. 1999;1(1):7-21.
98. Sievers B, Kirchberg S, Bakan A, Franken U, Trappe HJ. Impact of papillary muscles in ventricular volume and ejection fraction assessment by cardiovascular magnetic resonance. *J Cardiovasc Magn Reson*. 2004;6(1):9-16.
99. Hines R. Right ventricular function and failure: a review. *Yale J Biol Med*. 1991;64(4):295-307.
100. Lidegran M, Odhner L, Jacobsson LA, Greitz D, Lundell B. Magnetic resonance imaging and echocardiography in assessment of ventricular function in atrially corrected transposition of the great arteries. *Scand Cardiovasc J*. 2000;34(4):384-9.

101. Katz J, Whang J, Boxt LM, Barst RJ. Estimation of right ventricular mass in normal subjects and in patients with primary pulmonary hypertension by nuclear magnetic resonance imaging. *J Am Coll Cardiol.* 1993;21(6):1475-81.
102. Saba TS, Foster J, Cockburn M, Cowan M, Peacock AJ. Ventricular mass index using magnetic resonance imaging accurately estimates pulmonary artery pressure. *Eur Respir J.* 2002;20(6):1519-24.
103. Boxt LM, Katz J, Kolb T, Czegledy FP, Barst RJ. Direct quantitation of right and left ventricular volumes with nuclear magnetic resonance imaging in patients with primary pulmonary hypertension. *J Am Coll Cardiol.* 1992;19(7):1508-15
104. Holman ER, van Jonbergen HP, van Dijkman PR, van der Laarse A, de Roos A, van der Wall EE. Comparison of magnetic resonance imaging studies with enzymatic indexes of myocardial necrosis for quantification of myocardial infarct size. *Am J Cardiol.* 1993;71(12):1036-40.
105. Laissy JP, Messin B, Varenne O, Iung B, Karila-Cohen D, Schouman-Claeys E, et al. MRI of acute myocarditis: a comprehensive approach based on various imaging sequences. *Chest.* 2002;122(5):1638-48.
106. Teraoka K, Hirano M, Ookubo H, Sasaki K, Katsuyama H, Amino M, et al. Delayed contrast enhancement of MRI in hypertrophic cardiomyopathy. *Magn Reson Imaging.* 2004;22(2):155-61.
107. Choi KM, Kim RJ, Gubernikoff G, Vargas JD, Parker M, Judd RM. Transmural extent of acute myocardial infarction predicts long-term improvement in contractile function. *Circulation.* 2001;104(10):1101-7.
108. Lima JA, Judd RM, Bazille A, Schulman SP, Atalar E, Zerhouni EA. Regional heterogeneity of human myocardial infarcts demonstrated by contrast-enhanced MRI. Potential mechanisms. *Circulation.* 1995;92(5):1117-25.

109. Weinmann HJ LM, Mutzel W. Pharmacokinetics of Gd-DTPA after intravenous injection in Healthy Volunteers. *Physiology Chemistry Physics*. 1984;16:167-72.
110. Flacke SJ, Fischer SE, Lorenz CH. Measurement of the gadopentetate dimeglumine partition coefficient in human myocardium in vivo: normal distribution and elevation in acute and chronic infarction. *Radiology*. 2001;218(3):703-10.
111. Kim RJ, Chen EL, Lima JA, Judd RM. Myocardial Gd-DTPA kinetics determine MRI contrast enhancement and reflect the extent and severity of myocardial injury after acute reperfused infarction. *Circulation*. 1996;94(12):3318-26.
112. Nishimura T, Yamada Y, Hayashi M, Kozuka T, Nakatani T, Noda H, et al. Determination of infarct size of acute myocardial infarction in dogs by magnetic resonance imaging and gadolinium-DTPA: comparison with indium-111 antimyosin imaging. *Am J Physiol Imaging*. 1989;4(3):83-8.
113. Moon JC, Reed E, Sheppard MN, Elkington AG, Ho SY, Burke M, et al. The histologic basis of late gadolinium enhancement cardiovascular magnetic resonance in hypertrophic cardiomyopathy. *J Am Coll Cardiol*. 2004;43(12):2260-4.
114. Goldman MR, Brady TJ, Pykett IL, Burt CT, Buonanno FS, Kistler JP, et al. Quantification of experimental myocardial infarction using nuclear magnetic resonance imaging and paramagnetic ion contrast enhancement in excised canine hearts. *Circulation*. 1982;66(5):1012-6.
115. Cochet A, Zeller M, Cottin Y, Robert-Valla C, Lalande A, L'Huillier I, et al. The extent of myocardial damage assessed by contrast-enhanced MRI is a major determinant of N-BNP concentration after myocardial infarction. *Eur J Heart Fail*. 2004 Aug;6(5):555-60.

116. Ingkanisorn WP, Rhoads KL, Aletras AH, Kellman P, Arai AE. Gadolinium delayed enhancement cardiovascular magnetic resonance correlates with clinical measures of myocardial infarction. *J Am Coll Cardiol*. 2004 Jun 16;43(12):2253-9.
117. Wu KC, Zerhouni EA, Judd RM, Lugo-Olivieri CH, Barouch LA, Schulman SP, et al. Prognostic significance of microvascular obstruction by magnetic resonance imaging in patients with acute myocardial infarction. *Circulation*. 1998;97(8):765-72.
118. Kim RJ, Wu E, Rafael A, Chen EL, Parker MA, Simonetti O, et al. The use of contrast-enhanced magnetic resonance imaging to identify reversible myocardial dysfunction. *N Engl J Med*. 2000;343(20):1445-53.
119. Kim RJ, Fieno DS, Parrish TB, Harris K, Chen EL, Simonetti O, et al. Relationship of MRI delayed contrast enhancement to irreversible injury, infarct age, and contractile function. *Circulation*. 1999;100(19):1992-2002.
120. Choudhury L, Mahrholdt H, Wagner A, Choi KM, Elliott MD, Klocke FJ, et al. Myocardial scarring in asymptomatic or mildly symptomatic patients with hypertrophic cardiomyopathy. *J Am Coll Cardiol*. 2002;40(12):2156-64.
121. Kuribayashi T, Roberts WC. Myocardial disarray at junction of ventricular septum and left and right ventricular free walls in hypertrophic cardiomyopathy. *Am J Cardiol*. 1992;70(15):1333-40.
122. Kondo C, Caputo GR, Masui T, Foster E, O'Sullivan M, Stulbarg MS, et al. Pulmonary hypertension: pulmonary flow quantification and flow profile analysis with velocity-encoded cine MR imaging. *Radiology*. 1992;183(3):751-8. 38.
123. Bogren HG, Klipstein RH, Mohiaddin RH, Firmin DN, Underwood SR, Rees RS, et al. Pulmonary artery distensibility and blood flow patterns: a magnetic resonance study of normal subjects and of patients with pulmonary arterial hypertension. *Am Heart J*. 1989;118(5 Pt 1):990-9.

124. Kafi SA, Melot C, Vachiery JL, Brimiouille S, Naeije R. Partitioning of pulmonary vascular resistance in primary pulmonary hypertension. *J Am Coll Cardiol.* 1998 May;31(6):1372-6.
125. Ducas J, Stitz M, Gu S, Schick U, Prewitt RM. Pulmonary vascular pressure-flow characteristics. Effects of dopamine before and after pulmonary embolism. *Am Rev Respir Dis.* 1992 Aug;146(2):307-12.
126. Oosterhof T, Tulevski, II, Roest AA, Steendijk P, Vliegen HW, van der Wall EE, et al. Disparity between dobutamine stress and physical exercise magnetic resonance imaging in patients with an intra-atrial correction for transposition of the great arteries. *J Cardiovasc Magn Reson.* 2005;7(2):383-9.
127. Tulevski, II, Lee PL, Groenink M, van der Wall EE, Stoker J, Pieper PG, et al. Dobutamine-induced increase of right ventricular contractility without increased stroke volume in adolescent patients with transposition of the great arteries: evaluation with magnetic resonance imaging. *Int J Card Imaging.* 2000 Dec;16(6):471-8.
128. Tulevski I. Usefulness of magnetic resonance imaging dobutamine stress in asymptomatic and minimally symptomatic patients with decreased cardiac reserve from congenital heart disease (complete and corrected transposition of the great arteries and subpulmonic obstruction). *American Journal of Cardiology.* 2002;89(9):1077-81.
129. Rich S, Dantzker DR, Ayres SM, Bergofsky EH, Brundage BH, Detre KM, et al. Primary pulmonary hypertension. A national prospective study. *Ann Intern Med.* 1987;107(2):216-23.

130. Mikhail GW, Gibbs JS, Yacoub MH. Pulmonary and systemic arterial pressure changes during syncope in primary pulmonary hypertension. *Circulation*. 2001;104(11):1326-7.
131. Collidge TA, Thomson PC, Mark PB, Traynor JP, Jardine AG, Morris ST, et al. Gadolinium-enhanced MR imaging and nephrogenic systemic fibrosis: retrospective study of a renal replacement therapy cohort. *Radiology*. 2007 Oct;245(1):168-75.
132. Fuster V, Steele PM, Edwards WD, Gersh BJ, McGoon MD, Frye RL. Primary pulmonary hypertension: natural history and the importance of thrombosis. *Circulation*. 1984;70(4):580-7.
133. Downie PF, Talwar S, Squire IB, Davies JE, Barnett DB, Ng LL. Assessment of the stability of N-terminal pro-brain natriuretic peptide in vitro: implications for assessment of left ventricular dysfunction. *Clin Sci (Lond)*. 1999 Sep;97(3):255-8.
134. Souza R, Bogossian HB, Humbert M, Jardim C, Rabelo R, Amato MB, et al. N-terminal-pro-brain natriuretic peptide as a haemodynamic marker in idiopathic pulmonary arterial hypertension. *Eur Respir J*. 2005 Mar;25(3):509-13.
135. Fijalkowska A, Kurzyrna M, Torbicki A, Szewczyk G, Florczyk M, Pruszczyk P, et al. Serum N-terminal brain natriuretic peptide as a prognostic parameter in patients with pulmonary hypertension. *Chest*. 2006 May;129(5):1313-21.
136. Nagaya N, Nishikimi T, Uematsu M, Kyotani S, Satoh T, Nakanishi N, et al. Secretion patterns of brain natriuretic peptide and atrial natriuretic peptide in patients with or without pulmonary hypertension complicating atrial septal defect. *Am Heart J*. 1998 Aug;136(2):297-301.
137. Ndrepepa G, Braun S, Mehilli J, von Beckerath N, Vogt W, Schomig A, et al. Plasma levels of N-terminal pro-brain natriuretic peptide in patients with coronary

artery disease and relation to clinical presentation, angiographic severity, and left ventricular ejection fraction. *Am J Cardiol.* 2005 Mar 1;95(5):553-7.

138. Luchner A, Hengstenberg C, Lowel H, Riegger GA, Schunkert H, Holmer S. Effect of compensated renal dysfunction on approved heart failure markers: direct comparison of brain natriuretic peptide (BNP) and N-terminal pro-BNP. *Hypertension.* 2005 Jul;46(1):118-23.

139. Magnusson M, Melander O, Israelsson B, Grubb A, Groop L, Jovinge S. Elevated plasma levels of Nt-proBNP in patients with type 2 diabetes without overt cardiovascular disease. *Diabetes Care.* 2004 Aug;27(8):1929-35.

140. Alfakih K, Plein S, Thiele H, Jones T, Ridgway JP, Sivananthan MU. Normal human left and right ventricular dimensions for MRI as assessed by turbo gradient echo and steady-state free precession imaging sequences. *J Magn Reson Imaging.* 2003;17(3):323-9.

141. Lembcke A, Dohmen PM, Dewey M, Klessen C, Elgeti T, Hermann KG, et al. Multislice computed tomography for preoperative evaluation of right ventricular volumes and function: comparison with magnetic resonance imaging. *Ann Thorac Surg.* 2005 Apr;79(4):1344-51.

142. Raman SV, Shah M, McCarthy B, Garcia A, Ferketich AK. Multi-detector row cardiac computed tomography accurately quantifies right and left ventricular size and function compared with cardiac magnetic resonance. *Am Heart J.* 2006 Mar;151(3):736-44.

143. Longmore DB, Klipstein RH, Underwood SR, Firmin DN, Hounsfield GN, Watanabe M, et al. Dimensional accuracy of magnetic resonance in studies of the heart. *Lancet.* 1985 Jun 15;1(8442):1360-2.

144. MacNee W. Pathophysiology of cor pulmonale in chronic obstructive pulmonary disease. Part one. *Am J Respir Crit Care Med.* 1994;150:833-52.
145. Mogelvang J, Stubgaard M, Thomsen C, Henriksen O. Evaluation of right ventricular volumes measured by magnetic resonance imaging. *Eur Heart J.* 1988 May;9(5):529-33.
146. Pennell D, Casolo G. Right ventricular arrhythmia: emergence of magnetic resonance imaging as an investigative tool. *Eur Heart J.* 1997 Dec;18(12):1843-5.
147. Roeleveld RJ, Marcus JT, Faes TJ, Gan TJ, Boonstra A, Postmus PE, et al. Interventricular Septal Configuration at MR Imaging and Pulmonary Arterial Pressure in Pulmonary Hypertension. *Radiology.* 2005;5:5.
148. Vonk Noordegraaf A, Gan T, Marcus J, Boonstra A, Postmus P. Interventricular mechanical asynchrony is an important cause of cardiac dysfunction in pulmonary hypertension. *European Respiratory Society.* 2004;24(Supplement 48):203s.
149. Roeleveld RJ, Vonk-Noordegraaf A, Marcus JT, Bronzwaer JG, Marques KM, Postmus PE, et al. Effects of epoprostenol on right ventricular hypertrophy and dilatation in pulmonary hypertension. *Chest.* 2004;125(2):572-9.
150. Quaife RA, Chen MY, D. L, Badesch DB, Groves BM, Wolfel E, et al. Importance of right ventricular end-systolic regional wall stress in idiopathic pulmonary arterial hypertension: a new method for estimation of right ventricular wall stress. *Eur J Med Res.* 2006;11(5):214-20
151. Brown KA, Okada RD, Boucher CA, Strauss HW, Pohost GM. Right ventricular ejection fraction response to exercise in patients with coronary artery disease: influence of both right coronary artery disease and exercise-induced changes in right ventricular afterload. *J Am Coll Cardiol.* 1984 Apr;3(4):895-901.

152. Konstam MA, Salem DN, Isner JM, Zile MR, Kahn PC, Bonin JD, et al. Vasodilator effect on right ventricular function in congestive heart failure and pulmonary hypertension: end-systolic pressure--volume relation. *Am J Cardiol.* 1984 Jul 1;54(1):132-6.
153. Morrison D, Goldman S, Wright AL, Henry R, Sorenson S, Caldwell J, et al. The effect of pulmonary hypertension on systolic function of the right ventricle. *Chest.* 1983 Sep;84(3):250-7.
154. Zafir N, Zingerman B, Solodky A, Ben-Dayan D, Sagie A, Sulkes J, et al. Use of noninvasive tools in primary pulmonary hypertension to assess the correlation of right ventricular function with functional capacity and to predict outcome. *Int J Cardiovasc Imaging.* 2006 Sep 14.
155. Raymond I, Groenning BA, Hildebrandt PR, Nilsson JC, Baumann M, Trawinski J, et al. The influence of age, sex and other variables on the plasma level of N-terminal pro brain natriuretic peptide in a large sample of the general population. *Heart.* 2003 Jul;89(7):745-51.
156. Das A, Xi L, Kukreja RC. Phosphodiesterase-5 inhibitor sildenafil preconditions adult cardiac myocytes against necrosis and apoptosis. Essential role of nitric oxide signaling. *J Biol Chem.* 2005 Apr 1;280(13):12944-55.
157. Marcus JT, Vonk Noordegraaf A, Roeleveld RJ, Postmus PE, Heethaar RM, Van Rossum AC, et al. Impaired left ventricular filling due to right ventricular pressure overload in primary pulmonary hypertension: noninvasive monitoring using MRI. *Chest.* 2001;119(6):1761-5.
158. Gomez A, Bialostozky D, Zajarias A, Santos E, Palomar A, Martinez ML, et al. Right ventricular ischemia in patients with primary pulmonary hypertension. *J Am Coll Cardiol.* 2001;38(4):1137-42.

159. Cothran L, Hawthorne E, Sandler H. An analysis of left ventricular dimensional changes in conscious animals. In: Harrison L, editor. *Research Animals in Medicine*. Washington D.C.: D.E.W.Y. Publication; 1973. p. 553-65.
160. McKenzie JC, Kelley KB, Merisko-Liversidge EM, Kennedy J, Klein RM. Developmental pattern of ventricular atrial natriuretic peptide (ANP) expression in chronically hypoxic rats as an indicator of the hypertrophic process. *J Mol Cell Cardiol*. 1994;26(6):753-67.
161. Gurudevan SV, Malouf PJ, Auger WR, Waltman TJ, Madani M, Raisinghani AB, et al. Abnormal left ventricular diastolic filling in chronic thromboembolic pulmonary hypertension: true diastolic dysfunction or left ventricular underfilling? *J Am Coll Cardiol*. 2007 Mar 27;49(12):1334-9.
162. Mahmud E, Raisinghani A, Hassankhani A, Sadeghi HM, Strachan GM, Auger W, et al. Correlation of left ventricular diastolic filling characteristics with right ventricular overload and pulmonary artery pressure in chronic thromboembolic pulmonary hypertension. *J Am Coll Cardiol*. 2002 Jul 17;40(2):318-24.
163. Gan CT, Lankhaar JW, Marcus JT, Westerhof N, Marques KM, Bronzwaer JG, et al. Impaired left ventricular filling due to right-to-left ventricular interaction in patients with pulmonary arterial hypertension. *Am J Physiol Heart Circ Physiol*. 2006 Apr;290(4):H1528-33.
164. Louie EK, Rich S, Levitsky S, Brundage BH. Doppler echocardiographic demonstration of the differential effects of right ventricular pressure and volume overload on left ventricular geometry and filling. *J Am Coll Cardiol*. 1992 Jan;19(1):84-90.
165. Schena M, Clini E, Errera D, Quadri A. Echo-Doppler evaluation of left ventricular impairment in chronic cor pulmonale. *Chest*. 1996 Jun;109(6):1446-51.

166. Lotz J, Meier C, Leppert A, Galanski M. Cardiovascular flow measurement with phase-contrast MR imaging: basic facts and implementation. *Radiographics*. 2002 May-Jun;22(3):651-71.
167. Fontanet HL, Perez JE, Davila-Roman VG. Diminished contractile reserve in patients with left ventricular hypertrophy and increased end-systolic stress during Dobutamine stress echocardiography. *Am J Cardiol*. 1996 Nov 1;78(9):1029-35.
168. Holverda S, Gan CT, Marcus JT, Postmus PE, Boonstra A, Vonk-Noordegraaf A. Impaired stroke volume response to exercise in pulmonary arterial hypertension. *J Am Coll Cardiol*. 2006 Apr 18;47(8):1732-3.
169. Nootens M, Wolfkiel CJ, Chomka EV, Rich S. Understanding right and left ventricular systolic function and interactions at rest and with exercise in primary pulmonary hypertension. *Am J Cardiol*. 1995;75(5):374-7.
170. Vonk Noordegraaf A, Westerhof N. Right ventricular ejection fraction and NT-proBNP are both indicators of wall stress in pulmonary hypertension. *Eur Respir J*. 2007 Apr;29(4):622-3.
171. Raeside DA, Smith A, Brown A, Patel KR, Madhok R, Cleland J, et al. Pulmonary artery pressure measurement during exercise testing in patients with suspected pulmonary hypertension. *Eur Respir J*. 2000;16(2):282-7.
172. Daniels LB, Krummen DE, Blanchard DG. Echocardiography in pulmonary vascular disease. *Cardiol Clin*. 2004 Aug;22(3):383-99, vi.
173. Elzinga G, van Grondelle R, Westerhof N, van den Bos GC. Ventricular interference. *Am J Physiol*. 1974 Apr;226(4):941-7.
174. Baker AE, Dani R, Smith ER, Tyberg JV, Belenkie I. Quantitative assessment of independent contributions of pericardium and septum to direct ventricular interaction. *Am J Physiol*. 1998 Aug;275(2 Pt 2):H476-83.

175. Belenkie I, Sas R, Mitchell J, Smith ER, Tyberg JV. Opening the pericardium during pulmonary artery constriction improves cardiac function. *J Appl Physiol*. 2004 Mar;96(3):917-22.
176. Blanchard DG, Dittrich HC. Pericardial adaptation in severe chronic pulmonary hypertension. An intraoperative transesophageal echocardiographic study. *Circulation*. 1992 Apr;85(4):1414-22.
177. Groves BM, Reeves JT, Sutton JR, Wagner PD, Cymerman A, Malconian MK, et al. Operation Everest II: elevated high-altitude pulmonary resistance unresponsive to oxygen. *J Appl Physiol*. 1987 Aug;63(2):521-30.
178. Reeves JT, Groves BM, Sutton JR, Wagner PD, Cymerman A, Malconian MK, et al. Operation Everest II: preservation of cardiac function at extreme altitude. *J Appl Physiol*. 1987 Aug;63(2):531-9.
179. Suarez J, Alexander JK, Houston CS. Enhanced left ventricular systolic performance at high altitude during Operation Everest II. *Am J Cardiol*. 1987 Jul 1;60(1):137-42.
180. Barst RJ, Rubin LJ, McGoon MD, Caldwell EJ, Long WA, Levy PS. Survival in primary pulmonary hypertension with long-term continuous intravenous prostacyclin. *Ann Intern Med*. 1994;121(6):409-15.
181. Sitbon O, McLaughlin VV, Badesch DB, Barst RJ, Black C, Galie N, et al. Survival in patients with class III idiopathic pulmonary arterial hypertension treated with first line oral bosentan compared with an historical cohort of patients started on intravenous epoprostenol. *Thorax*. 2005 Dec;60(12):1025-30.
182. Ogino H, Ando M, Matsuda H, Minatoya K, Sasaki H, Nakanishi N, et al. Japanese single-center experience of surgery for chronic thromboembolic pulmonary hypertension. *Ann Thorac Surg*. 2006 Aug;82(2):630-6.

183. Riedel M, Stanek V, Widimsky J, Prerovsky I. Longterm follow-up of patients with pulmonary thromboembolism. Late prognosis and evolution of hemodynamic and respiratory data. *Chest*. 1982 Feb;81(2):151-8.
184. Peacock A, Naeije R, Galie N, Reeves JT. End points in pulmonary arterial hypertension: the way forward. *Eur Respir J*. 2004 Jun;23(6):947-53.
185. Grunig E, Janssen B, Mereles D, Barth U, Borst MM, Vogt IR, et al. Abnormal pulmonary artery pressure response in asymptomatic carriers of primary pulmonary hypertension gene. *Circulation*. 2000 Sep 5;102(10):1145-50.
186. Hughes RJ, Jais X, Bonderman D, Suntharalingam J, Humbert M, Lang I, et al. The efficacy of bosentan in inoperable chronic thromboembolic pulmonary hypertension: a 1-year follow-up study. *Eur Respir J*. 2006 Jul;28(1):138-43.